國立成功大學

太空與電漿科學研究所

碩士論文

National Cheng Kung University

Institute of Space and Plasma Sciences

Master Thesis

磁控電子束轟擊金屬離子推進器之開發

Development of Metallic Ion Thruster using Magnetron Electron-beam Bombardment

陳國益

Kuo-Yi Chen

指導教授:張博宇

Advisor: Po-Yu Chang, Ph.D

中華民國一百零八年七月

July, 2019

doi:10.6844/NCKU201900538

國立成功大學

碩士論文

磁控電子束轟擊金屬離子推進器之開發

Development of Metallic Ion Thruster using Magnetron Electron-beam Bombardment

研究生：陳國益

本論文業經審查及口試合格特此證明

論文考試委員：

指導教授：

系(所)主管：

中　華　民　國　108　年　7　月　1　日

doi:10.6844/NCKU201900538

摘要

我們開發出了一種使用固態金屬作為推進劑的新型態離子推進器:磁控電子束轟擊金屬離子推進器 Metallic Ion Thruster using Magnetron E-beam Bombardment (MIT-MEB)。不同於使用惰性氣體作為推進劑的經典離子推進器/電漿推進器,MIT-MEB 使用固體金屬作為推進劑，因此有儲存密度高、成本低廉、易於儲存、安全等優點。可以使用任何導體作為推進劑。而元素週期表上有八成是金屬，因此相較傳統離子推進器而言，MIT-MEB 在材料選擇上有絕對的優勢。本設計分為三個部分：金屬離子產生器和離子加速器以及中和器。首先自由電子從熱燈絲發射並被電場加速衝向金屬靶，使得金屬被加熱並蒸發。而金屬靶表面和燈絲之間具有約 0.2~0.3T 的磁場用於聚焦電子，當金屬蒸氣通過被磁場侷限而形成的高密度的電子雲時，會被其中的高能電子碰撞並游離。金屬被游離成離子後會被電場加速並排出裝置，而外部的中和器則釋放電子並與離子一同離開推進器。推進器最終排出等量的高速離子與電子藉以保持裝置的電中性。由於電子束工作條件與真空條件無關，因此可在超高真空環境中運作。我們已經製作並測試了原型機，通過電子束轟擊將金屬靶加熱至超過 415℃。在 5 kV/3 mA 和 1 kV/15 mA 的電子束電流轟擊下，使用鋅片作為測試靶材，測得其質量流率為（2.2±0.4）×10^{-4}（g/s）與（1.8±0.3）×10^{-5}（g/s），游離率為 0.03±0.01 %和 1.1±0.3 %。因此，離子貢獻之推進力理論值分別為 9.0±1.0 μN 和 10.3±0.7 μN，總功率約為 25 W 左右。比衝 I_{sp} 理論值分別為 12300 s 和 5500 s。若考慮未游離之蒸氣的貢獻，則總推進力分別為 99±40 μN 和 17.3±4.0 μN.

關鍵字: 電推進器；物理氣相沉積；電子束蒸發技術；固態推進劑

doi:10.6844/NCKU201900538

Abstract

The electric thruster is a device that uses electromagnetic fields to control and accelerate ions. An ion thruster using a metallic target as the propellant has been developed. Different from the inert gas used in conventional plasma thrusters, the metallic target is in the solid state, high density, easy to be stored and cheap. The design is divided into three parts: a metallic evaporator and an ion accelerator and a neutralizer. The principle of electron-beam (E-beam) evaporation, where a metal target is evaporated and ionized by thermal-emitted electrons, is used. The working condition is independent of the vacuum condition so that it works in the ultra-high vacuum space. A focusing magnet with a magnetic field about 0.2~0.3 T between the target surface and the filament is used to guide electrons toward the center of the target so that the metal is evaporated and ionized. A prototype has been built and tested. The metallic targets were heated to more than 415 °C by electron bombardment. A mass flow rate of $(2.2\pm0.4)\times10^{-4}$ (g/s) and $(1.8\pm0.3)\times10^{-5}$ (g/s) using Zn at 5 kV/3 mA and 1 kV/ 15mA E-beam current was measured. An ionization rate of 0.03±0.01 % and 1.1±0.3 % using Zn at 5 kV and 1 kV E-beam current was measured. Therefore, the estimated thrust is 9.0±1.0 μN and 10.3±0.7 μN with a power of about 25 W. The Estimated I_{sp} is 12,300 s and 5,500 s respectively. Considering the contribution of vapors, the total thrust is 99±40 μN and 17.3±4.0 μN respectively.

Key word: Electric thrust；Physical vapor deposition；Electron-beam vaporizer；Solid propellant

doi:10.6844/NCKU201900538

致謝

感謝張博宇教授的指導，在您的帶領下順里完成我的碩士學位。還記得推甄成大時帶著幾個想做的題目尋找指導教授，有幸讓教授對我想做的東西感興趣，經過幾天的討論就導定題目便一路研究到碩二畢業。從理論模型建立道計畫申請通過，再到建立原型並實驗驗證，一切都令人難以想像的順利。其皆歸於教授深厚的專業科學素養，總是能夠很快的發現問題的癥結並給予我犀利的建議。在您的指導下經常激盪出新的想法。感謝科技部通過我的計畫讓我無上的經費限制放膽嘗試。感謝實驗室的朋友們時常幫忙跑腿到處買東西，在大家的努力下一點一滴的把新實驗室建立起來。感謝名城這兩年的相伴，到處陪我去吃好吃的吃到破產。感謝宛儀在實驗上幫我測量各種繁瑣的數據。最後感謝男朋友立綱，有幸在這個時間點遇到你，陪我一起申請博士班並包容我走過心情最低落的時光，希望未來我們能順利完成博士學位去想去的地方生活。

doi:10.6844/NCKU201900538

Contents

doi:10.6844/NCKU201900538

doi:10.6844/NCKU201900538

doi:10.6844/NCKU201900538

doi:10.6844/NCKU201900538

List of tables

doi:10.6844/NCKU201900538

List of figures

doi:10.6844/NCKU201900538

doi:10.6844/NCKU201900538

doi:10.6844/NCKU201900538

doi:10.6844/NCKU201900538

doi:10.6844/NCKU201900538

Chapter 1

INTRODUCTION

The principle of an ion thruster is to ionize the gas first then use the electric force to accelerate ions. Therefore, spacecrafts are pushed by reaction forces from ejecting ions. The thrust can be adjusted by changing the electric field strength. Exhausted ions can reach a very high speed so that it is very efficient. This is the most efficient way in rocket technologies that has been put into practical use. Since the specific impulse (I_{sp}), a measure of how efficient propellant is used, is much larger than other existing propulsion technologies, only a small amount of propulsion is required. The total weight can be reduced so that a smaller and economical launch vehicle can be used and the fuel saved is significant. The downside is that thrusts form ion thrusters are very small, in the range of millinewton (mN). Current ion propulsion systems can only blow a piece of paper and can't be used to launch spacecrafts out of the planet. Further, it takes a long time to accelerate spacecraft even in space. Never the less, after a long period of running time, the spacecraft using ion thrusters is much faster than those using chemical propulsion. It makes the ion thruster very attractive for deep-space mission. Furthers, small thrusts are suitable for attitude and orbit control or satellite attitude control.

1-1 Principle of ion thrusters

An ion thruster is a device that emits high-speed electrical quasi-neutral particles. The momentum change of the propellant provides the thrust. A thruster is characterized by its thrust and specific impulse (I_{sp}).

doi:10.6844/NCKU201900538

1-1-1 Thrusts

The propellant is accelerated and exhausted from the thruster. The thrust is provided by reaction force from the exhausted propellant. Assuming the propellant is accelerated to a specific kinetic energy E_k before being exhausted, the thrust F is given by:

$$F = \frac{d}{dt}(mv_{ex}) = \frac{dm}{dt} v_{ex} = \dot{m} \times \sqrt{\frac{2E_k}{m_i}} \quad (1)$$

where $\dot{m}$ is the ion mass flow rate of the propellant, v_{ex} is the ion exhaust velocity, m_i is atom mass of ions and E_k is the kinetic energy of ions obtained by passing through the accelerating grid.

1-1-2 Specific impulse (I_{sp})

Specific impulse is a parameter that measures the thrust efficiency. The unit of I_{sp} is in seconds, meaning the time that an 1 kg propellant lasts while keeping 9.8 N of thrust. Specific impulse is only related to exhaust speed of the propellant. It is defined as

$$I_{sp} \equiv \frac{F}{\dot{m}g} = \frac{v_{ex}}{g} \text{ (sec)} \quad (2)$$

where g is the gravitational acceleration. When the propellant is exhausted with high speed, the I_{sp} is larger meaning higher efficiency. A spacecraft has a higher final speed using a thruster with a higher I_{sp}. It can be obtained from the conservation of linear momentum.

$$p(t) = p(t + dt), \quad (3)$$

$$mv = (m - dm_p)(v + dv) + dm_p(v - v_{ex}), \quad (4)$$

$$dv = -v_{ex}\frac{dm}{m} \text{ where } dm_p dv \text{ is neglected and } dm_p = -dm, \quad (5)$$

$$v_f = v_i + v_{ex} \ln\left[\frac{m_i}{m_f}\right] = v_i + I_{sp} g \ln\left[\frac{m_i}{m_f}\right] \quad (6)$$

doi:10.6844/NCKU201900538

where p is the total linear momentum of the whole system, dm and dm_p are the mass changes of the thruster and the exhausted propellant, respectively, m is the total mass, and m_i, m_f, v_i, and v_f are the initial and final mass and velocity, respectively. To obtain a higher final speed, either larger m_i/m_f or larger I_{sp} is needed. Notice that a thruster with higher I_{sp} does not necessarily have a larger thrust since a larger thrust can be provided by large mass flow rate of exhausted propellant such as chemical rockets. Shown in Fig. 1.1[1,2] is the comparison between different types of thrusters. Ion thrusters provide larger I_{sp} but with a much smaller thrust density defined as force per unit area. Thrusts of ion thrusters are generally insufficient for a rocket to overcome the gravitational force on earth. However, its high I_{sp} indicates a higher final speed once the spacecraft has left the gravitational influence from earth than using other thrusters such as chemical rockets. Therefore, an ion thruster is one of the best options for deep-space missions.

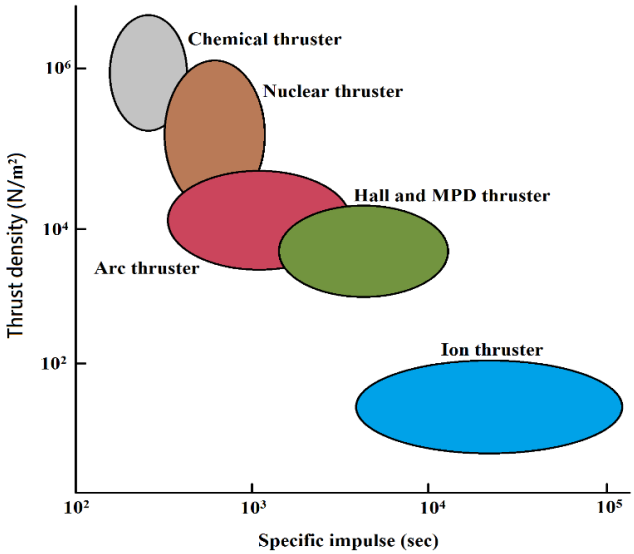

Figure 1.1: Thrust density vs specific impulse for different types of thrusters [1,2].

doi:10.6844/NCKU201900538

1-2 Different types of electric propulsions

Depending on how propellants are accelerated, electric thrusters are categorized as electrothermal, electrostatic, and electromagnetic thrusters. Three different thrusters, gridded ion thrusters, Hall thrusters, pulsed-plasma thrusters, are introduced below.

1-2-1 Gridded ion thrusters

The gridded ion thruster is a classical ion thruster that usually uses large mass inert gas as the propellant, like Xenon gas. As shown in Fig. 1.2, the device can be mainly divided into two parts: an ionizer and an accelerator. The ionizer is used to ionize neutral inert gas. Electron guns are commonly used for electron impact ionization processes. However, we can also use any other methods for ionizing gas such as microwave and high energy particle impact ionizing by nuclear radioactive material. When (Xenon) ions generated by the ionizer diffuse to the accelerator part, they are accelerated by the electric field provided by the electric grids. As a result, high-speed (Xenon) ions are exhausted from the thruster into the space and provide the thrust. Gridded ion thruster usually provide a moderate specific impulse (2000 ~ 4000s) with a thrust of 20–200 mN.

doi:10.6844/NCKU201900538

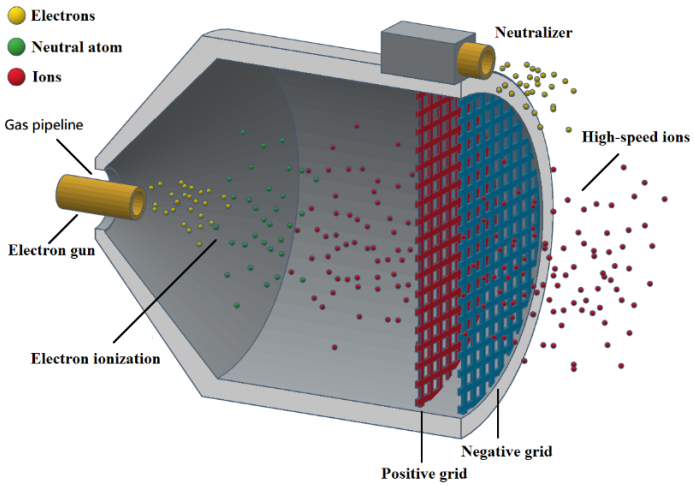

Figure 1.2: Schematic of gridded ion thrusters.

1-2-2 Hall thrusters

The operation principle of the Hall thruster is shown in Fig. 1.3. An electron gun is used to provide electron currents. Magnetic fields are used to confine the electron motion in axial direction extending the time that electrons reach the anode. Electrons are used to ionize the propellant via electron impacts. The magnetic fields are generated by an electromagnet located at the center cylinder. The strength of the magnetic field is designed to confine electrons but not ions. Electrons moving around the cylinder forms a so-called electron Hall current. It greatly extends the time of electron motions in the cavity. When propellant gas is injected in to the chamber, it is ionized by electron impacts. Since ions are too heavy to be confined by the magnetic field, they will be accelerated by the electric field and leave the thruster with high speed and provide the thrust. The electron gun is responsible for providing both the Hall current and the neutralizing electrons. Hall thrusters usually provide a moderate specific impulse (1000 ~ 5000 s) with a thrust of 40–600 mN.

doi:10.6844/NCKU201900538

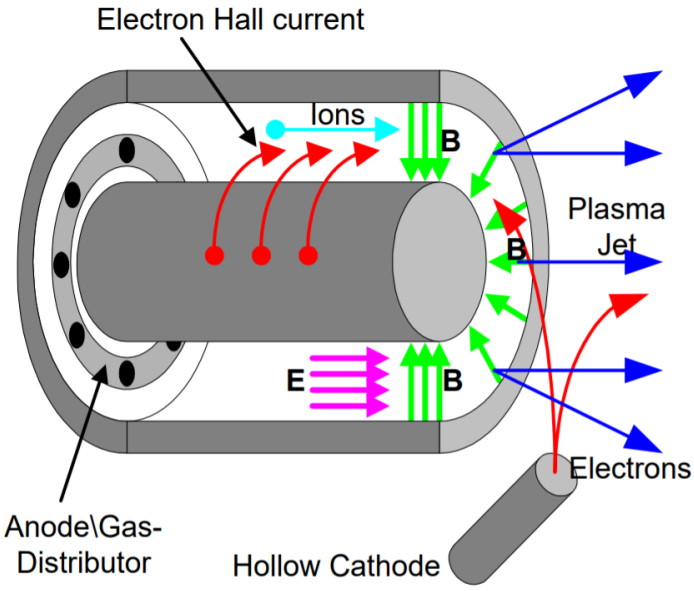

Figure 1.3: Schematic of the Hall effect thruster. Courtesy of Ref [3].

1-2-3 Pulsed-plasma thrusters (PPT)

A pulsed-plasma thruster (PPT) is also the simplest form of electric spacecraft propulsion. Shown in Fig. 1.4, PPT uses pulsed arc discharge to erode propellant momentary [4]. When the propellant turns from solid to vapor and plasma, it is accelerated by the Lorentz force. High temperature gas also diffuses at the same time providing some thrusts. The arc thruster has low ionization rate and low I_{sp} but has higher thrust compared to ion thrusters because it has a large mass flow rate.

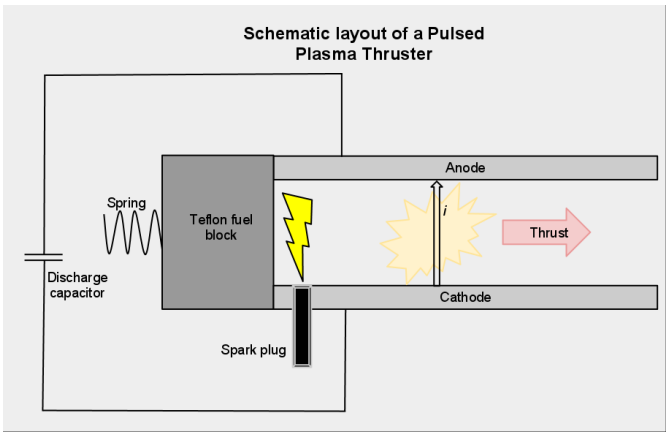

Figure 1.4: Schematic of the pulsed-plasma thruster. Courtesy of Ref [5].

doi:10.6844/NCKU201900538

1-3 Metallic Ion Thruster using Magnetron Electron-beam Bombardment

Metallic Ion Thruster using Magnetron Electron-beam Bombardment (MIT-MEB) is a new type of electric thrusters we are developing. The structure of MIT-MEB is shown in Fig. 1.5. Instead of using inert gas, it uses a solid metal as the propellant. I apply electron-beam evaporation technology and electron impact ionization to the electric thruster. It can use any conductors as propellants. Our metallic ion thruster can be used on deep space exploration because it is possible to collect metallic propellants from asteroids, planets, star dusts, etc. Solid propellants do not need huge gas cylinders. It can also be fitted in a CubeSat. We built a prototype with a size of ~ 5×5×5 cm^3, and a weight less than 500 g. Final results of the best power and thrust and I_{sp}. The MIT-MEB concept is never used in any electric thruster and is very competitive internationally. MIT-MEB provides high specific impulse (I_{sp}) like any conventional ion thrusters. Comparing to conventional ion thrusters where inert gas is used as the propellant, the metallic propellant is in solid state, high density, easy to be stored and cheap. The thesis is arranged as following: the E-beam principle will be given in chapter 2. The details of MIT-MEB will be shown in chapter 3. The high vacuum system will be shown in chapter 4. The measurement methods and experimental results will be shown in chapter 5 & 6. The Future woks and summary will be given in chapter 7 & 8.

doi:10.6844/NCKU201900538

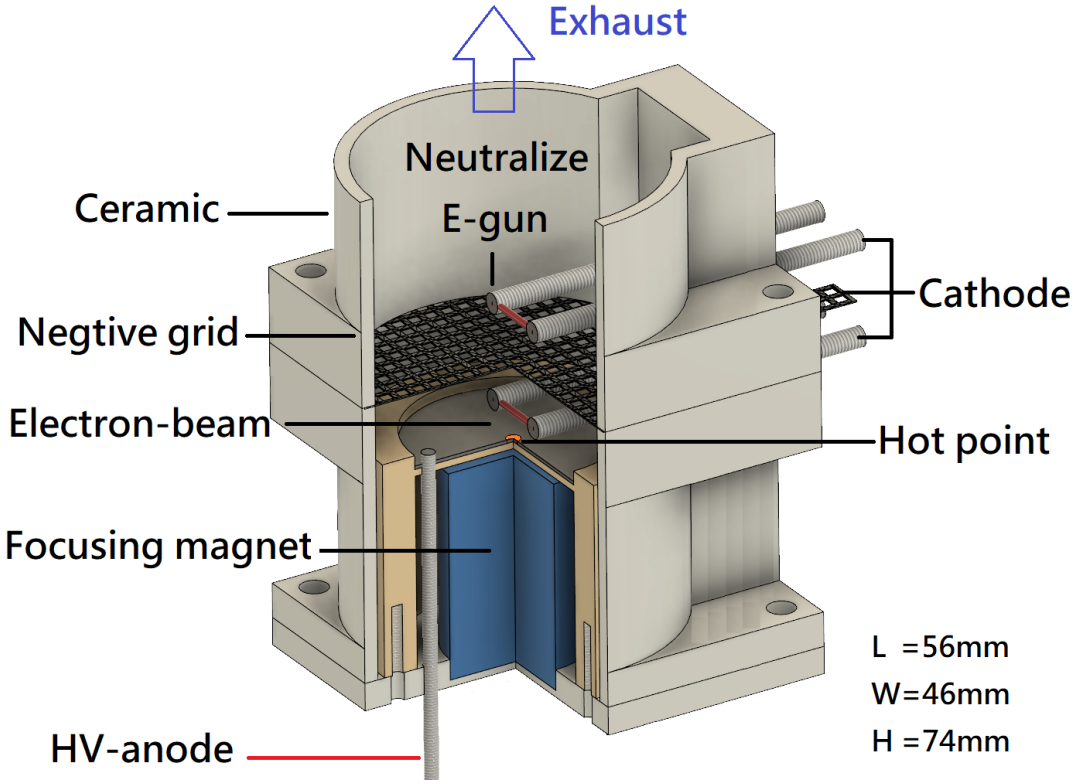

Figure 1.5: Schematic of the Metallic Ion Thruster using Magnetron Electron-beam Bombardment (MIT-MEB).

doi:10.6844/NCKU201900538

Chapter 2

Concepts of the new ion thruster

In this chapter, I will introduce ideas and backgrounds on developing the new thruster. The biggest difference between MIT-MEB and traditional ion propulsions is that we use solid metal targets as propellants. So, first step I have to find a way to make the target change its phase to vapor and must also be able to operate in ultra-high vacuum. The second step is to change the vapor to a plasma. Combining two conditions above, I chose electron-beam (E-beam) evaporation to generate ions. It is because using electrons as working particles can work in ultra-high vacuum and can ionize vapor through electron impact ionization effect. We will start from introducing vapor deposition and the principle of MIT-MEB in this chapter.

2-1 Physical vapor deposition

Physical Vapor Deposition (PVD) is a physical deposition mechanism for thin film deposition processes. The so-called physical mechanism is the phase change of matter. The methods that can be used are evaporation and sputtering. Evaporation is the evaporation of the target by heating such as joule heating, laser heating and E-beam heating. In the case of sputtering, the target is bombarded by ions in the plasma. The momentums of working particles, ions, are converted to the kinetic energy of the material atoms, making atoms detach from the surface. However, no matter which method is used, the purpose of PVD is to change the material from a solid state into a gaseous state.

doi:10.6844/NCKU201900538

2-1-1 Thermal evaporation

The principle of thermal evaporation uses joule heating to heat the target till it evaporates to vapor. Tungsten and molybdenum are the materials most commonly used to carrier the evaporated material because they have high electrical resistance, high melting point and are difficult to form alloys with other metals. For example, tungsten wire is commonly used as a carrier to melt and evaporate aluminum. Aluminum attached on the tungsten wire evaporates into aluminum vapor after it is heated. For other materials, instead of attaching them on tungsten wires, they are put in tungsten boats which are used as carriers. Shown in Fig. 2.1. (a) is the schematic of the evaporation equipment, (b) is a tungsten wire and a tungsten boat. Thermal evaporation is not suitable as an ion source of ion thrusters for the following three reasons: (1) efficiency of joule heating is very low; (2) although the target can be turned into vapor, it is difficult to ionize it; (3) it is hard to evaporate materials with high melting point.

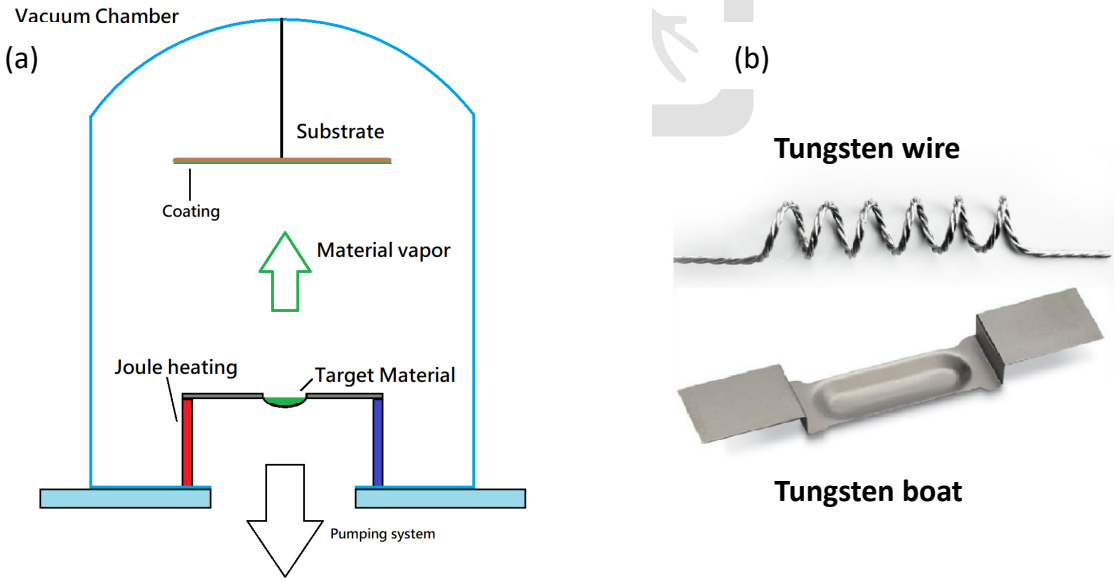

Figure 2.1: Principle of thermal evaporation in (a) and tungsten wire/boat in (b) [6,7].

doi:10.6844/NCKU201900538

2-1-2 Magnetron sputtering

Sputtering is a physical phenomenon that refers to the physical process in which atoms in a target are struck by high-energy ions (usually from plasma) and leave the target surface. In PVD technology, sputtering is generally carried out in a vacuum system filled with inert gas. By the action of a high-voltage electric field, causing argon gas to be ionized, generating an argon ion stream. Target is bombarded with argon ions into gas. As a result, material vapor forms a film on the substrate.

Sputtering is very inefficient because the plasma is occupied in a larger volume around the cathode in the chamber rather than concentrating on the target. In order to increase the efficiency of sputtering, we must guide the ion bombardments in specific areas. Fortunately, the ions are charged and therefore can be controlled by magnetic fields. Therefore, we can easily use a variety of permanent magnets to achieve the effect of condensed plasma called “magnetron sputtering.” Differences between the regular sputtering and magnetron sputtering are shown in Fig. 2.2, and Fig 2.3. You can see that plasmas distribute significantly differently. The advantage of sputtering is that it can produce a film of high melting point material on a substrate at a lower temperature. But sputtering is still not suitable as an ion source for new thrusters because it needs to carry extra working gas to produce plasma. If the new thruster still needs to carry a gas cylinder, it loses its original purpose.

doi:10.6844/NCKU201900538

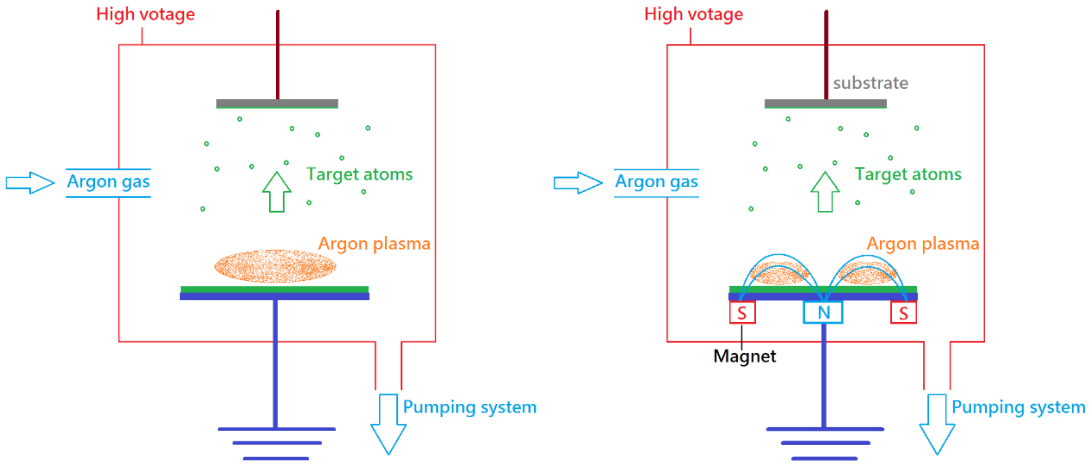

Figure 2.2: Principle of sputtering in (a) and magnetron sputtering in (b). You can see the plasma bombardment region is different.

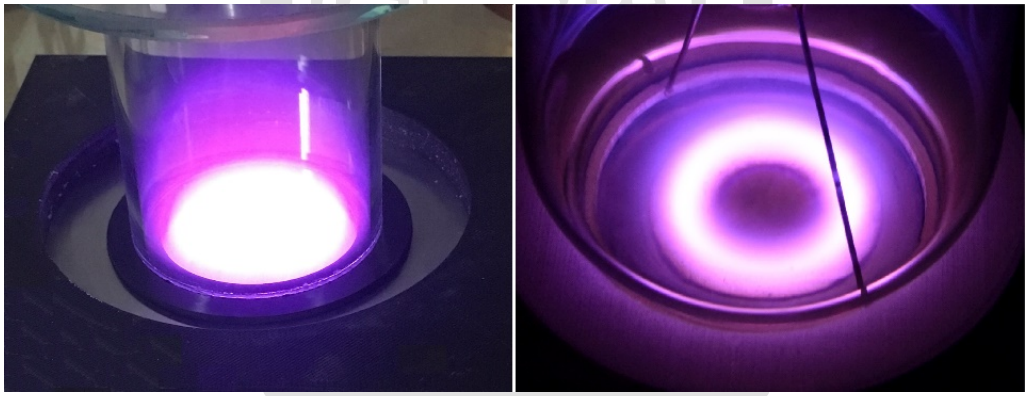

Figure 2.3: Comparison between sputtering (left) and magnetron sputtering (right). You can clearly observe the confining effect of the magnetic field on the plasma.

2-1-3 Electron beam evaporation

Electron-beam (E-beam) evaporation uses accelerated electrons bombarding the coating material. The kinetic energy of the electrons is converted into heat and evaporate the coating material and eventually form a film on the substrate. Since electron beam heating provides extremely high energy density, materials can be heated to temperatures up to 3000~6000 °C. Therefore,

doi:10.6844/NCKU201900538

refractory metals or compounds can still be evaporated. An example of E-beam evaporation is shown in Fig. 2.4. At the bottom there is a hot filament as an electron source using the thermal-emission effect. The E-beam is deflected by Lorentz force from a magnetic field. Therefore, we can control the bombardment location of E-beam. Free electrons accelerated by an external electric field get kinetic energy. When an electron hits the target, it converts its kinetic energy into heat and heats the target efficiently. After the material evaporates, it forms a vapor diffusing and depositing around and forming a thin film on the chamber wall.

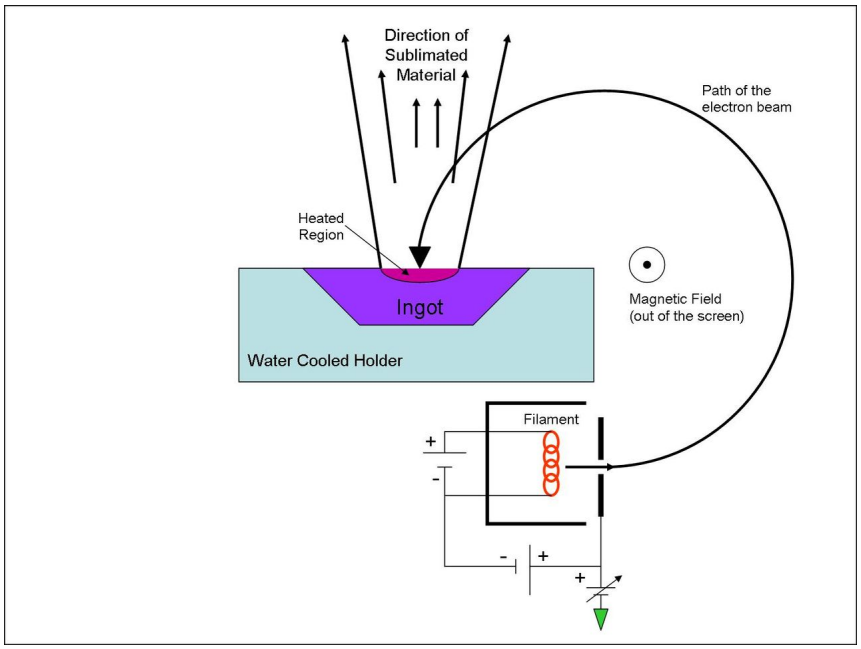

Figure 2.4: Electron beam evaporation deposition. Courtesy of Ref [8].

The biggest advantage of E-beam evaporation over evaporation by electric resistance is that it can provide higher heat for the substance to be evaporated. Therefore, the evaporation rate is higher; the E-beam is positioned accurately to avoid evaporation and contamination of the crucible material. On the other hand, secondary electrons on the target surface generated by high-energy electrons

doi:10.6844/NCKU201900538

bombardments may ionize residual gas molecules, which may also cause pollution in the film. In addition, since the heated area of the evaporator is small. The thermal efficiency is higher, but the structure is complicated. The large number of compounds are likely to be decomposed due to electron bombardment. Thus, E-beam heating are not suitable for vapor deposition of most compounds.

2-1-4 Choice of the appropriate evaporation method for ion thrusters

Joule heating, magnetron sputtering, and E-beam heating are three PVD methods all can achieve the purpose of evaporating propellant. However, not every PVD method is suitable for us to develop a new type of ion thrusters. Disadvantages of joule heating evaporation is that the thermal efficiency is too low and it does not ionize the vapor. The efficiency of magnetron sputtering is high and can ionize materials. However, it needs to carry extra working gas because it can only work under certain pressures. It is contrary to the purpose we want to use solid targets.

Electron beam evaporation is our final choice. First, since that working particles are electrons and come from thermal-emission electrons. They circulate in the loop and can operate in ultra-high vacuum. This means that I don't need to worry about the source of working particles in outer space. Second, electron beam bombardments will ionize the material through the electron impact ionization. Third, electron beam induced secondary electrons and backscattered electrons can further increase the ionization rate. These three advantages make us choose an E-beam evaporation to vaporize the propellant.

doi:10.6844/NCKU201900538

2-2 Background knowledge of the electron-beam technology

In this section, I will introduce related technologies related to the E-beam technology. It contains knowledge on how to generate free electrons, how electrons move in an electromagnetic field, secondary electrons, and backscattered electrons generated from electron bombarding on a target, and electron impact ionization.

2-2-1 Electron generation

An electron beam is a bundle of free electrons moving in the space. Free electrons are not bounded by atoms and can be well affected by electric and magnetic fields. Therefore, we can focus electrons into electron beams using electric or magnetic fields. Thus, how to generate free electrons that are available is an important topic in the E-beam technology. There are four common methods: (1) thermal electron emission; (2). field emission; (3) photoelectric effect; (4) beta decay. I will introduce how and advantages of generating free electrons using four different ways in the following sections.

2-2-1-1 Thermal electron emission

When the temperature of the metal rises, the kinetic energy of electrons in the metal increases and the number of electrons whose kinetic energy exceeds the work function gradually increases. It the temperature is above a certain value, a large number of electrons escape from the metal. This phenomenon is called thermal electron emission. Thermal electron emission has a wide range of applications in radio technology, and various electron tubes and electron beam tubes. In 1901, Richardson gave the mathematical form of thermal emission:

doi:10.6844/NCKU201900538

$$J = \lambda_R \, A_G \, T^2 \, e^{\frac{-w}{k_B T}} \quad [9] \ , \tag{7}$$

where J is the emission current density, T is the temperature of the metal, w is the work function of the metal, k_B is the Boltzmann constant and A_G is a universal constant and $A_G = 4\pi m k_B^2 e/h^3 = 1.2\times10^6\ Am^{-2}K^{-2}$. λ_R is a correction factor for different material and is typically in the order of 0.5. Tungsten filaments will be used due to its high melting point. Shown in Fig. 2.5 is the saturation current of the thermionic emission from a tungsten wire as a function of temperature. It will be used to estimate the required tungsten temperature.

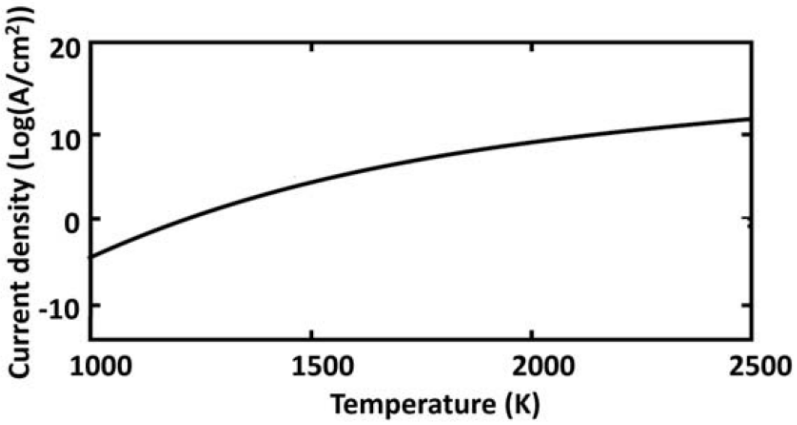

Figure 2.5: Saturation current densities of the thermionic emission from tungsten as a function of temperature. [10]

Generally, when the temperature of the metal is above 1000 K, the number of electrons whose kinetic energy exceeds the work function of the metal increases sharply so that a large number of electrons can escape from the metal. If there is no external electric field, the escaping hot electrons are accumulated near the metal surface and become a space charge which will prevent more hot electrons being emitted as shown in Fig. 2.6. Therefore, we have to apply an external electric field to pull out the electrons.

doi:10.6844/NCKU201900538

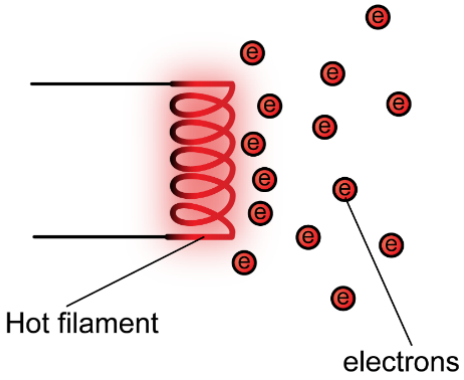

Figure 2.6: Hot filament emits free electrons. Courtesy of Ref [11].

2-2-1-2 Field emission

Field emission which is also called cold cathode emission refers to the phenomenon that electrons are released from the surface of the cathode by a strong electric field. The escape of free electrons from the metal from the metal requires a certain amount of work, called the work function of the metal, so that free electrons in the metal conductor are confined in a certain electron potential well. When metal acts as a cathode and a certain voltage is applied between the anode and the cathode, a certain potential barrier is formed on the surface of the cathode. If the applied voltage is increased, the width of potential barrier is reduced and the free electrons can penetrate through the barrier and be released from the metal through the quantum-tunneling effect. Shown in Fig. 2.7 is an example, a needle is usually used as an electrode to strengthen the electric field in a field-emission electron source.

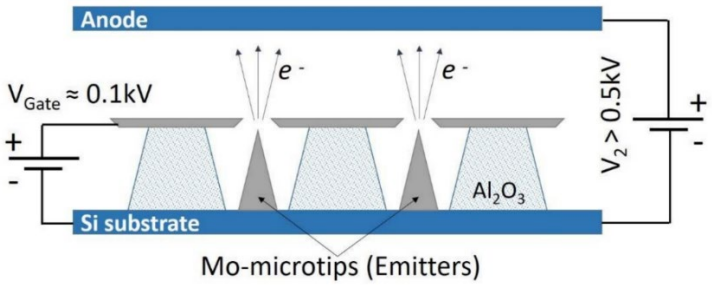

Figure 2.7: Field-emission micro needle electrode. Courtesy of Ref [12].

doi:10.6844/NCKU201900538

2-2-1-3 Photoelectric effect

Photoelectric Effect is the physical effect that a surface of an object emits electrons when light illuminates on the surface of the object. The emitted electrons are called "photoelectrons." In 1887, German physicist Heinrich Hertz discovered that ultraviolet radiation on metal electrodes can help generate electric sparks. Electron source using photoelectric effect is shown in Fig.2.8. Electron flows formed by free photoelectrons can be observed when the cathode is impacted by photons. This technique is often used in photomultiplier tubes. However, it is not suitable as an electron source for our ion thruster because it is inefficient to first convert energy into photons and then use them to generate electrons.

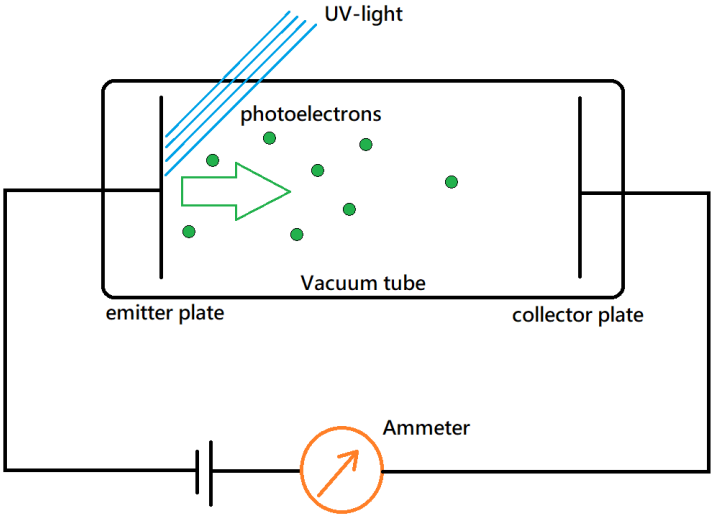

Figure 2.8: Electron source of photoelectric effect.

2-2-1-4 Beta decay

Beta decay is the process of radiates electrons (β particles) and antineutrino converting into another nucleus. Shown in Fig.2.9 is an example of beta decay process. A neutron in the atom releasing an electron and an antineutrino becomes a proton and the atom decays into another element. Beta decay is a spontaneous

doi:10.6844/NCKU201900538

nuclear reaction that generates free electrons without supplying additional energy. However, since using nuclear radioactive materials is very dangerous, we are not considering decay electron sources for the time being. Nevertheless, we are still thinking about the possibility of applying nuclear decay to the ion thruster. If you don't consider its danger, nuclear decay is a great source of electrons.

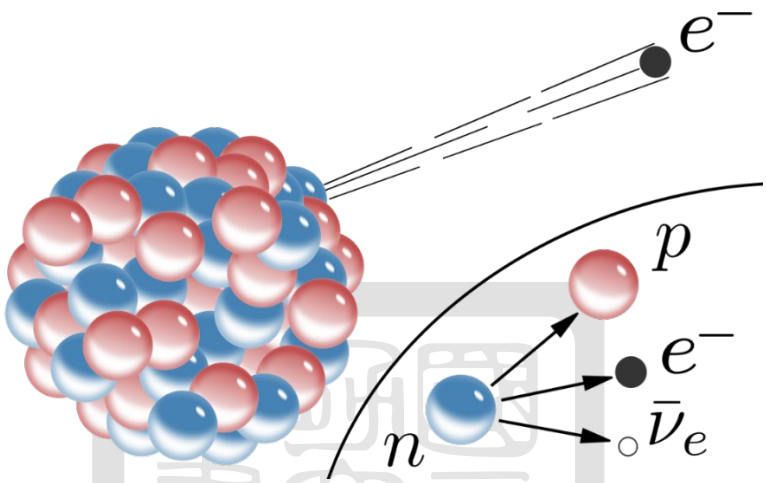

Figure 2.9: The atom decays into other elements through beta decay. Courtesy of Ref [13].

2-2-2 Electron manipulations

In order to use free electrons, we must be able to control the energy and directions of electrons. Charged particles interact with electromagnetic fields, i.e., electrons can be controlled by electromagnetic forces. We can use the Lorentz force to describe the interactions between charged particles and electric and magnetic fields to predict the trajectories of electrons and achieve the purpose of controlling electrons. In this section, I will introduce Lorentz force, electron volts, gyroradius, electron motion in electric and magnetic fields, secondary and backscattered electrons, and electron impact ionization.

doi:10.6844/NCKU201900538

2-2-2-1 Lorentz force

The Lorentz force is the force felt by an charged particle in an electromagnetic field expressed as

$$\vec{F}= q(\vec{E}+\vec{v}\times\vec{B}) \quad (8)$$

where $\vec{F}$ is the Lorentz force, q is the charge of the charged particle, $\vec{E}$ is the electric field, $\vec{v}$ is the velocity of the charged particle, and $\vec{B}$ is the magnetic field. The positive charged particle will be accelerated by the electric field. When a magnetic field presents, the positive charge will be turned by the magnetic field in the direction of $\vec{v}\times\vec{B}$. The effect of the magnetic field on a charged particle is shown in Fig. 2.10.

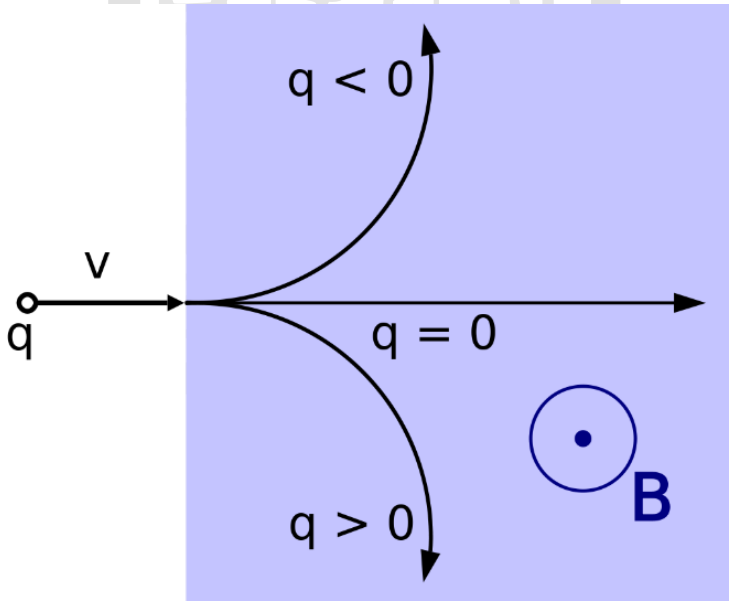

Figure 2.10: The charge is deflected by the influence of the magnetic field. Courtesy of Ref [14].

Therefore, we can use the Lorentz force to achieve the purpose of controlling electrons. Electric field is responsible for accelerating electrons to high kinetic energy and magnetic field is responsible for guiding electrons. An

doi:10.6844/NCKU201900538

example is given in Fig. 2.11. Electrons are emitted from the hot cathode and accelerated into the vacuum chamber by the electrode while the magnetic field is responsible for deflecting the electrons. You can see the purple light produced by the E-beam, because the air was ionized by electrons impact.

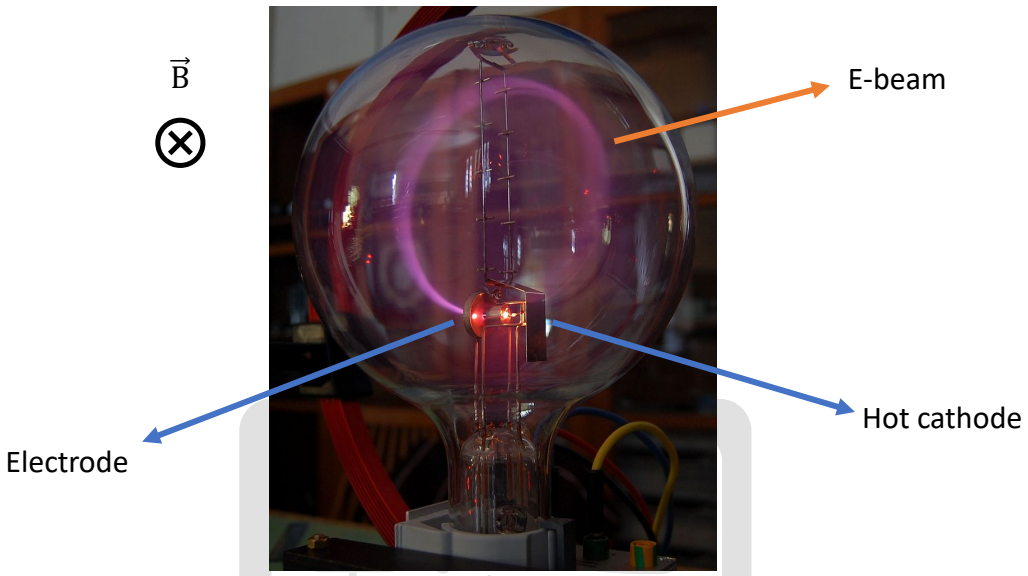

Figure 2.11: The cathode ray is deflected by the magnetic field. Courtesy of Ref [15].

2-2-2-2 Electron volt

Electron volt (eV) is a unit of energy for measuring kinetic energy of charged particles. One eV is defined as the energy obtained by a singly charged particle such as an electron accelerated by an electric potential of 1 volt. As shown in Fig. 2.12, electrons are accelerated by electric fields. The conversion relationship between eV and Joule is

$$1\ \text{eV} = 1.6\times10^{-19}\ \text{J}\ . \qquad (9)$$

We only need to know the electric potential at the initial and the final positions of an electron to obtain the energy of the electron at the final point. This is why eV is a useful unit.

doi:10.6844/NCKU201900538

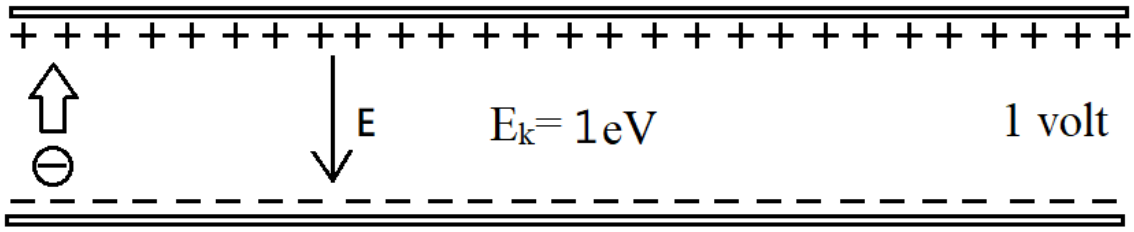

Figure 2.12: The electrons are accelerated by electric fields.

2-2-2-3 Gyroradius

From the Lorentz force equation, we can see that charged particles are subjected to do circular motion in a magnetic field which provides the centripetal force. The gyroradius is defined as the radius of the circular motion of a charged particle in the presence of a uniform magnetic field. It is given by:

$$r_g = \frac{mv}{|q|B} = \frac{1}{|q|B}\sqrt{\frac{2E_k}{m}} \quad (10)$$

where m is the mass of the particle, v is the component of the velocity perpendicular to the direction of the magnetic field, q is the electric charge of the particle, B is the strength of the magnetic field and E_k is the kinetic energy of the charge particle. It can be seen from the above equation that the larger the magnetic field, the smaller the gyroradius, and the larger the energy, the larger the gyroradius.

An example is shown in Fig. 2.13, when the electron moves from the weak magnetic field to the strong magnetic field, its gyroradius will gradually become shorter. Therefore, we can use the magnetic field to achieve the purpose of focusing electrons. When electrons enter a strong magnetic field, they will be focused into a thin beam.

doi:10.6844/NCKU201900538

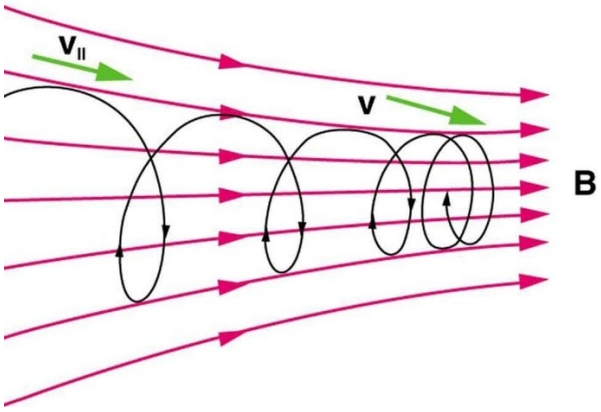

Figure 2.13: Focusing electrons using a magnetic field. Courtesy of Ref [16].

2-2-2-4 Electron impact ionization

Electron Impact is an ionization method that achieves ionization through using high-energy electrons to impact atoms or molecules [17]. A common method is to use a hot filament as an electron source and an external electric field to accelerate electrons. A gas is provided so that electrons collide with the gas to remove the electron of the gas molecular. The ionization reaction formula can be written as:

$$M + e^{-} = M^{+} + 2e^{-} \quad (11)$$

where M is atom, e^{-} is electron. The kinetic energy of the electron must be greater than the first ionization energy of target elements. The relationship between first ionization energy and atomic number is shown in Fig. 2.14. Zinc which has a first ionization energy of 9.4 eV will be used in this thesis.

doi:10.6844/NCKU201900538

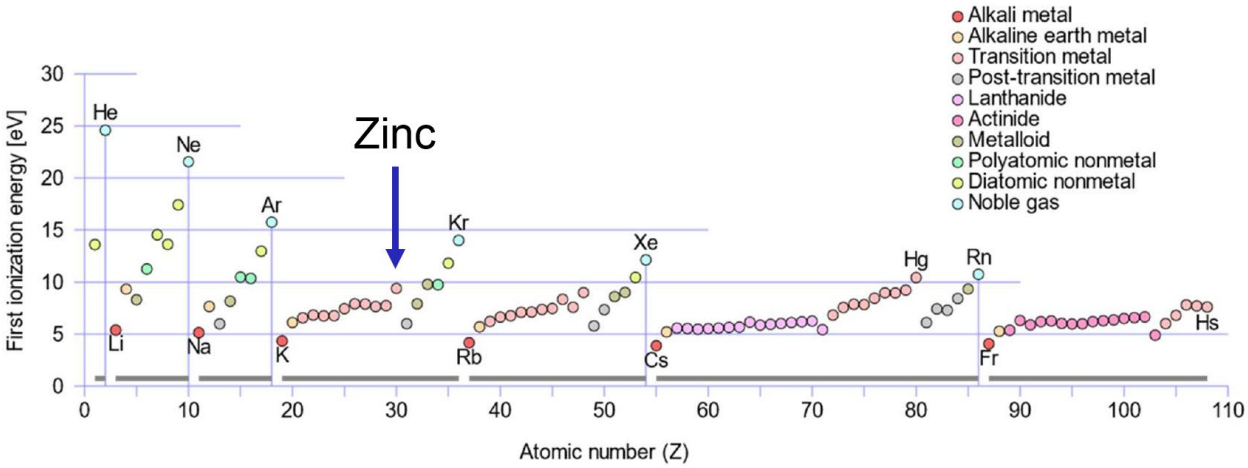

Figure 2.14: Relationship between first ionization energy and atomic number. Courtesy of Ref [18].

2-2-2-5 Secondary and backscattered electrons

Secondary electrons are low-energy electrons that are initially in an object and emitted when the surface of the object is irradiated with radiation. The radiation can be ions, electrons or photons with sufficient energy.

Backscattered electrons are a portion of incident electrons that are bounced back by nuclei in a target. There is a considerable amount of backscatter electrons with energy closed to that of the incident electrons. The backscattering phenomena is mainly divided into elastic backscattering and inelastic backscattering. Elastic backscattered electrons are incident electrons that are bounced back by the nuclei in the sample with a scattering angle greater than 90° without losing much of their initial, i.e., with no energy losses. Since the energy of incident electrons is very high, the energy of elastic backscattered electrons can reach thousands to tens of thousands of electron volts. The inelastic backscattered electrons are generated by the incident electrons and by the electrons inside the sample. They not only change directions but also have

doi:10.6844/NCKU201900538

different degrees of energy losses. Some electrons may be bounced off from the surface of the sample after multiple scattering. Their energy distribution ranges from tens of electron volts to thousands of electron volts.

Secondary electrons and backscattered electrons are commonly used in electron beam technologies. In electron microscopy, it is often used for imaging fine structure. In this study, secondary electrons and backscattered electrons are mainly used to increase electron density for increasing opportunity of ionizing metal atoms [19].

2-3 Metallic ions generated by E-beam bombardments

The core concept of MIT-MEB is using E-beam to generate metallic ions to achieve the new type of ion thrusters which do not require working gas and uses solid metal as propellants. Electron are used as working particles, which are generated by a hot filament and accelerated by an electric field toward a metallic target. When electrons move toward the target, they are focused to the center of the target surface by the strong magnetic field provided by a magnet located in the back side of the target. When the target is bombarded by energetic electrons, it is heated and evaporated into gas. The metallic vapor is then bombarded and ionized by energetic electrons, secondary electrons and backscattered electrons. The process is shown in Fig 2.15 and will be described in Chapter 3.

doi:10.6844/NCKU201900538

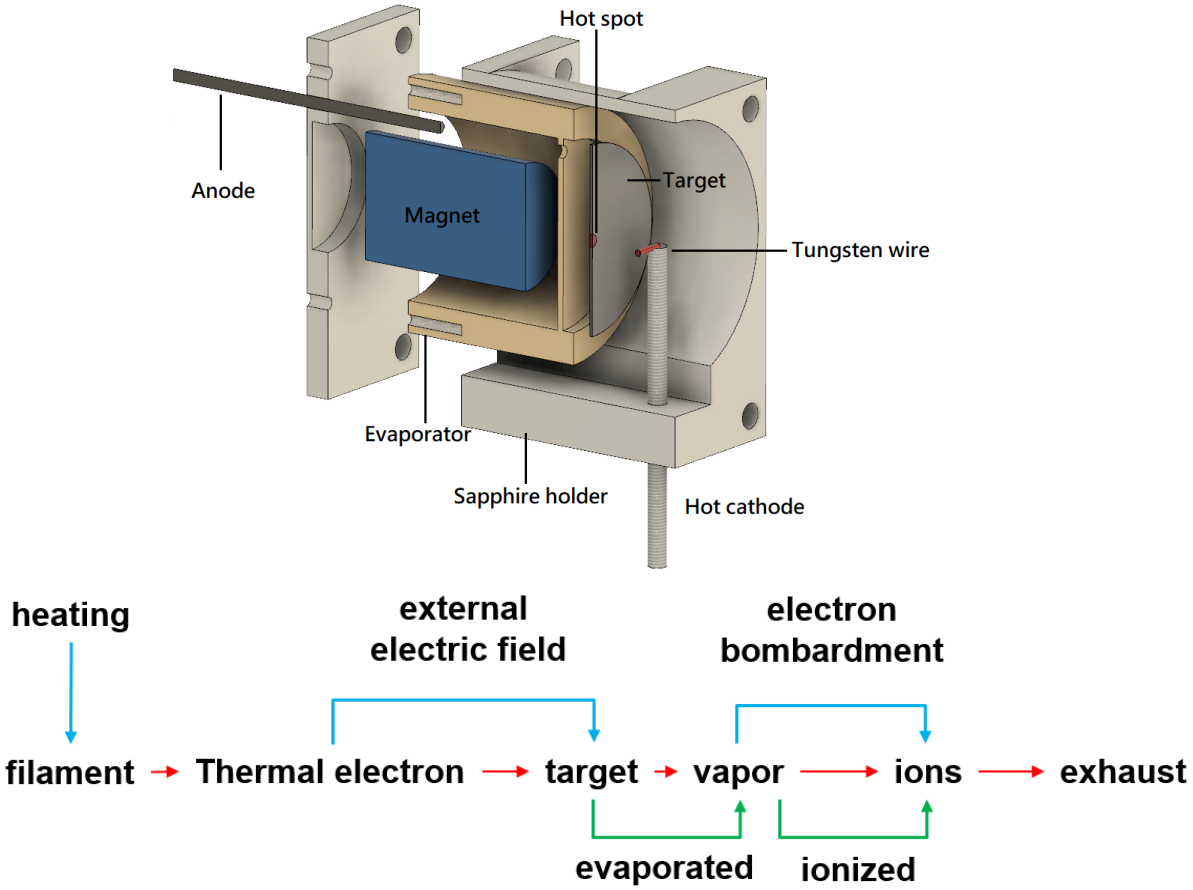

Figure 2.15: New type of metallic ion sources for ion thrusters.

doi:10.6844/NCKU201900538

Chapter 3

Metallic Ion Thruster using E-beam Bombardment

Metallic Ion Thruster using E-beam Bombardment (MIT-MEB) is a solid propellant ion thruster that uses E-beam to generate and accelerate metallic ions. An ion thruster using a metal target as the propellant was built. The prototype and the performance will be given in Chapter 4. The design of MIT-MEB is shown in Fig. 3.1. The design is divided into three parts: a metallic ion source, an ion accelerator, and a neutralizer. In this chapter, I will introduce the magnetron E-beam and the structural design and operation principle of MIT-MEB.

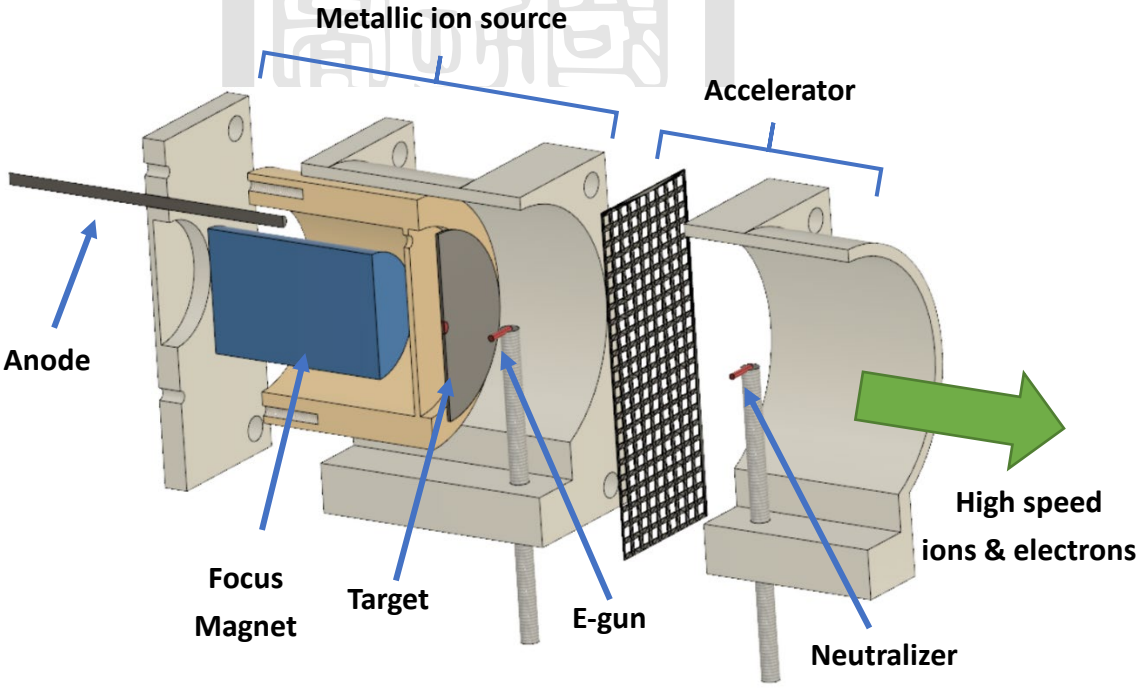

Figure 3.1: Structural design blueprint of MIT-MEB.

3-1 Magnetron E-beam

The main innovation of MIT-MEB is using the solid ion source. According to Chapter 2, the magnetron E-beam is used in evaporation and ionization for

doi:10.6844/NCKU201900538

generating metallic ions. I will use a cylindrical magnet to provide a magnetic field that confines electrons. The field will magnetize the electron beam and guide electrons toward a spot at the target surface. Since we must know the distribution of electromagnetic fields to predict the traveling trajectories of electrons, I will explain how to focus the electron beam. I will show the magnetic field simulation results and electric field simulation results. Finally, I will calculate the distribution of gyro radius through the profile of the electric field and the magnetic field.

3-1-1 Principle of guiding electron-beams

In section 2-2-2, I introduced the principle of controlling electrons through a magnetic field. Gyromotion occurs when electrons enter a region with a magnetic field. The gyroradius is proportional to the speed of the electron and inversely proportional to the strength of the magnetic field. If gyroradius is much smaller than the system size, we call the electrons being magnetized by the magnetic field. When the electron is magnetized, it moves along the magnetic field line. I use this principle to control the bombarding region of the E-beam.

3-1-2 Magnetic field measurements

In order to simulate the distribution of the magnetic field, I need to know the magnetic field of magnets. Therefore, I used a Gauss meter to measure the magnetic field of the magnet. Shown in Fig .3.2, the Gauss meter was used to measure the magnetic fields of the magnet in the X, and Z-directions. The sensor measures the magnetic field moves in the X-direction. We measured magnetic field strength at 0.92 mm, 1.42 mm, 1.92 mm, and 2.42 mm above the magnet's top surface of Z-direction. We measured magnetic field strength at 2.04 mm, 2.42

doi:10.6844/NCKU201900538

mm, 2.92mm, and 3.42mm above the magnet's top surface of X-direction. The size of each step of the stage is 0.5 mm. Since the magnet is cylindrically symmetrical, we mirror the measurement results to obtain the magnetic field distribution of the entire magnet. The magnet we used is a 1 cm thick neodymium magnet with a diameter of 2 cm. The magnetic field measurement results are shown in Fig. 3.3 and Fig. 3.4.

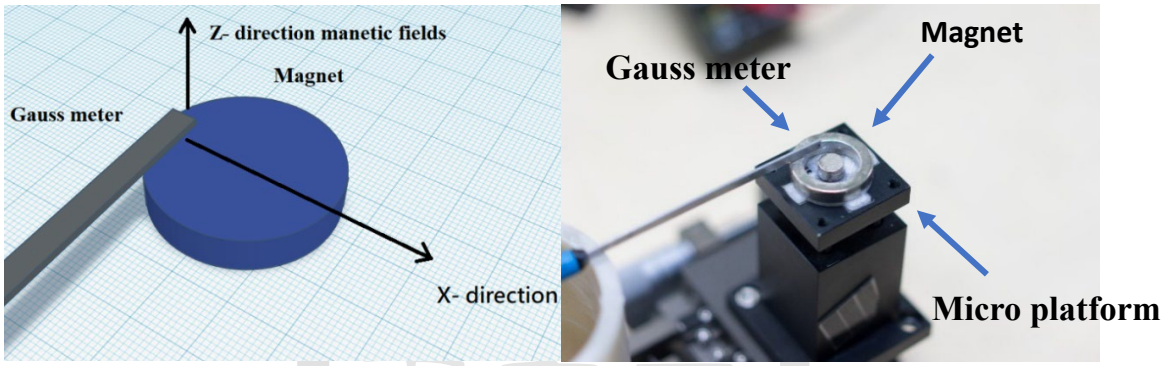

Figure 3.2: Gauss meter is used to measure the magnetic fields of the magnet in the Z direction.

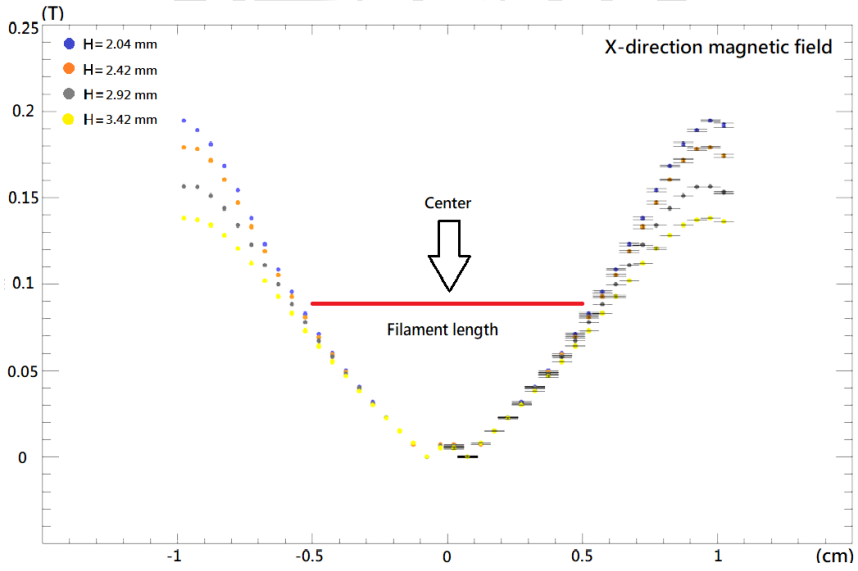

Figure 3.3: Magnetic fields distribution of X-direction of the focusing magnet.

doi:10.6844/NCKU201900538

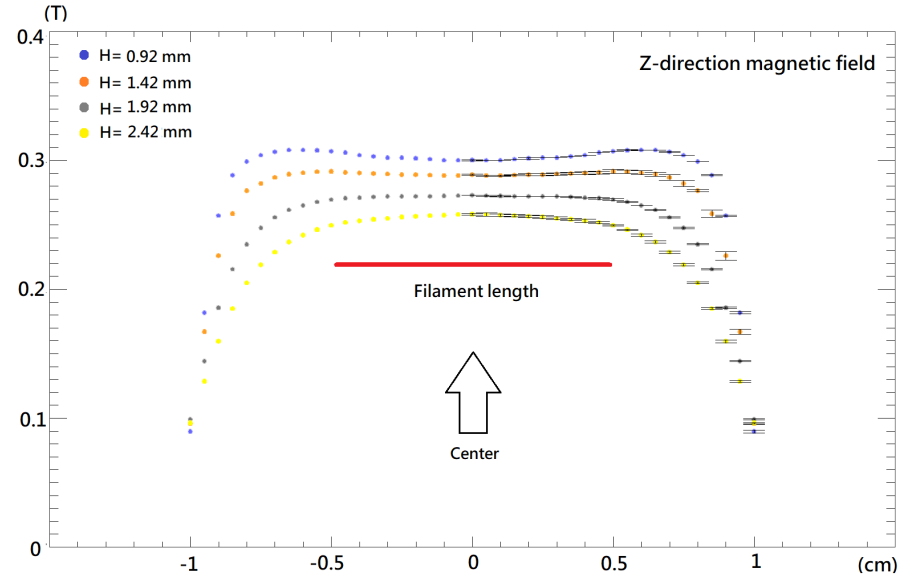

Figure 3.4: Magnetic fields distribution of Z-direction of the focusing magnet.

3-1-3 Simulation results of the magnetic field

I only measured the magnetic field at some important locations which are between the filament and the target. Since the magnetic field of a magnet is only determined by the shape of the magnet and its magnetization, I constructed a magnet in Comsol with the same dimensions to that of the actual one and adjust the magnetization of the magnet to 1050,000 [A/m] to fit the experimental data. Thus, I can construct the profile of the magnetic field in the space. Since we only care about the gyroradius of the electrons in the radial direction, we only simulate the magnetic field in the Z direction. The comparison between simulations and experiments of the z-direction magnetic field is shown in Fig. 3.5 where magnetization 1.05×10^{6} A/m is used in the simulation. Solid lines are from the simulations and points are from the measurements. You can see that both the simulated and measured magnetic fields at the center of the magnet are not the highest meaning simulations catch the same feature of the actual field.

doi:10.6844/NCKU201900538

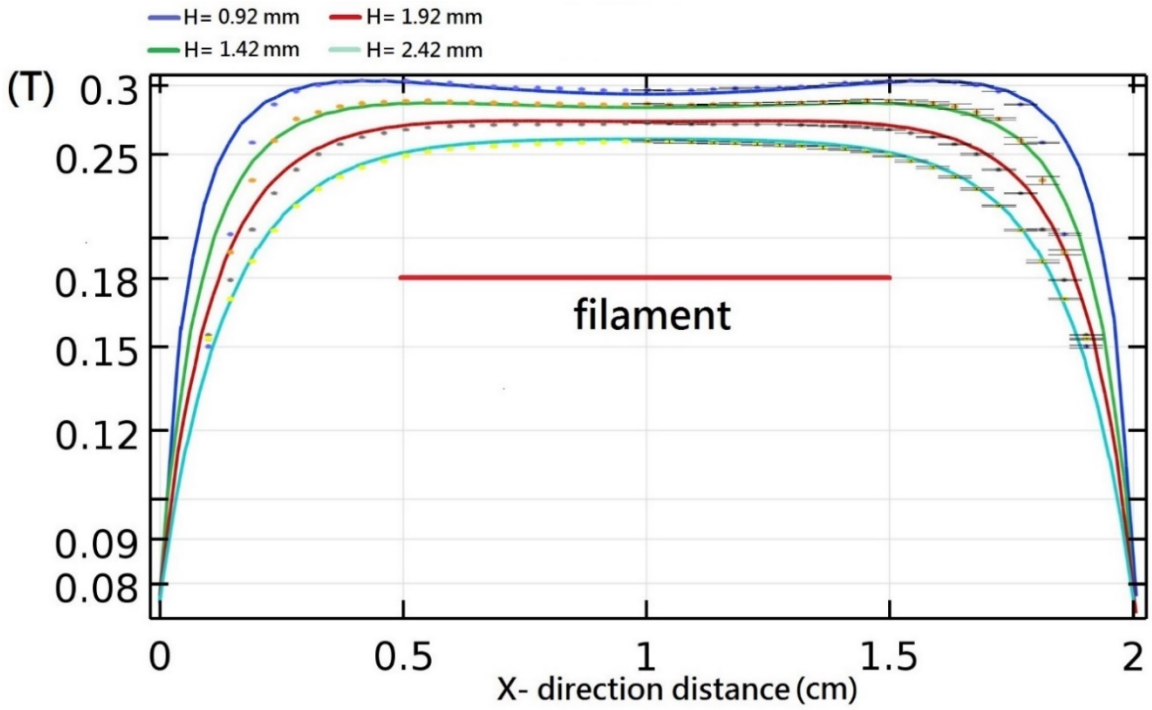

Figure 3.5: Curve fitting with magnet fields of focus magnet.

3-1-4 Simulation results of electric fields

The profile of the electric field is obtained by using Comsol to solve the Poisson equation. The metallic target is connected to positive high voltage in order to attract electrons for bombardments. Filament is at ground and the target is at the positive high voltage. The electric field distribution can be easily obtained by taking the negative gradient of the potential. The simulation result of the electric field is shown in Fig. 3.6. You can expect that electrons move away from the filament and follow the electric fields if there is no magnetic field.

doi:10.6844/NCKU201900538

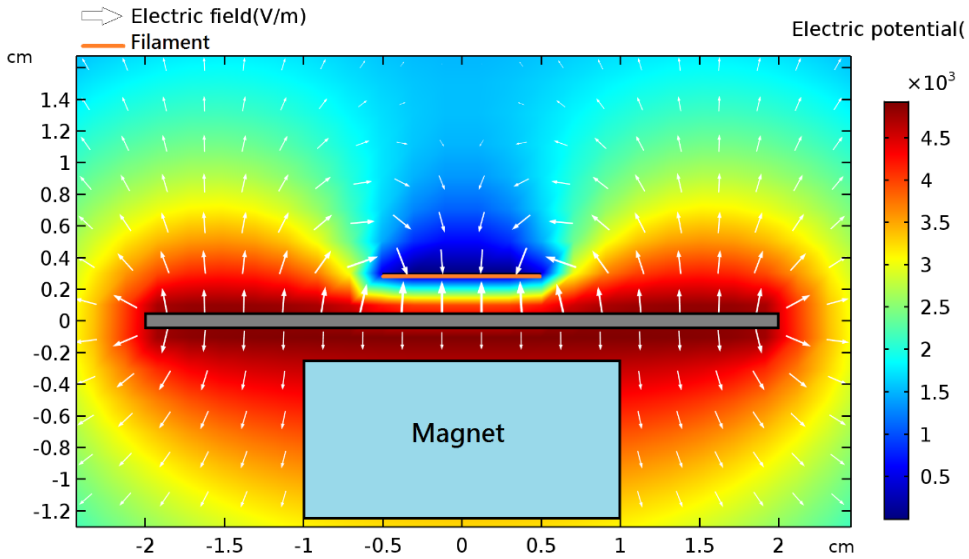

Figure 3.6: Simulation result of electric field.

3-1-5 Calculations of gyroradius

When we get the profiles of electric and magnetic fields, we can obtain the kinetic energy of electrons and the magnetic field strength at any locations. Fig. 3.7 shows the simulated electric and magnetic fields.

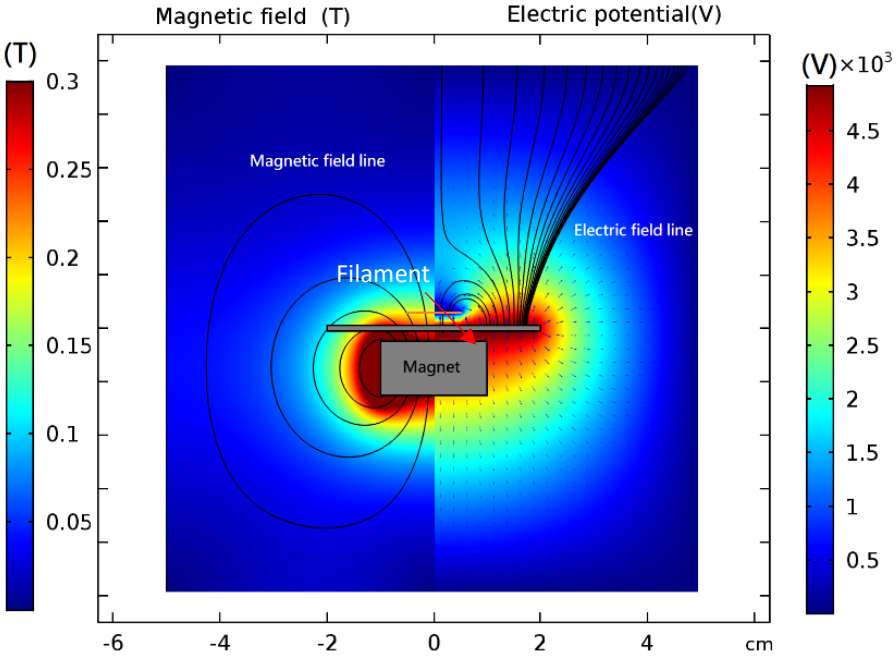

Figure 3.7: Electric field and magnetic field profile.

doi:10.6844/NCKU201900538

Through these two pieces of information, we can calculate the gyroradius when electrons move from the filament to different positions. The potential of the filament is 0 and we know the distribution of the potential. Therefore, the kinetic energy of the electron equals to the potential at the location of the electron, i.e. E_k=e*V. We can then substitute the kinetic energy of the electron into the Equation (10) to get the gyroradius. The formula of gyroradius written in Comsol is

$$r_g = ((me\_const)*((2*esbe.V*e\_const)/(me\_const))\text{^}0.5)/((e\_const)*(mf.normB)) \quad (12)$$

where me_const is the electron mass, esbe.V is the electric potential, e_const is the elementary charge, mf.normB is the magnetic field strength. Simulated gyroradius is shown in Fig. 3.8. You can see that gyroradius is only 0.02-0.1 cm between the filament and the target. The value is much smaller than the scale of the target, 5 cm in diameter. Therefore, electrons are magnetized and move along magnetic field lines.

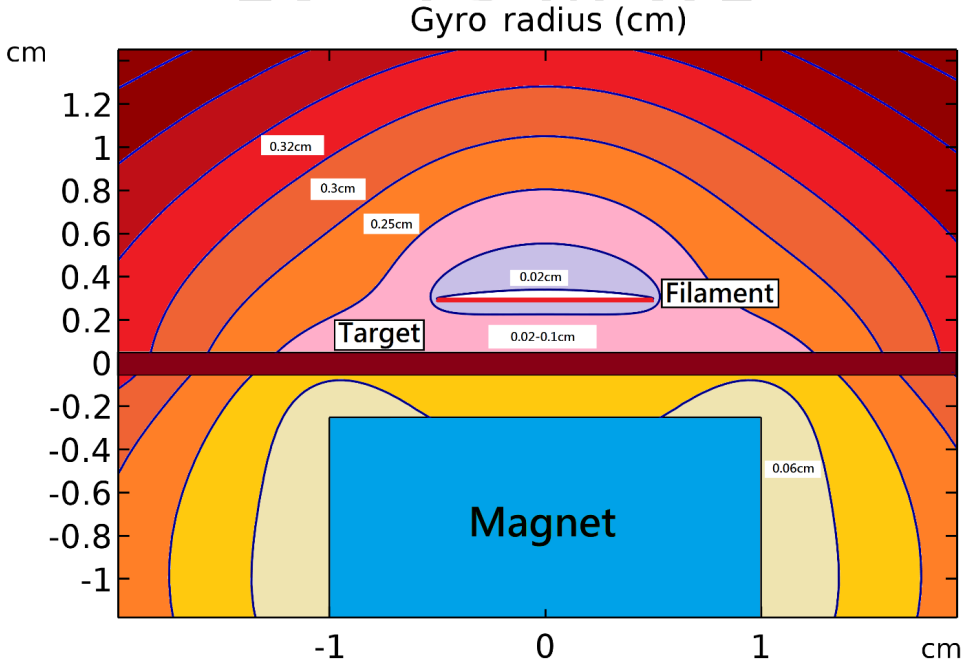

Figure 3.8: Simulation result of gyroradius profile.

doi:10.6844/NCKU201900538

3-2 The structure of MIT-MEB

In this section I will introduce functions and principles of components of MIT-MEB. The magnetron E-beam introduced in section 3-1 will be used in the ion generator. I will explain how I choose the material of the propellant and how to calculate evaporation rate, ionization rate, thrust and specific impulse I_{sp}.

3-2-1 The Ion generator

The ion generator provides ions needed for the ion thruster. A tungsten filament is placed on top of the metallic target. The tungsten filament will be joule heated to 1000°C ~ 1500°C so that it emits free electrons. We can use Richardson's law to describe the relationship between the emitted current density and the filament temperature. The emitted electrons will be accelerated by high voltage (HV1) shown in Fig. 3.9 and bombard the solid metal target. Therefore, electrons with high energy transfer their kinetic energy into thermal energy of metallic target. To increase the efficiency of heating the target, electrons will be guided by magnetic field provided by the focusing magnet behind the target. We can control electrons so that they heat a small region on the metallic target and create a high-density electrons cloud on the metal surface. Note that electrons not only come from the hot filament but also from the backscattered and secondary electrons from the metal surface when energetic electrons hit the target. When the metal is evaporated, its vapor will pass through the electron cloud and be ionized by electron impact. As a result, metallic ions are generated.

doi:10.6844/NCKU201900538

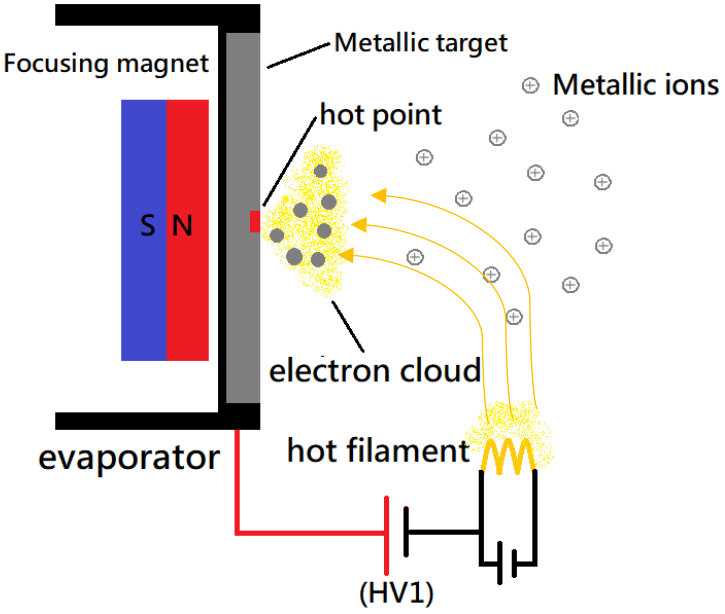

Figure 3.9: metallic ions are generated by E-beam bombardment.

Since electrons with the highest energy in the system are magnetized, other electrons whose energy is much lower than the energetic electrons are also confined by the magnetic field. Therefore, a local high-density electron cloud above the target is formed. In other words, the formation of the electron cloud is mainly due to the confinement of magnetic fields in radial direction and electric fields on axial direction. The composition of the electron cloud is probably from secondary and backscattered electrons as introduced in 2-2-2-4. The detail studies of the electron density will be one of our future research topics.

3-2-2 The accelerator

The momentum change of the propellant will let the device get a thrust. Since the higher the speed of the ions, the better we need an acceleration device to accelerate ions. The accelerator is shown in Fig. 3.10. When metallic ions leave the ions generator and pass through the grid, they will be accelerated by a second electric field. Ions will leave the thruster with high exhausted speed.

doi:10.6844/NCKU201900538

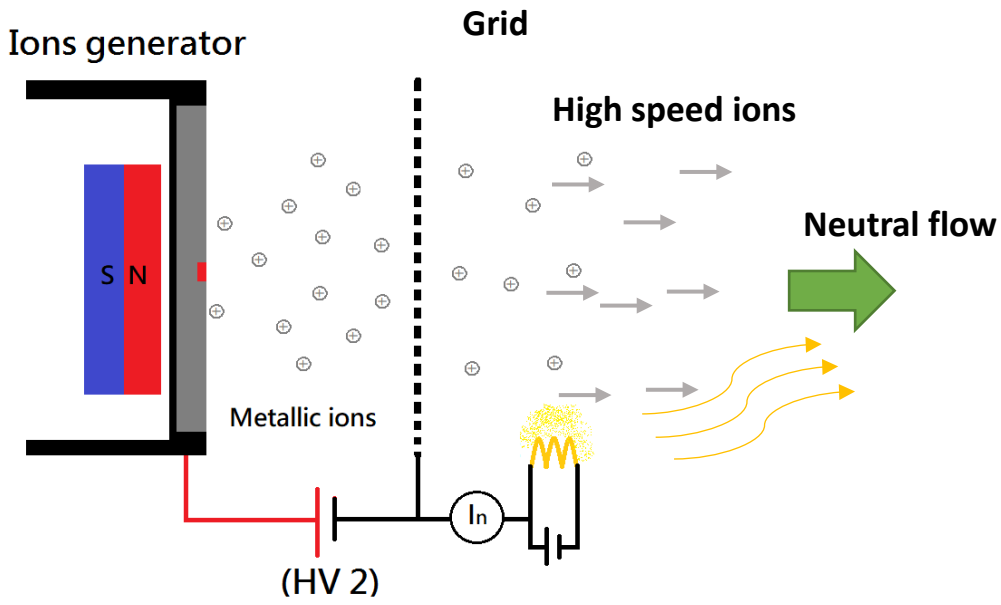

Figure 3.10: Ions are accelerated by the grid and neutralized with neutralizer.

Accelerator section located downstream of the ion source section where an electrostatic grid with negative potential further away from the ion source section is used to accelerate ions. Ions simply get the energy from the electrical potential difference between accelerator grid and the metallic target. From the definition of specific impulse from Eq. (2) and assuming that ions are singly charged, the specific impulse of the thrust can be calculated as

$$I_{sp} = \frac{1}{g}\sqrt{\frac{2E_k}{M}} = \frac{1}{9.8}\sqrt{\frac{2V_{(volt)}\times 1.6\times 10^{-19}}{M_{(amu)}\times 1.67\times 10^{-27}}} = 1413\sqrt{\frac{V_{(volt)}}{M_{(amu)}}}\ (sec). \qquad (13)$$

3-2-3 The neutralizer

In order to prevent charge accumulation, we place a second electron gun as a neutralizer at the end of the thruster. The electrons are emitted from the second electron gun. Therefore, MIT-MEB emits high-speed ions and electrons and remain neutral. Neutralizer located downstream of the accelerator emits electrons to neutralize accelerated ions. If ions are not neutralized before leaving the thruster, the thruster becomes negatively charged. The thruster not only

doi:10.6844/NCKU201900538

collects ions in space but also attracts the accelerated ions back to the thruster canceling the thrust. The neutralizer is made of filaments that are similar to the one emitting electrons in the ion source section. The thermal-emitted electrons are attracted by ions and neutralize ions via colliding with accelerated ions. Since the neutralizing electron current I_n should equal to the ion current, we can obtain the ion flux by measuring the electron current I_n.

$$I_n = I_{ion} \tag{14}$$

3-2-4 Choice of the material for the propellant

We can see that the easier the material is evaporated, the better it is for our ion thruster. How easily the material is evaporated depends on its vapor pressure. If the vapor pressure of the material A is higher than that of the material B at the same temperature, material A is easier to become a vapor than the material B. In other words, the temperature required for the material A will be lower than that of the material B to reach the same vapor pressure. The formula for thermal evaporation is given by [20]:

$$\dot{m}_{Metal}\left(\frac{g}{s}\right) = A \times \alpha_e \, 5.84 \times 10^{-2} \sqrt{\frac{M}{T}} \, (P_v - P_h) \tag{15}$$

where $\dot{m}_{Metal}$ is the vaporizing mass flow rate, A is the heated area, α_e is a constant depending on the material, M is the atomic mass of the material, T is the heated temperature, P_v is the vapor pressure of the material at temperature T and P_h is the background pressure. Assuming that the heating conditions are the same, the larger the P_v, the larger the mass flow rate of the vapor can be obtained. An alternative way to see this is the lower the temperature to reach the same P_v, the easier to vaporize the material leading to a higher mass flow rate. We use the look-up table to select metals with high vapor pressure as targets. Vapor pressure P_v of common metals is listed in Table 3.1. It shows that zinc and lead the metal

doi:10.6844/NCKU201900538

are with the highest vapor pressure at the same temperature and are obtained easily. According to the formula (1) for calculating thrusts, lead can provide us with high thrust because of its high atomic mass. However, it is highly toxic. Therefore, in practical considerations, we chose zinc as the material for experiments. Note that materials with lower melting points does not mean they are evaporated easier. For example, the melting point of tin is only 231.9 °C while zinc needs 419.5 °C to be melted. However, when the tin reaches the vapor pressure of 10^{-3} Torr, its temperature must reach 1315 °C while zinc only needs 565 °C. In other words, zinc is easier to be vaporized. This is another reason that we pick zinc as the propellant.

PE (torr) / T (K) / Material	10^{-3}	10^{-2}	10^{-1}	10^{0}	10^{1}	10^{2}
Al ($M = 27.0$ amu)	1162	1269	1396	1552	1760	2022
Fe ($M = 55.8$ amu)	1583	1720	1875	2056	2312	2633
Cu ($M = 63.5$ amu)	1414	1546	1705	1901	2152	2480
Zn ($M = 65.4$ amu)	565	616	678	760	866	1009
Ag ($M = 107.9$ amu)	1209	1320	1457	1626	1848	2138
Sn ($M = 118.7$ amu)	1315	1462	1646	1882	1976	2241
Au ($M = 197.0$ amu)	1589	1738	1919	2140	2427	2794
Pb ($M = 207.2$ amu)	898	991	1105	1248	1440	1690

Table 3.1: Temperature T in kelvin for different PE in Torr for different metallic materials [21].

3-2-5 Evaporation rate and Ionization rate

The evaporation rate was given in equation (15). However, the practical evaporation rate $\dot{m}_{\text{Metal}}$ measured in experiments is expressed as:

$$\dot{m}_{Metal}\left(\frac{g}{s}\right) = \frac{m_i - m_f}{\Delta t} = \frac{\Delta m}{\Delta t} \tag{16}$$

where m_i is the mass of the target before the experiment, m_f is the mass of the target after the experiment, Δt is the time the experiment lasts. Equation (16)

doi:10.6844/NCKU201900538

gives the mass of the target that leaves the evaporator per second. Therefore, by dividing $\dot{m}_{Metal}$ by atomic mass, we can know how many atoms per second are evaporated:

$$\Gamma_{Atom}\left(\frac{\#}{s}\right) = \frac{\dot{m}_{Metal}}{M_{atom}} \tag{17}$$

where Γ_{Atom} is the atom number flow rate and M_{atom} is the atomic mass of the target.

We have mentioned in 3-2-3 that the neutralizing electron current I_n equals to the ion current. Assume that ions leave are all singly charged, i.e., Z = +1, the electron flux equals to the ion flux. Therefore, we can calculate the ionization rate:

$$\beta = \frac{I_n}{q} \times \left(\frac{\dot{m}_{Metal}}{M_{atom}}\right)^{-1} \tag{18}$$

where I_n is the neutralizing electron current in ampere, and $q=1.6\times10^{-19}$ coulomb is the elementary charge. The ionization rate is the ratio between the number of ions to that of the neutral gas so the value of β is between 0 and 1.

3-2-6 The ion mass flow rate

Since ions that are accelerated in the ion thrusters are the main source of thrusts, only ions are considered when calculating the thrust. The thrust F is written as:

$$F = \dot{m}_{ion} \times V_{ion} \tag{19}$$

where $\dot{m}_{ion}$ is Ion mass flow rate and

$$\dot{m}_{ion}\left(\frac{g}{s}\right) = \beta \times \dot{m}_{Metal} \tag{20}$$

3-2-7 Estimation of thrusts

Based on Eq. (1) and Chapter 3-2, we can write down the estimated thrust:

doi:10.6844/NCKU201900538

$$T(N) = v_{ion}\dot{m}_{ion} = \sqrt{\frac{2E_k}{M}}\dot{m}_{ion} \quad (21)$$

where v_{ion} is exhausted ions velocity, $\dot{m}_{ion}$ is ion mass flow rate, β is the ionization coefficient depending on the atom and is between 0 and 1. Note that coefficients α_e and β depend on materials, temperatures, and electron energies and need to be measured via experiments.

3-3 Prototype of MIT-MEB

I built two type of prototypes of MIT-MEB. Due to the need for high temperature and insulation, I use either quartz or sapphire ceramics as materials for the body of the thrusters. It is because the melting points of quartz and ceramics are 1650 ° C and 2054 ° C, respectively. The density of quartz is 2.65 g/cm^3 and the density of ceramics is 3.97 g/cm^3. Quartz is crystal brittle but transparent So that it is easier for observation. Sapphire ceramic is strong and durable. Both have irreplaceable advantages so I used both to build four prototypes according to different needs. Fig. 3.11 shows prototypes of MIT-MEB: (a) is the structure of MIT-MEB (b) is made of sapphire ceramic (c) is made of quartz.

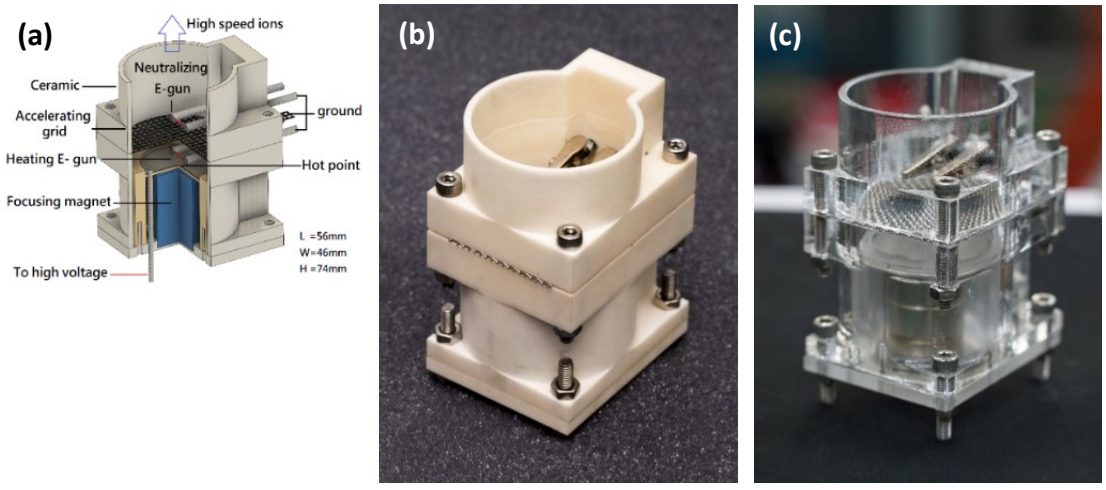

Figure 3.11: (a) prototype of MIT-MEB (b) is sapphire ceramic (c) is Quartz.

doi:10.6844/NCKU201900538

Dimensions of MIT-MEB as shown in Fig. 3.12. In order to prevent the electrons from escaping from the thruster, we sealed the conductive tape at the seam. And, we use a BNC connector to shield the positive electrode.

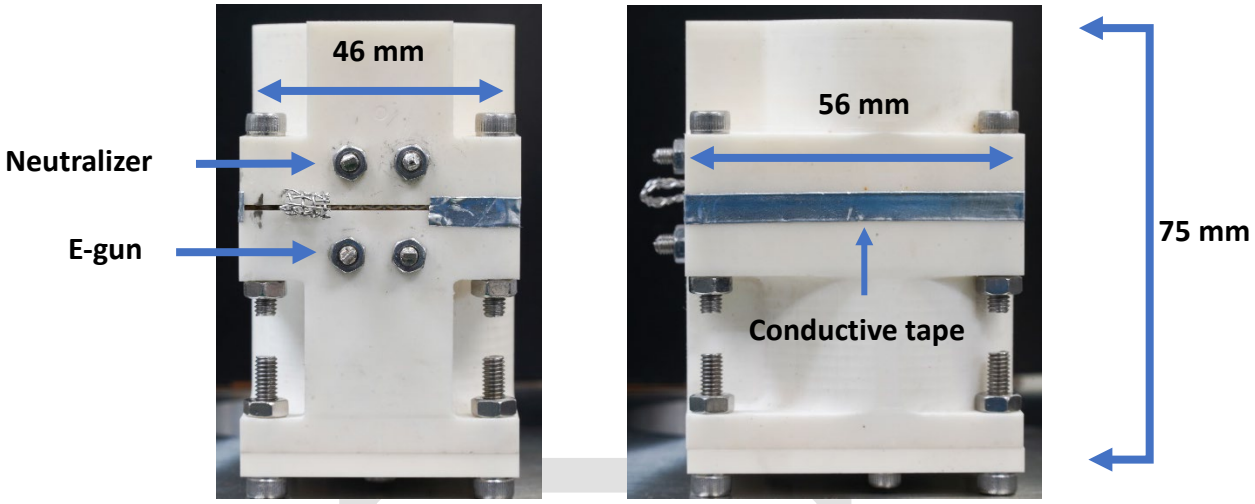

Figure 3.12: Length and width and height of MIT-MEB.

In order to prevent electrons from reaching the anode from other paths, I used aluminum alloy to make a grounding plate to shield the anode. The grounding plate is attached to the bottom of MIT-MEB. As shown in Fig 3.13, the anode is connected through a BNC connector.

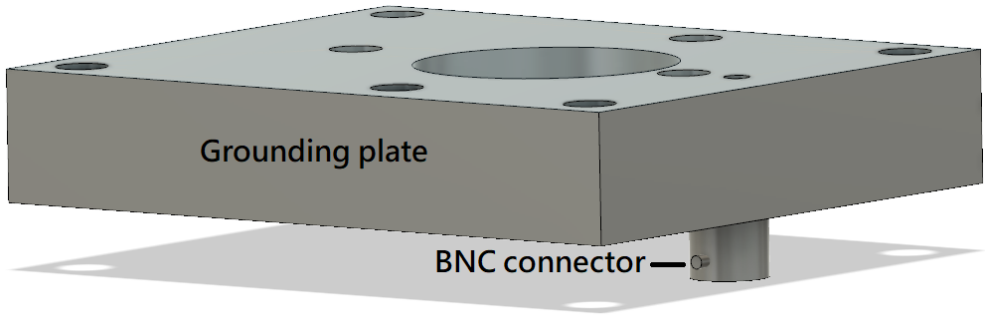

Figure 3.13: An aluminum alloy grounding plate to shield the anode.

doi:10.6844/NCKU201900538

3-4 Physical picture of MIT-MEB

As shown in Fig. 3.13, magnetic field lines that pass through the filament are shown. The hot filament is used as the electron source. When the electrons emit from the filament to the anode, they have an electrostatic repulsion tendency to diverge from each other. Since the electrons leave the filament, they feel a huge magnetic field strength. Electrons will be magnetized and follow magnetic field lines. When these magnetic field lines converge to a point on the target, the electrons can be focused on the surface of the target. With the information of electric fields, magnetic fields, gyroradius, ionization we can construct a clear physical picture of MIT-MEB:

(1) The filament as the electron source emits free electrons.

(2) Electrons are magnetized by the magnetic field and follow magnetic field lines.

(3) Electrons are accelerated by the electric field obtaining kinetic energy and move toward the metallic target along magnetic field lines.

(4) Energetic electrons bombard the metallic target and convert their kinetic energy into heat.

(5) The target is heated until it becomes vapor.

(6) The metallic vapor is ionized through electron impact ionizations when it pass through the region between the filament and the target.

(7) The metallic ions are accelerated by the accelerating grid.

(8) Ions are neutralized by the neutralizer.

(9) Ions as well as electrons leave the thruster with high exhausted speed and provide the thrust.

doi:10.6844/NCKU201900538

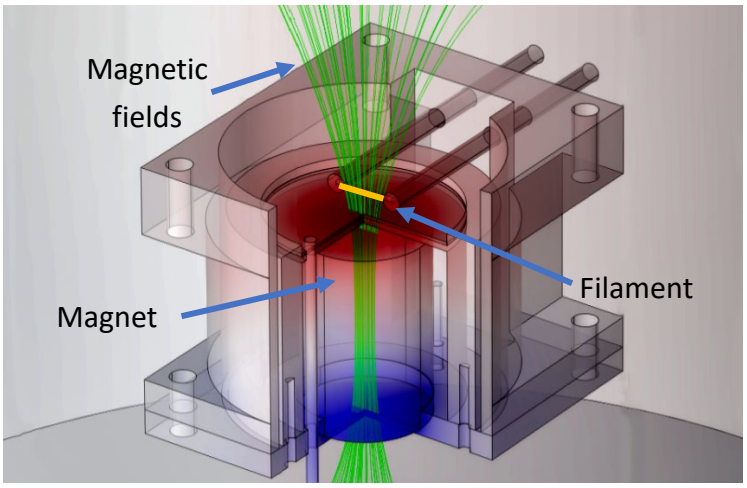

Figure 3.14: The magnetic field lines pass through the electrons source of MIT-MEB.

doi:10.6844/NCKU201900538

Chapter 4

High vacuum system

In this chapter, I will introduce how to build a high vacuum system as the main testing environment. I will explain why high vacuum environment is so important in my research.

4-1 Basic Vacuum knowledge

In this section, I will introduce basic vacuum knowledges. I will explain why we need a high vacuum environment, the mean free path and the various components of the high vacuum system. The vacuum system I built is shown in Fig. 4.1. It consists of a cylindrical vacuum chamber made of quartz, a turbomolecular pump, a roughing pump, a hot cathode ion gauge and a thermocouple gauge. Quartz tube creates an excellent sealed environment and is transparent for observation. The roughing pump and the turbomolecular pump are for creating the high vacuum environment. The hot cathode ion gauge and the thermocouple gauges are responsible for monitoring the vacuum pressure from 1 atmosphere to high vacuum. The vacuum requirement of my experiment is a background pressure less than 10^{-5} Torr. My system can reach a pressure of 10^{-6} Torr.

doi:10.6844/NCKU201900538

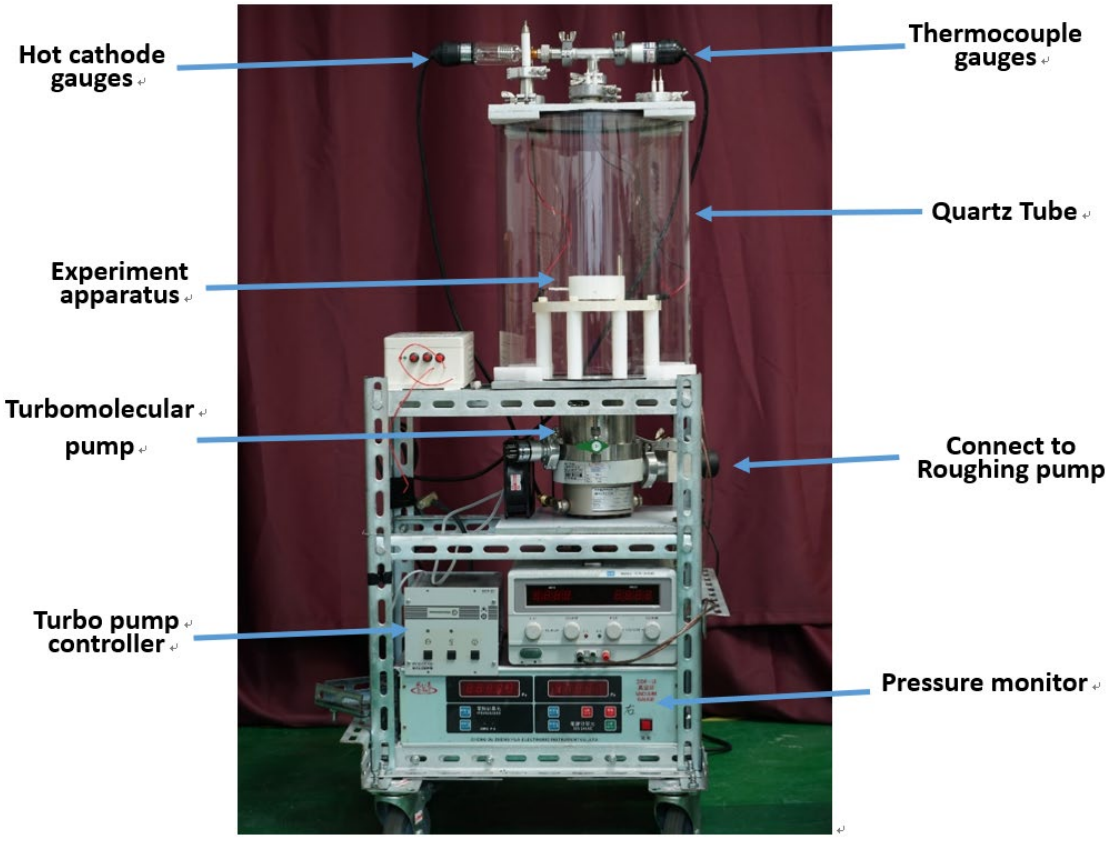

Figure 4.1: High vacuum system for experimental.

4-1-1 Units and range of vacuum pressure

The definition of vacuum is that there are no particles in space. But in reality, it is impossible to remove everything in the space. So we measure how many gas particles are left in the environment as the degree of vacuum. According to the ideal gas equation:

$$PV = NKT \tag{22}$$

where P is the pressure in Pa, V is the volume in m^3, K is Boltzmann constant, T is the temperature in Kelvin, N is the particles number. In the case of constant volume and constant temperature, we can get the following formula for particle number N:

$$N = \frac{KT}{PV} \ . \tag{23}$$

doi:10.6844/NCKU201900538

In the general case, we only need to know the pressure of a container to calculate the number of residual gas particles. Therefore, the vacuum is defined as an environment with a pressure of less than 1 atm. The vacuum pressure units commonly used in engineering are Torr, mbar, Pa. Their relationships with atm are as follows:

$$1 \text{ Torr} = 1.333 \text{ mbar} = 133.3 \text{ Pa} \fallingdotseq 1.316 \times 10^{-3} \text{ atm} . \quad (24)$$

The degree of vacuum is mainly divided into three types. The medium vacuum is from a 25 to 10^{-3} Torr. The high vacuum is 10^{-3} to 10^{-9} Torr. The ultra-high vacuum is less than 10^{-9} Torr. As shown in Table 4.1, they correspond different gas particle residual levels.

Degree of vacuum	*Torr*	*Pa*	*atm*
Atmospheric	760	1.013×10^{5}	1
Rough Vacuum	760~25	10^{5}~10^{3}	1~0.03
Medium Vacuum	25~10^{-3}	10^{3}~10^{-1}	0.03~1.3×10^{-6}
High Vacuum	10^{-3}~10^{-9}	10^{-1}~10^{-7}	1.3×10^{-6}~1.3×10^{-12}
Ultra-High Vacuum	10^{-9}~10^{-12}	10^{-7}~10^{-10}	1.3×10^{-12}~1.3×10^{-15}
Outer Space	10^{-6}~3×10^{-17}	10^{-4}~3×10^{-15}	1.3×10^{-15}~1.3×10^{-20}
Absolute Vacuum	0	0	0

Table 4.1: Different vacuum pressures levels.

4-1-2 Velocity of moleculars

The velocity of gas moleculars is a very important quantity because it will determine how we reach the high vacuum. In the regime of molecular flow, only when the pumping speed exceeding the molecular motion speed can the gas

doi:10.6844/NCKU201900538

molecules be taken away. Average velocity v is given by:

$$v_{av} = 1.45\times10^{4}\ (T/M\times N_A)^{1/2}\ (cm/s) \quad (25)$$

where v_{av} is the average velocity, T is the gas temperature in Kelvin, M is the mass of molecular in a.m.u., N_A is Avogadro constant 6.02×10^{23} molecules/mole. [22]

4-1-3 Mean free path

The average distance that a particle travels between two sequential collisions with other particles is called the mean free path. In order to accelerate electrons emitted from the hot filament, and accelerate ions in the acceleration system, a long accelerating path without losing energy via collisions is required. Therefore, it is important to have sufficiently long mean free path in our experiments. The mean free path is given by [22]:

$$\lambda = \frac{1}{\sqrt{2}\pi d^2 n} = \frac{kT}{\sqrt{2}\pi d^2 P} = 2.33\times10^{-20}\frac{T}{d^2 P} \quad (27)$$

where d is the molecular diameter in centimeters and n is the number of molecules per cubic centimeter. For air at standard temperature, the mean free path (MFP, λ) can be calculated [22]:

$$\lambda_{(cm)} = \frac{5\times10^{-3}}{P_{(torr)}}\ . \quad (28)$$

If the average MFP is too short, electrons and ions are likely to be scattered during acceleration. As a result, they will never obtain the required energy. Further, when the background pressure is too high, the filament is easily oxidized and burned due to the surface being quickly attached with a layer of oxygen. As shown in table. 4.2, different vacuum pressures correspond to different molecular densities, molecular moving flux, mean free path, and the time of forming a monolayer on a surface. You can check this table to find the right vacuum

doi:10.6844/NCKU201900538

pressure according to different needs. The MFP is 5 m when P is 10^{-5} Torr, which is larger than our system size. Thus, I need a vacuum environment with a pressure less than 10^{-5} Torr.

Pressure (Torr)	Molecular Density (molecules/cm^3)	Molecular Incidence (molecules/cm^2/sec)	Mean free path (cm)	Monolayer Formation Time (sec)
760	2.49×10^{19}	2.87×10^{23}	3.9×10^{-6}	1.7×10^{-9}
1	3.25×10^{16}	3.78×10^{20}	5.1×10^{-3}	2.2×10^{-6}
10^{-3}	3.25×10^{13}	3.78×10^{17}	5.1	2.2×10^{-3}
10^{-6}	3.25×10^{10}	3.78×10^{14}	5.1×10^{3}	2.2
10^{-9}	3.25×10^{7}	3.78×10^{11}	5.1×10^{6}	2.2×10^{3}
10^{-12}	3.25×10^{4}	3.78×10^{8}	5.1×10^{9}	2.2×10^{6}

Table 4.2: Vacuum parameters corresponding to different pressures [22].

4-2 Building a vacuum system

A vacuum system consists mainly of three subsystems: (1) a pump system, (2) a pressure monitoring system, and (3) a vacuum chamber.

4-2-1 Viscous flows and molecular flows

There is no pump that can pump from atmospheric pressure to ultra-high vacuum. It is because the airflow pattern can be divided into two types: viscous flows and molecular flows. The viscous flow occurs when the mean free path is extremely short compared to the system scale and the distance between molecules is short. Therefore, collisions between molecules are very frequent. Momentums can be transferred between molecules and molecules efficiently. In this regime, gas flow can be pumped through aerodynamics.

doi:10.6844/NCKU201900538

On the other hand, when the mean free path is far longer than the system size, there is almost no collisions between molecules and molecules will hit the chamber wall. In this regime, the gas molecules are pumped away by mechanical motions. Speeds of blades of a pump must exceed velocities of molecules to transfer momentums to molecules. Schematic of viscous flows and molecular flows are shown in Fig. 4.2.

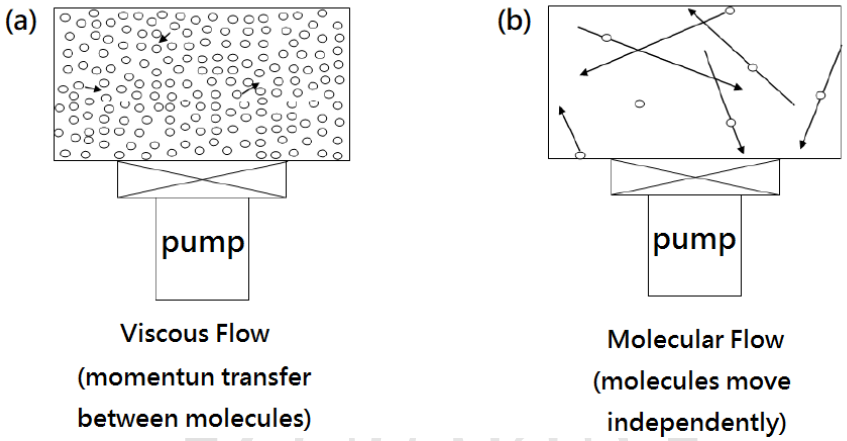

Figure 4.2: (a) Viscos flow and (b) molecular flow. Courtesy of Ref [22].

4-2-2 Roughing pumps

A roughing pump is a type of vacuum pumps that works at atmospheric pressure. Its main function is to pump the vacuum chamber to a rough vacuum of 10^{-2} to 10^{-3} Torr. It is mainly used as the first stage of the pumping system. The purpose is to create a working environment for high vacuum pumps. It is divided into two major categories: oil pumps and dry pumps. Among them, the oil pump is cheap and easy to maintain but there will be oil and gas contaminated. The dry pump can provide a clean vacuum but its price is extremely high compared to the oil pump. Dry pumps are mainly used in electron microscopy or chemical analysis to create a clean vacuum. Since our ion thrusters are not sensitive to oil gas, so we use a cheaper oil pump as the roughing pump.

doi:10.6844/NCKU201900538

4-2-3 High vacuum pumps

If I want to get a pressure below 10^{-3} Torr as described in Section 4-2-1, I must use a pump that can work under molecular flow. Therefore, I will introduce two commonly used high vacuum pumps in this section: diffusion pumps and turbomolecular pumps. Both of these pumps transfer momentums to molecules using physical collisions. Therefore, their working media speeds must exceed molecular motion speeds. Note that all high vacuum pumps cannot be operated directly at atmospheric pressure. Therefore, the working pressure must be achieved by the roughing pump.

4-2-3-1 Diffusion pumps

The diffusion pump is a pump that uses high-speed diffusion of oil molecules. It uses long-chain liquid oil as the working medium because the molecular mass is larger and the effect of momentum transfer is better. The structure of the diffusion pump is shown in Fig. 4.3. There is a heater outside the bottom of the diffusion pump. The working oil is heated by the heater and evaporated. When the oil vapor moves upwards, it collides the mushroom-like umbrellas and changes direction. High-speed cone-shaped pressure jets are formed when oil gas moves downward. The speed of these pressure jets can exceed the speed of sound and therefore effectively push nearby gas molecules down when they collide them. Because of the large molecular mass of oil gas, the diffusion pump has excellent pumping efficiency for very light molecules such as hydrogen. When the gas molecules are compressed in multiple stages achieving the viscous flow regime, they are pumped out by the following roughing pump.

doi:10.6844/NCKU201900538

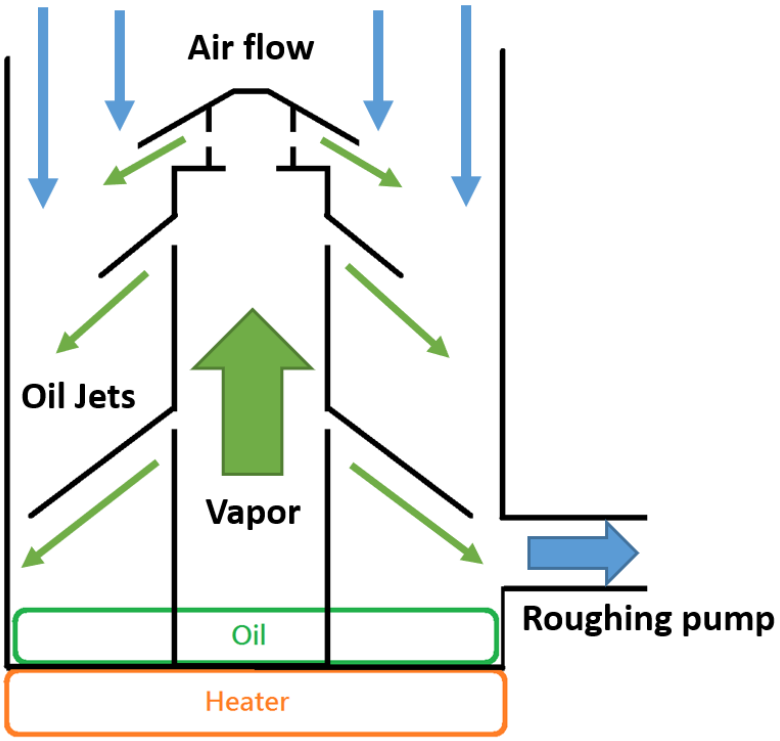

Figure 4.3: The Structure of diffusion pump.

4-2-3-2 Turbomolecular pumps

Different from diffusion pumps, turbomolecular pumps use solid blades with high rotation speed to transfer momentums to gas molecules. The structure turbomolecular pump is shown in Fig. 4.4. Turbomolecular pumps are multi-stage of a rotating rotor blade and a stationary stator blade as a pair in each stage. In order to make the speed of the blade exceed the molecular thermal speed, the rotor rotates at extremely high speed (30000 ~ 90000 rpm). When gas molecules hit the blade through random motion, they are hit by high-speed blades and obtain a little downward momentum. Gas molecules get a little downward momentum every time they pass through a stage. Gas molecular that are compressed to viscous flow regime when they finally reach the bottom of the pump. Therefore, gas molecules are pumped to the atmosphere by the roughing pump after they pass through the turbomolecular pump.

doi:10.6844/NCKU201900538

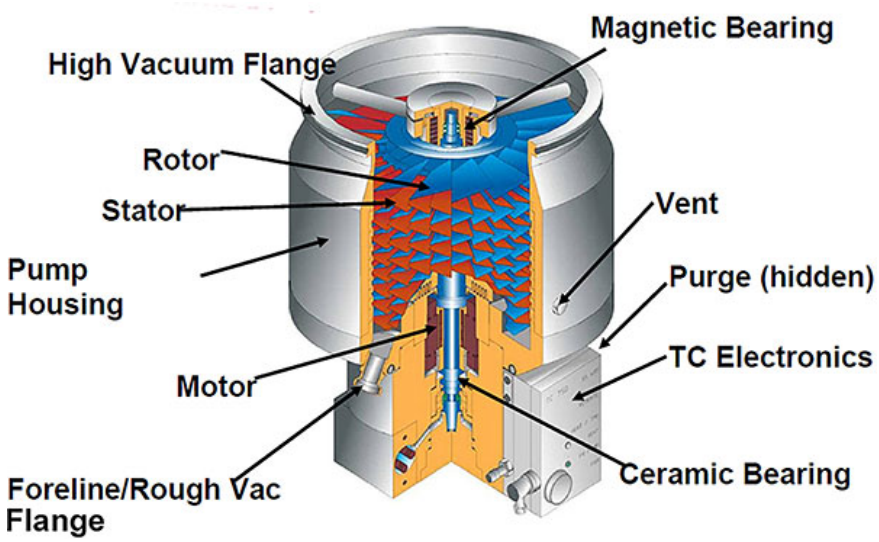

Figure 4.4: Turbomolecular pump structure. Courtesy of Ref [23].

As shown in Fig. 4.5, is the actual rotor we use and a photo when the turbomolecular pump is working. I took it apart for maintenance occasionally.

Figure 4.5: The real rotor of turbomolecular and the way it works.

Both the diffusion pump and the turbomolecular pump can reach an ultra-high vacuum of 10^{-9} Torr. The advantage of the diffusion pump is that the structure is simple and the cost is extremely low but there is a problem of oil and gas contamination. The advantage of the turbomolecular pump is that it is very clean but the structure is extremely complicated and the cost is high. The price

doi:10.6844/NCKU201900538

of the same level of diffusion pump and turbomolecular pump can be nearly 100 times different. Therefore, unless the experimental system is sensitive to oil gas, it is generally more economical to use a diffusion pump.

4-2-4 Vacuum gauges

Just like no pumps can work from atmospheric pressure to ultra-high vacuum, there is no vacuum gauge that can measure from atmospheric pressure to ultra-high vacuum. In general, high vacuum systems have two vacuum gauges to measure the low vacuum regime and the high vacuum regime. A thermocouple gauge is usually used in low vacuum while a hot cathode ion gauge is used in high vacuum.

4-2-4-1 Thermocouple gauges

The thermocouple gauge measures the degree of vacuum by using the principle that the potential of the thermocouple is related to the temperature of the heating element and the temperature of the element is related to the heat conduction of the gas. The thermocouple is attached to a thin filament of platinum or tungsten. This thin filament is heated by a current. The heat is conducted to the surrounding gas molecules. The vacuum pressure is proportional to the heat transfer. Since the resistance of the filament is depended on the temperature, the voltage will also change. Therefore, we can calculate the pressure through the change of voltage. Thermocouple gauge can measure a pressure range from 760 Torr to 10^{-3} Torr.

doi:10.6844/NCKU201900538

4-2-4-2 Hot cathode ion gauges

The measurement range of the hot cathode ion gauge is 10^{-3} Torr to 10^{-9} torr. Since the gas is too thin in this range, there is no way to cause observable pressure changes and there is no way to take away the considerable heat. Therefore, the thermocouple gauge does not work. A hot cathode ion gauge collects the ionic current generated when thermal emitted electrons collide the residual gas. As shown in Fig. 4.6, there is a hot filament which provides free electrons. When hot electrons bombard the residual gas molecules, they will be ionized when free ions pass through the accelerating grid and reach the collector forming an ion current, the amoumt of the current is then converted to the reading of the pressure.

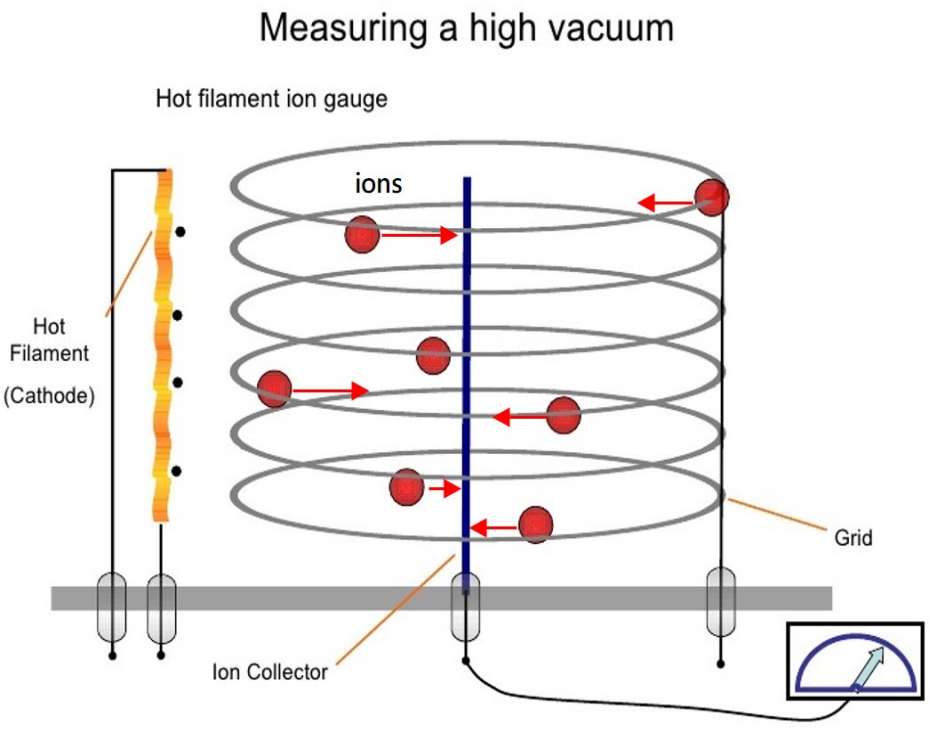

Figure 4.6: Structure of hot cathode ion gauge. Courtesy of Ref [24].

doi:10.6844/NCKU201900538

4-2-5 The Vacuum chamber

A vacuum chamber is a device used to isolate gas particles in external and internal environments. It must have good sealing and low outgassing performance. On the other hand, due to the huge pressure difference with 1 atm (about 1kg/cm^2), the chamber must withstand huge stresses. Therefore, vacuum chambers are usually made of hard materials such as stainless steel, aluminum alloy, quartz, etc., and the shape is usually in circular, barrel and spherical to disperse stress while keeping wall thin.

In order to observe experiments, I choose quartz tube as the vacuum chamber. The quartz tube has a height of 400 mm, a diameter of 300 mm and a wall thickness of 5 mm. Two aluminum alloys plates were used as the cover plate. Holes were made on the plates and connected to the turbo pump and vacuum flanges. Shown in Fig. 4.7 and Fig. 4.8 are the top cover plate and the bottom cover plate for the vacuum chamber. The top cover plate has five KF 25 flanges connecting to the vacuum gauge、feedthroughs and the up to air valve. The bottom cover plate has a 102 mm hole for connecting the turbomolecular pump and a KF 25 flange for connecting a feedthrough. In order to seal the quartz tube and the aluminum alloy cover plates well, I use a 5 mm thick rubber plate which was cut into a ring with an outer diameter of 350 mm and an inner diameter of 280 mm as a sealing ring. The final system with the cover plates and the quartz chamber is shown in Fig. 4.9 and 4.10.

doi:10.6844/NCKU201900538

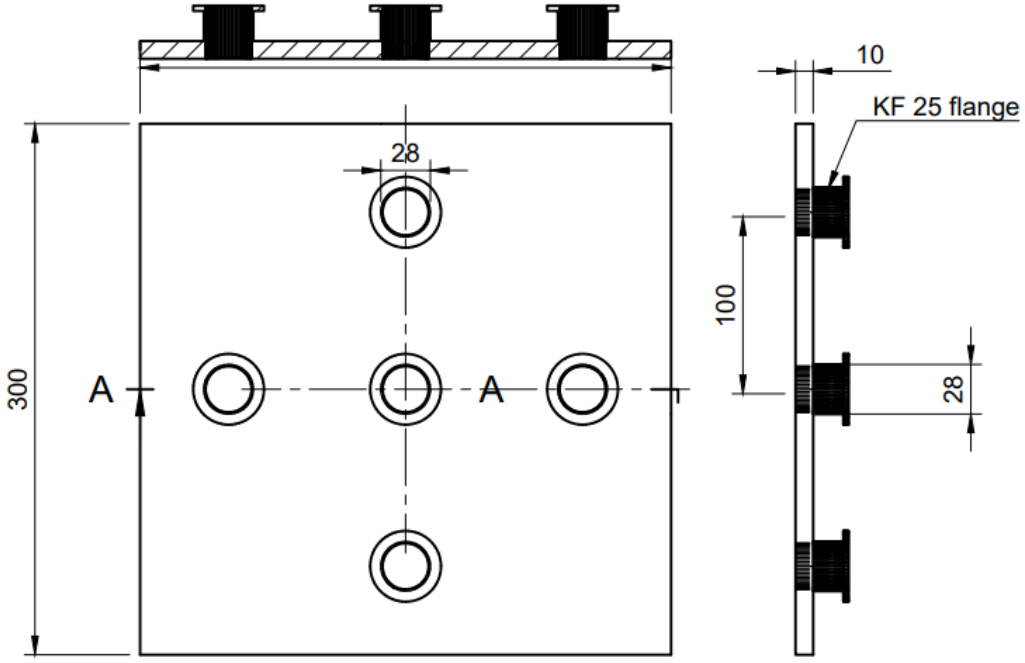

Figure 4.7: Vacuum chamber top cover plate.

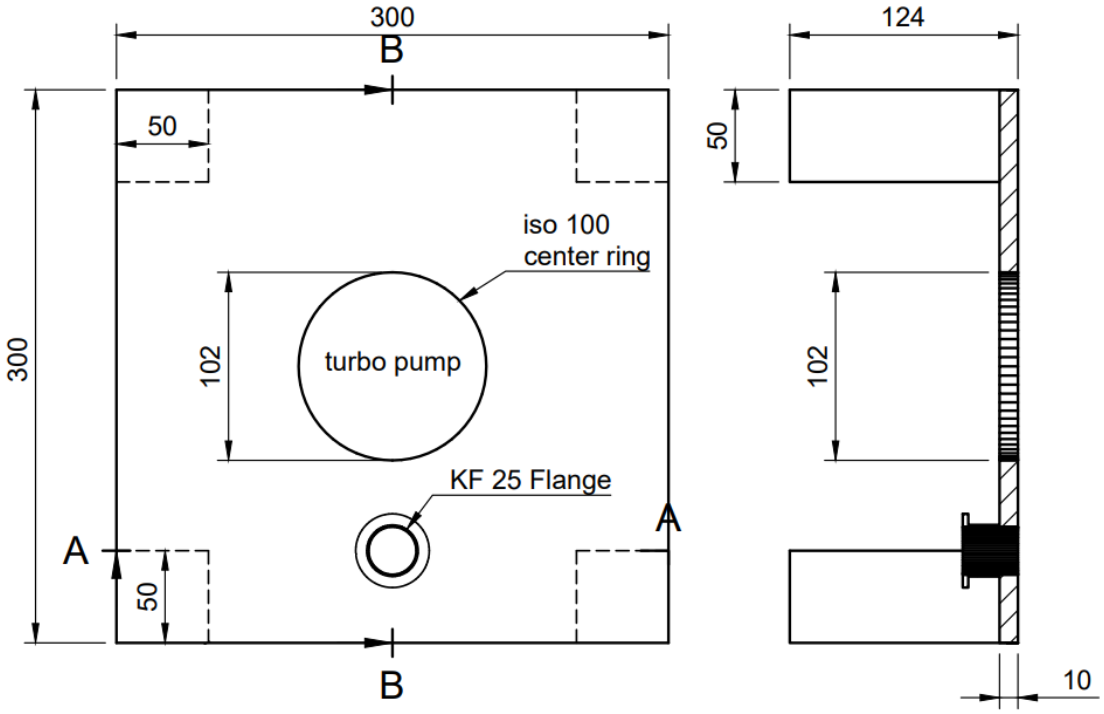

Figure 4.8: Vacuum chamber bottom cover plate.

doi:10.6844/NCKU201900538

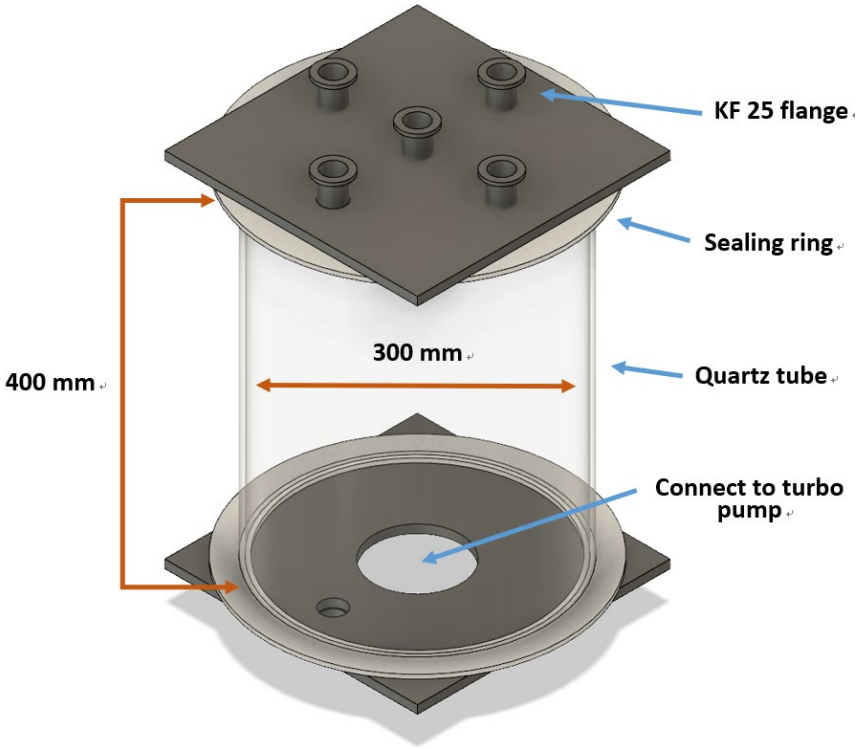

Figure 4.9: The quartz high vacuum chamber.

As shown in Fig. 4.10, it is the configuration of top cover plate. Flanges are connected feedthrough for vacuum gauges、filaments、anode and the cathode respectively.

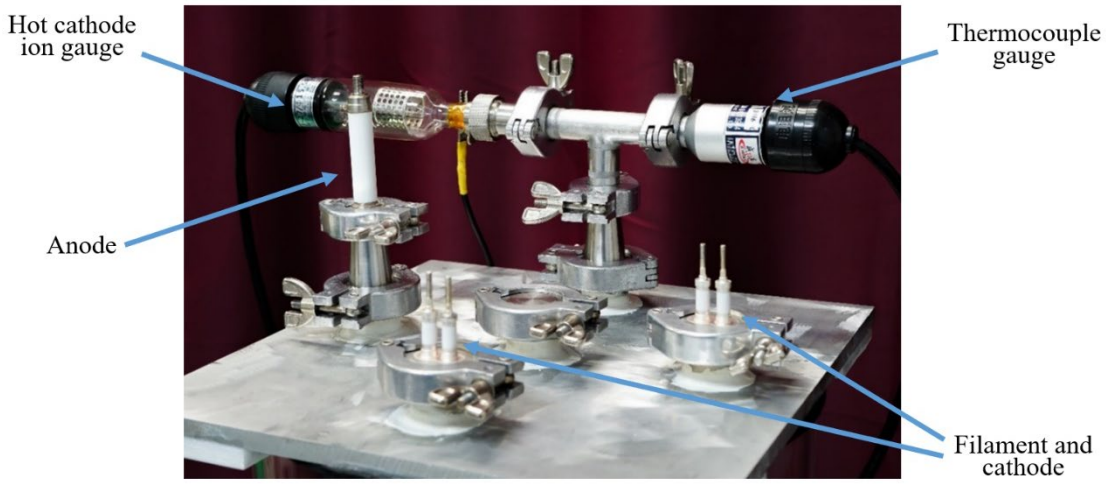

Figure 4.10: Configuration of top cover plate.

doi:10.6844/NCKU201900538

Chapter 5

Measurement methods

In this chapter, I will introduce measurement methods for obtaining parameters of MIT-MEB. They include the electrical characteristics, the evaporation rate and the ionization rate.

5-1 Experimental procedures

The whole experimental process is divided into two parts: (1) pump the pressure in the chamber down to experimental requirements；(2) perform MIT-MEB discharge experiments and measure data.

5-1-1 Process of vacuuming the chamber

The pump down process is very long. It normally takes more than 12 hours. Minimizing the plastic and high-outgassing materials in the chamber can speed up the process. Process of pumping down the chamber is shown in Fig. 5.1.

(1) I use a roughing pump to reduce the pressure in the turbo pump and the chamber to 10^{-3} Torr.

(2) Confirm that the pressure reaches the operating range of the turbo pump ($<10^{-3}$ Torr) then turn on the turbo pump.

(3) Wait until the turbo pump reaches the rated rotation speed then turn the ion gauge on.

(4) Wait until the pressure in the chamber reaches 10^{-6} Torr. The vacuum system is them ready for experiments.

doi:10.6844/NCKU201900538

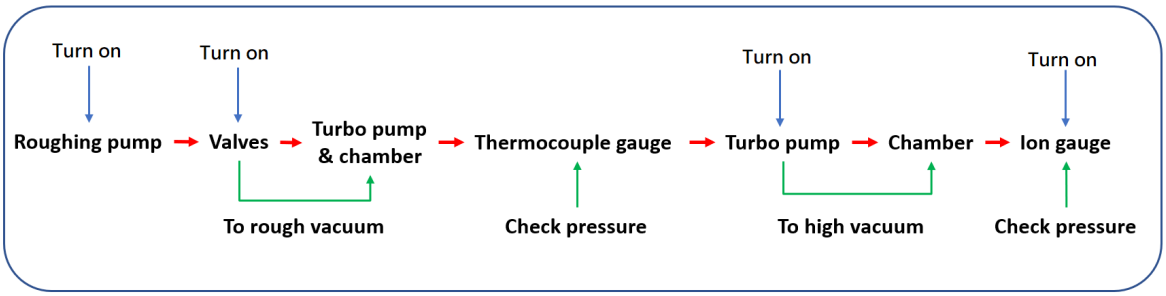

Figure 5.1: Process of vacuuming the chamber.

5-1-2 Testing procedures

As shown in Fig. 5.2, when the pressure drops below 10^{-5} Torr, we can conduct MIT-MEB discharge experiments. The process is as following:

(1) Turn on the power supply for the filament of the E-gun I_f.

(2) Turn on the HV-power supply to the target voltage HV.

(3) Adjust the I_f for heating the filament of the E-gun, so that the E-beam current I_e reaches the set current.

(4) Turn on the heating power of the neutralizer filament and set the heating current I_{nf} to 2.5 A.

(5) Record the voltage and the current of E-gun Filament power (I_f,V_f), the voltage and the current of HV-power (HV、I_e)、the voltage and the current of neutralizer filament power (I_{nf}, V_{nf}) and neutralizing electrons current (I_n) every minute for 5 minutes.

doi:10.6844/NCKU201900538

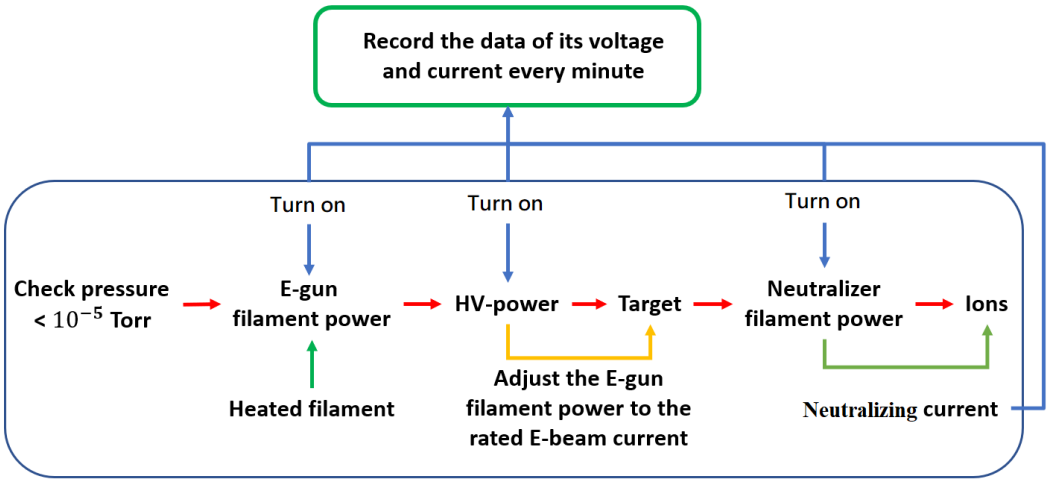

Figure 5.2: Process of testing MIT-MEB.

5-2 Parameter measurements

As shown in Fig. 5.3, it is the circuit of MIT-MEB. We have measure high voltage (HV), E-beam current (I_e), E-gun filament voltage (V_f), E-gun filament current (I_f), neutralizing filament voltage (V_{nf}), and neutralizing filament current (I_{nf}) and neutralizing electrons current (I_n). Below I will explain the physical meaning of the seven data. The experimental power supply system of MIT-MEB is shown in Fig. 5.4.

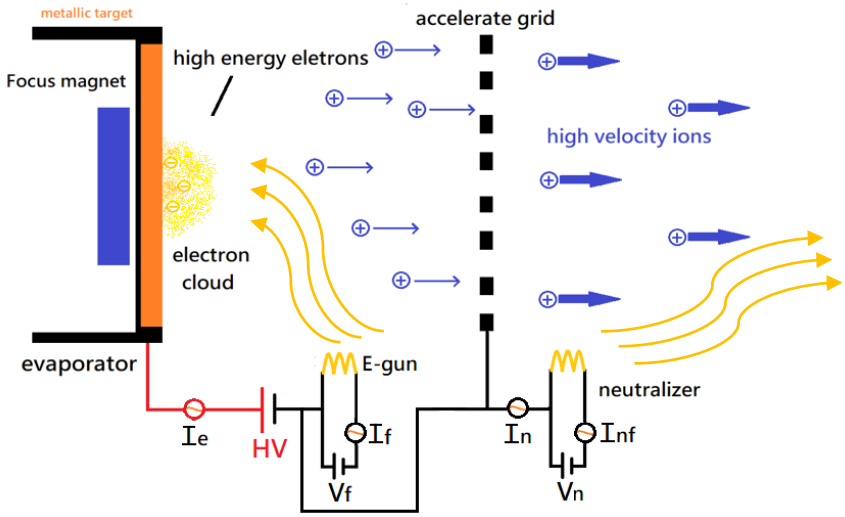

Figure 5.3: The circuit of MIT-MEB.

doi:10.6844/NCKU201900538

Figure 5.4: Power supply system of MIT-MEB.

(1) HV: the voltage between the E-gun/grid and the metallic target. It is used to accelerate thermal electrons to hit the metallic target and accelerate the ions leaving the thruster. Therefore, HV corresponds to the kinetic energy and speed of electrons and ions. As shown in Fig. 5.5 is the measurement of HV. It is set by the power supply directly.

(2) I_e: the current of the high voltage power supply. It should equal to the sum of the electron beam current and the ion beam current. The value of I_e is actually determined by the ability of releasing free electrons of the E-gun filament. The product of HV and I_e is the thrust power consumption of MIT-MEB. Shown in Fig. 5.5 is the reading of I_e. Note that I_e is controlled by adjusting the power supply of the E-gun filament I_f.

doi:10.6844/NCKU201900538

Figure 5.5: Measurement of HV and I_e on high voltage power supply.

(3) V_f: the voltage of the power used to heat the E-gun filament. Shown in Fig. 5.6 is the reading of V_f. V_f is determined by I_f and the resistance of the filament. It is normally ~ 2.3 V.

(4) I_f: the current of the power used to heat the E-gun filament. It is used to control the filament temperature and thus the emitted electron current from the filament. Therefore, by adjusting I_f, we can control the E-beam current I_e. The product of V_f and I_f is the total power consumption of the E-gun filament. Shown in Fig. 5.6 is the reading of I_f.

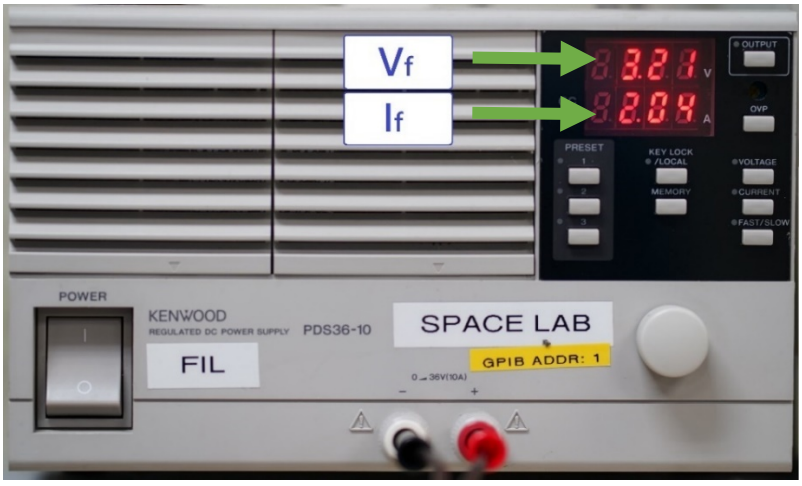

Figure 5.6: Measurement of V_f and I_f on E-gun filament power supply.

doi:10.6844/NCKU201900538

(5) V_{nf}: the voltage of power used to heat the neutralizer filament. Shown in Fig. 5.7 (a) is the reading of V_{nf}. V_{nf} is determined by I_{nf} and the resistance of the neutralizer filament. It is normally ~ 2.45 V.

(6) I_{nf}: the current of the power used to heat the neutralizer filament. Shown in Fig. 5.7 (b) is the reading of I_{nf}. The product of V_{nf} and I_{nf} is the total power consumption of the neutralizer filament.

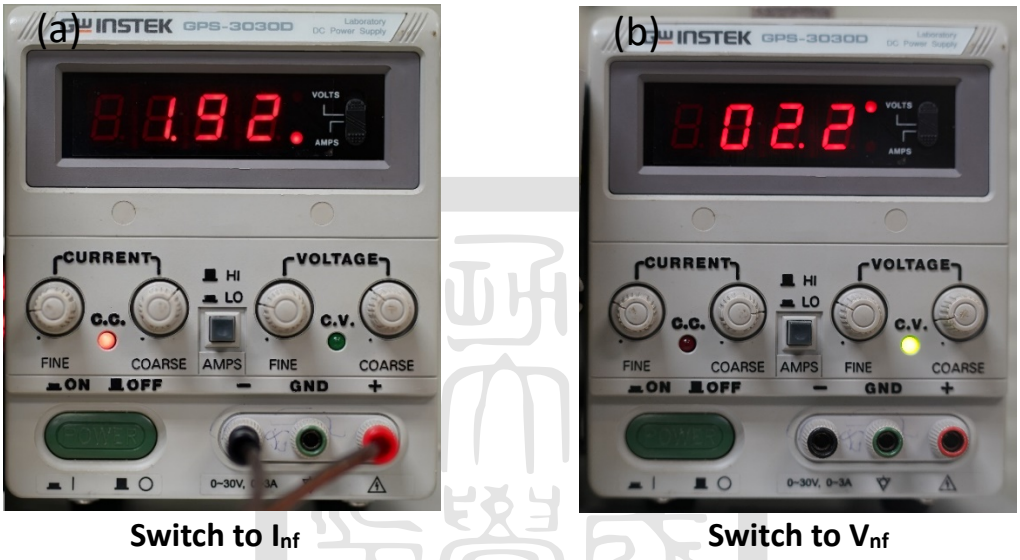

Figure 5.7: Measurement of V_{nf} and I_{nf} on E-gun filament power supply.

(7) I_n: It is a current between neutralizer filament and the whole ion source. Since the neutralizer filament will release free electrons, they will follow the ions and leave the thruster. Therefore, theoretically, I_n equals the ion current. However, ions may attract some electrons from the E-gun filament. Therefore, I_n should be less than or equal to the ion current, i.e., the lower bond of the ion current. I use an ammeter to measure I_n in the circuit.

doi:10.6844/NCKU201900538

5-3 Evaporation rate

I introduced the formula for evaporation rate Eq. (17) in section 3-2-5. We know from Eq. (16) in section 3-2-5 that the evaporation rate $\dot{m}_{Metal}=\frac{m_i-m_f}{\Delta t}$. In the measurement, by measuring the mass difference of the targets before and after the experiments and the experimental time, we can obtain the evaporation rate. After several tries, we found that the mass difference is 0.1 to 0.001 g after each experiment. Therefore, the precision of the scale must be 0.0001 g. The model of the scale we used is Sartorius TE124S. It can meet our needs as shown in Fig. 5.8. In order to reduce the error, we measured the target and the evaporator together.

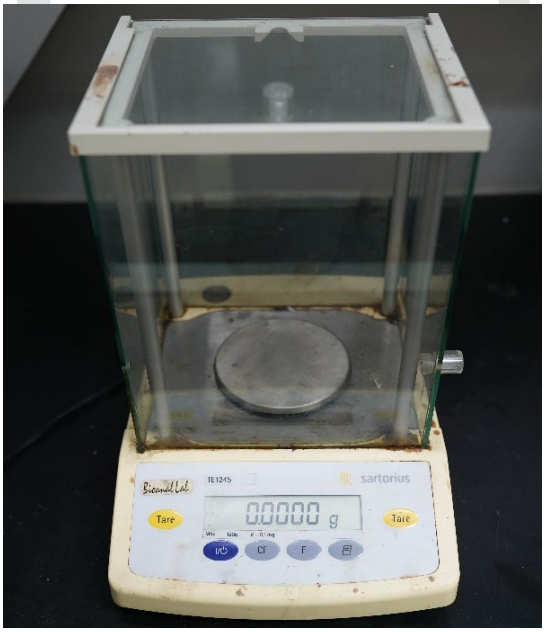

Figure 5.8: The electronic balance Sartorius TE124S.

5-4 Ionization rates

The equation for ionization rate was given by Eq. (18) section in 3-2-5. We have $\beta = \frac{I_n}{q} \times (\frac{\dot{m}_{Metal}}{M_{Atom}})^{-1}$. Therefore, by measuring I_n and evaporation rate $\dot{m}_{Metal}$, we can calculate ionization rate β.

doi:10.6844/NCKU201900538

Chapter 6

Experimental Results

In this Chapter, I will show the experimental data which contains the electrical characteristics, evaporation rates and ionization rates of the MIT-MEB. I will use these data to calculate the theoretical thrust and specific impulse I_{sp}. Metallic Ion Thruster using Magnetron E-beam bombardment in operation is shown in Fig. 6.1. I used a quartz case for easy viewing and the one made of ceramics was used for testing evaporator to keep the consistency of data.

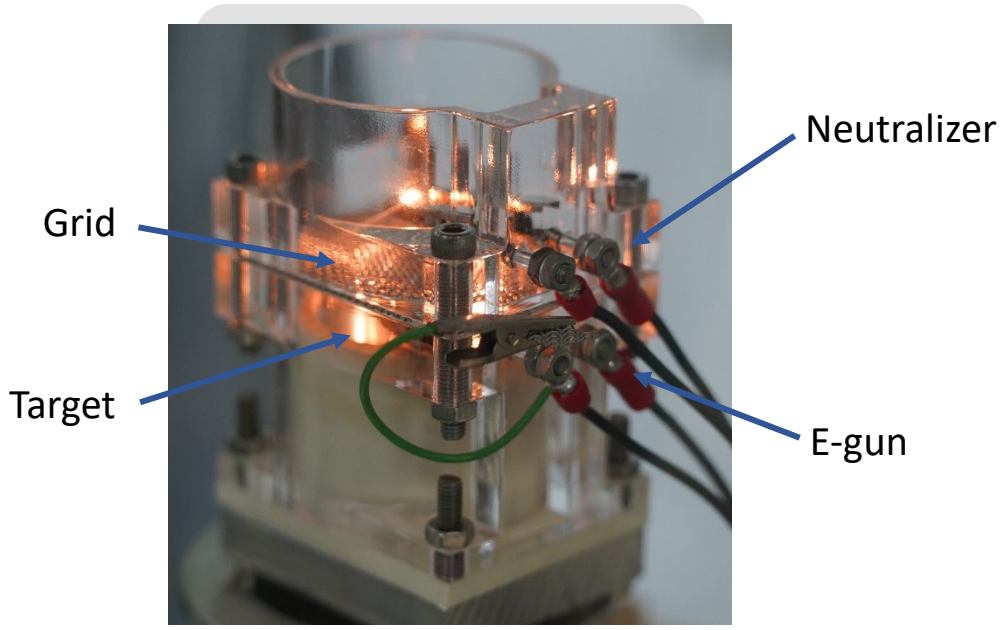

Figure 6.1: The MIT-MEB in operation.

6-1 Targets after being bombarded by E-beams

When the metallic target is bombarded by electrons, the center of the target is melted significantly as shown in Fig. 6.2. This proves our simulation results that the magnetic field can well confine the electrons forming an E-beams and guide them to the center of the target. This greatly increases the evaporation

doi:10.6844/NCKU201900538

efficiency. We can see that the degree of melting from 5 kV accelerating voltage and 3 mA E-beam current (5 kV/3 mA) is higher than that from 1 kV accelerating voltage and 15 mA E-beam current (1 kV/15 mA). We conclude that the higher the accelerating voltage under the same power, the kinetic energy of the electrons can be converted into the thermal energy of the target more efficiently.

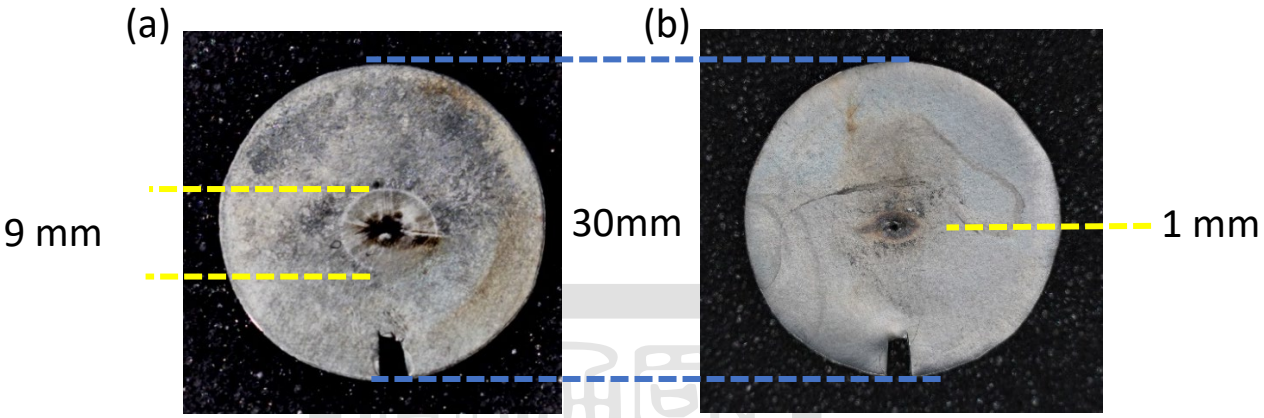

Figure 6.2: The zinc target is heated by electrons and melted (a) in 5 kV/3 mA/5 min, (b). in 1 kV/15 mA/5 min.

However, if you look closer at the result of 1 kV/15 mA as shown in Fig. 6.3, you will find that the target is burned out forming a hole with diameter about 1 mm. It seems like it sublimated directly from the solid-state into a gaseous state rather than melting first then evaporating into a gaseous state. This shows that 1-keV E-beam heating effect is better than 5-keV E-beam. According to Eq. (10), it is possible that the smaller the energy of electrons in the same magnetic field, the smaller the gyroradius. So that, the heat was more concentrated.

doi:10.6844/NCKU201900538

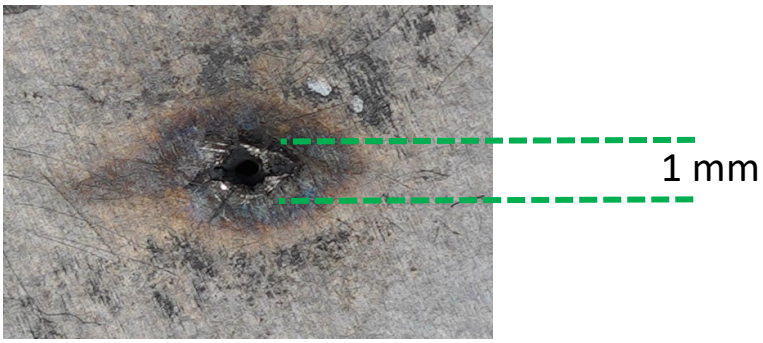

Figure 6.3: The target is burned out a hole at an acceleration voltage of 1 kV.

6-2 E-beam evaporators

Before building the prototype of MIT-MEB, I must first confirm the feasibility of the E-beam evaporation. Therefore, I built an E-beam evaporator for proving the concept. Ceramic (Al_2O_3) was used to build the evaporator. Since Al_2O_3 has very high melting point, 2,072 °C, and low thermal conductivity, 40 W/mK, the metal can be heated very efficiently. It makes ceramic ideal for making evaporators. On the other hand, the magnet will not be heated due to lack of contact between magnets and the heated target. Therefore, the magnets can be kept cold enough and their magnetism is not lost. Therefore, one ceramic tube and two clips were used to carry the filament and the other tube is used to place the target as shown in Fig. 6.4.

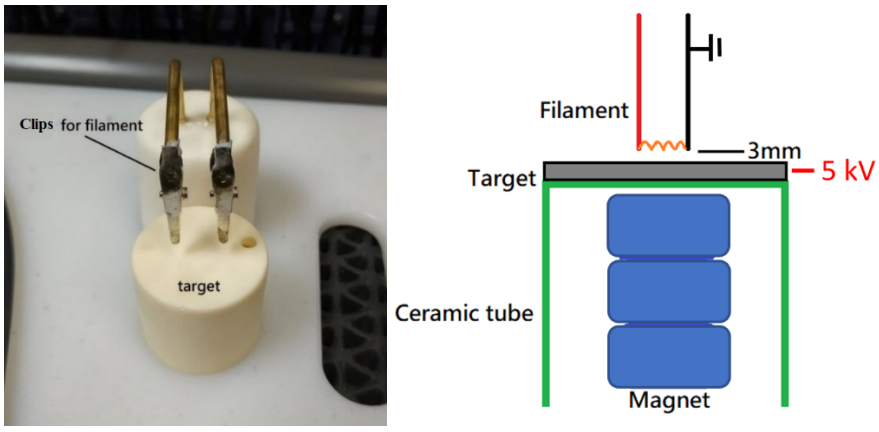

Figure 6.4: Ceramic evaporator and clips for filament.

doi:10.6844/NCKU201900538

The ceramic evaporator worked well. Zinc was used as the target. The filament was heated by a power supply with a current of 1.864±0.004 A and a voltage of 1.74 V. The high voltage HV between the filament and the target was 5002.2±0.5 kV. The E-beam current I_e that heated the target was 3.00±0.06 mA. The experiments were repeated 5 times. In only ten minutes, the quartz chamber was obviously coated by Zn as shows in Fig. 6.5. The mass difference of the target was 0.17±0.03 g. Evaporation rates was $(2.8\pm0.5)\times10^{-4}$ (g/s).

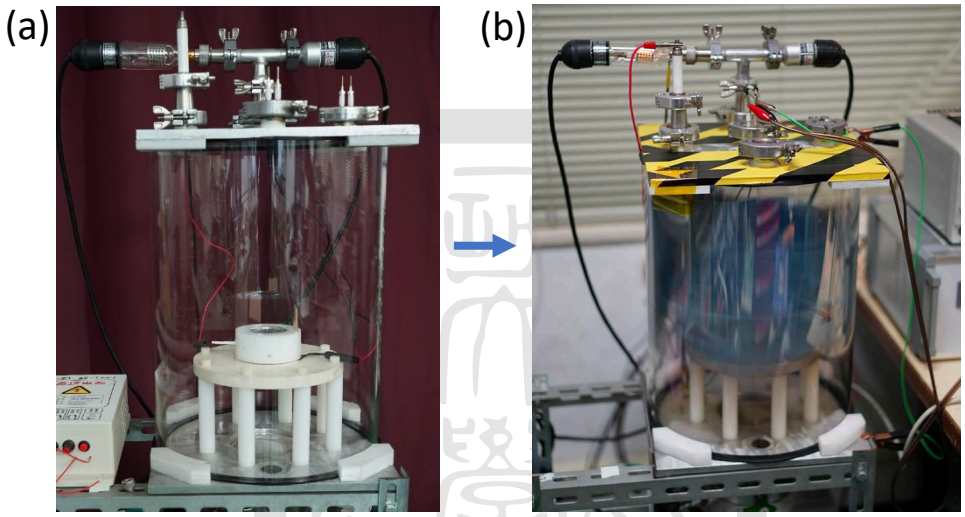

Figure 6.5: the quartz chamber was coated by zinc, (a) before experiment (b) after experiment.

6-2-1 Characteristics of the E-beam

The voltage of the power supply and the current of the E-beam is shown in Fig. 6.6. Both curves were from the average of five sets of experiments. The power consumption of the electron beam was $HV\times I_e = 15.0\pm0.3$ W.

doi:10.6844/NCKU201900538

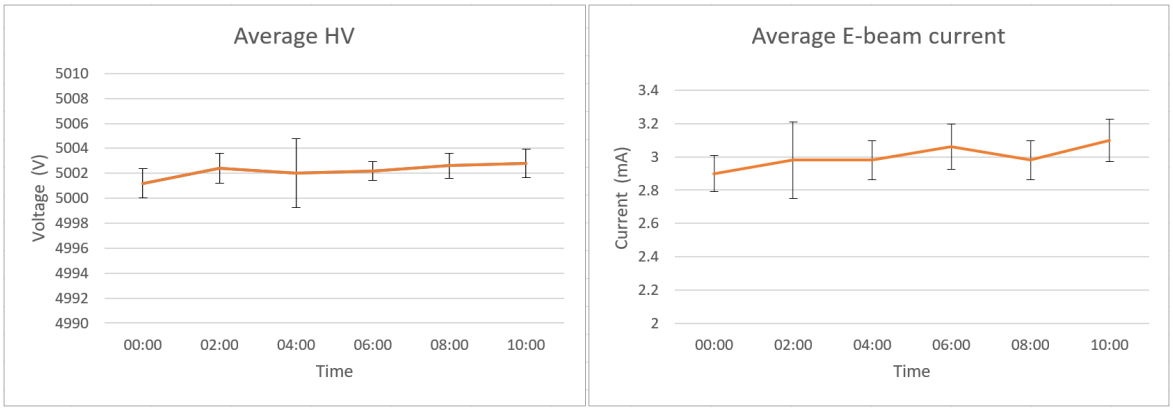

Figure 6.6: E-beam discharge curve with 5 kV/3 mA evaporation rate experiment.

6-2-2 Characteristics of the E-gun filaments

The heating voltage and the current of the electron gun filament is shown in Fig. 6.7, I_f=1.86±0.05 A and V_f=1.74±0.1 V. Since the tungsten wire must be replaced after each experiment, it is hard to ensure that the resistance of the filament is exactly the same. Therefore, the voltage and the current of the filament fluctuated greatly. The power consumption of the E-gun filament is $I_f \times V_f$= 3.2±0.2 W.

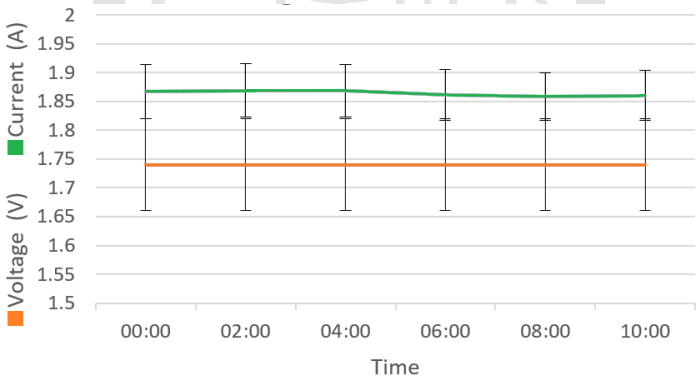

Figure 6.7: The average heating voltage and current change of the E-gun filament.

6-2-3 Vacuum conditions

The background pressure of the system was about 10^{-6} Torr. You can see that the pressure rises rapidly to 10^{-5} Torr when experiments started as shown in

doi:10.6844/NCKU201900538

Fig. 6.8. This proves that when the E-beam started, something evaporated into a gaseous state causing the pressure in the chamber rise.

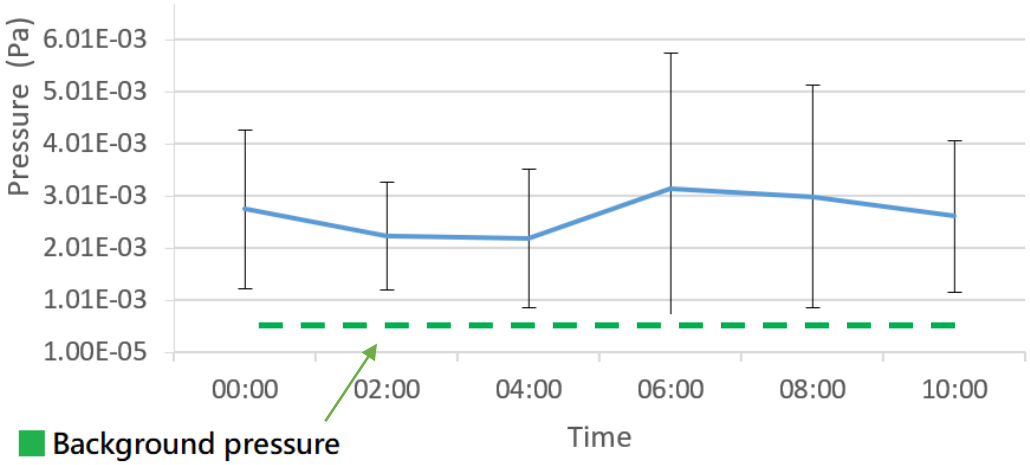

Figure 6.8: Averaged vacuum pressure over time.

6-2-4 Evaporation rates

The evaporation rate for each experiment and the average evaporation rate are shown in Fig. 6.9. The averaged evaporation rate is $(2.8\pm0.5)\times10^{-4}$ (g/s). This proves that our idea of using electron beam evaporation to generate metallic vapor is feasible.

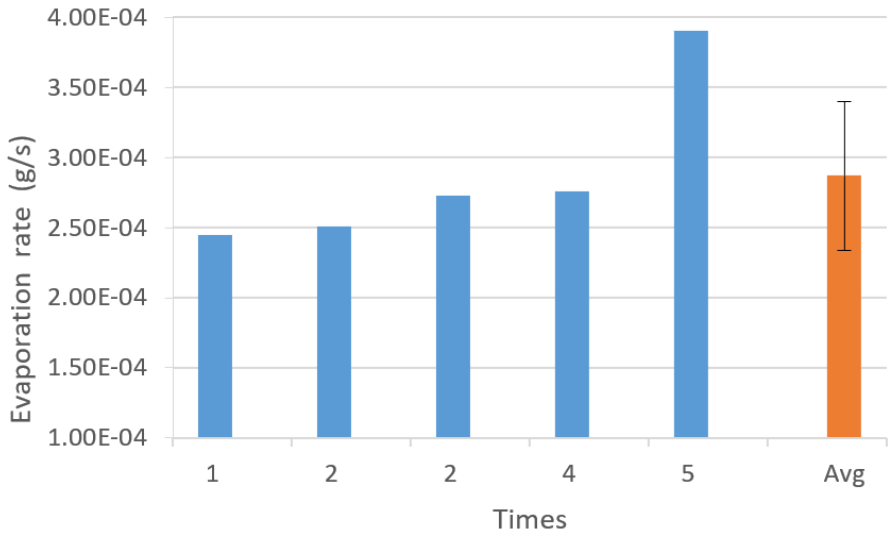

Figure 6.9: Evaporation rate of ceramic evaporator.

doi:10.6844/NCKU201900538

6-3 Results of MIT-MEB of 5 kV/3 mA E-beam

In this section I will show the results of MIT-MEB using a 5 kV accelerating voltage with 3 mA E-beam current (5 kV/3 mA). All results are averages of 5 sets of experiments.

6-3-1 Electrical characteristics of the E-beam

The current curve of the E-beam is shown in Fig. 6.10. The voltage and the current of the E-gun filament is shown in Fig. 6.11. It is to heat the filament of the E-gun. The voltage and the current of the neutralizer are shown in Fig. 6.12. It is to heat the filament of the neutralizer. The total power is

$$W = (HV \times I_e)+(V_f \times I_f)+(V_{nf} \times I_{nf})$$

$$= (5000\times(3\pm0.1)\times10^{-3})+((1.83\pm0.04)\times(2.2\pm0.1))+((2.3\pm0.1)\times(2.5\pm0.1))$$

$$= 24.8\pm1.1 \text{ W}$$

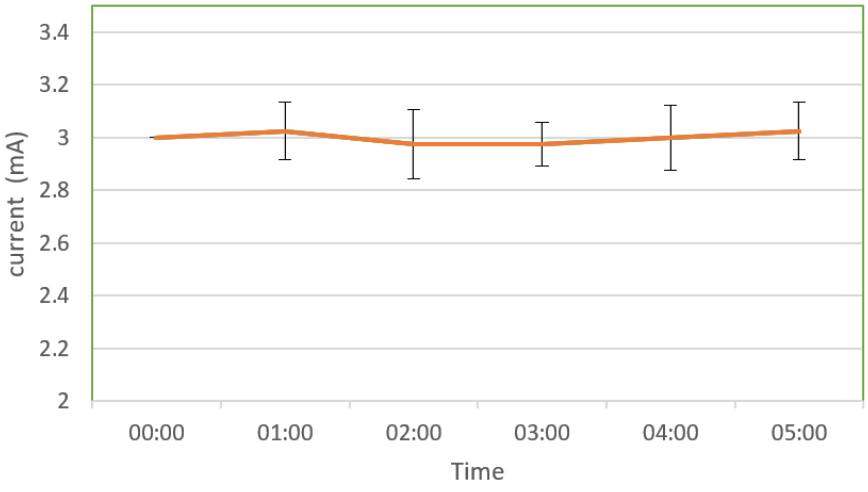

Figure 6.10: The current curve of the E-beam of MIT-MEB at 5 kV.

doi:10.6844/NCKU201900538

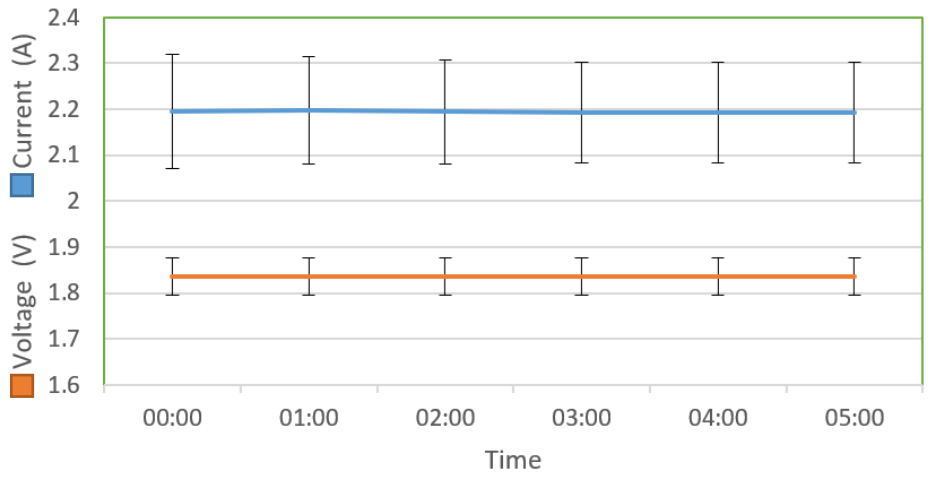

Figure 6.11: The discharge curve of voltage and current of the E-gun filament.

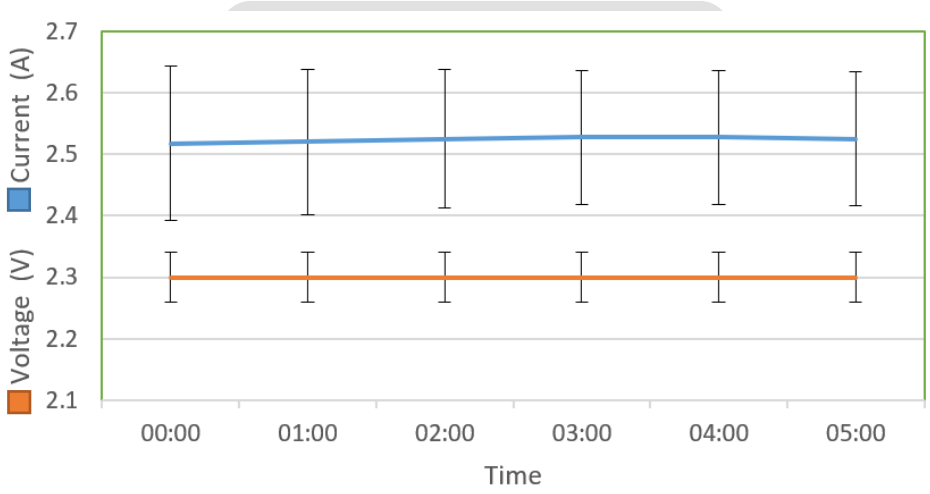

Figure 6.12: The discharge curve of voltage and current of the Neutralizer.

6-3-2 Evaporation rates

The mass different of the target is $(7.0\pm0.8)\times10^{-2}$ (g). The evaporation rate is $(2.2\pm0.4)\times10^{-4}$ (g/s) as shown in Fig. 6.13. Since the parameters are equivalent to the E-beam evaporator in section 6-2, the result is similar to that of section 6-2-4.

doi:10.6844/NCKU201900538

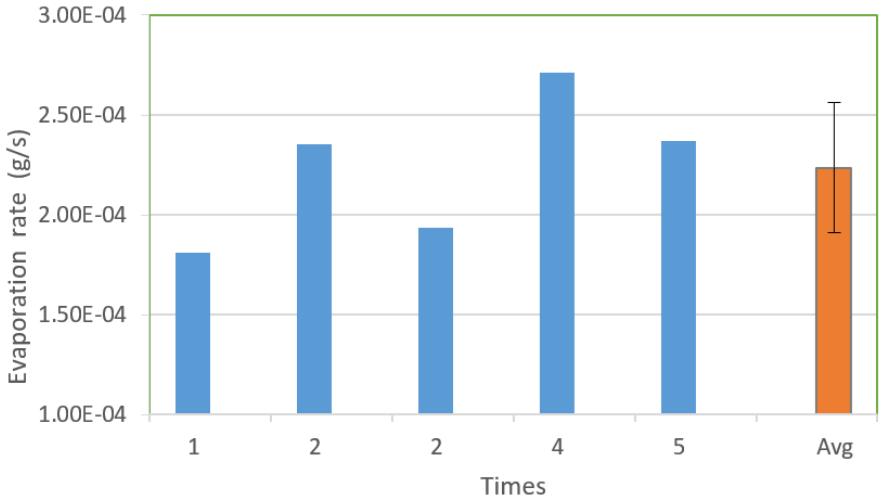

Figure 6.13: The evaporation rate of MIT-MEB at 5 kV.

6-3-3 Ionization rates

The current curve of the neutralizer of MIT-MEB is shown in Fig. 6.14. The maximum 0.11±0.01 mA occurs at the fifth minute. Since I_n gradually become saturated, we choose the maximum value to calculate. According to formula (18) the ionization rate is

$$\beta = \frac{(0.11\pm0.01)\times10^{-3}}{1.6\times10^{-19}} \div \frac{(2.2\pm0.4)\times10^{-4}}{65\times1.67\times10^{-24}} = 0.03\pm0.01\ \%$$

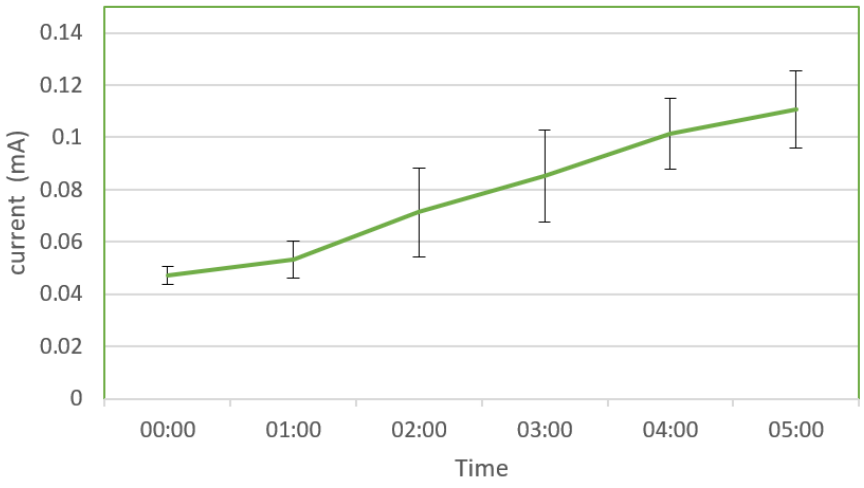

Figure 6.14: The current curve of the Neutralizer of MIT-MEB at 5 kV.

doi:10.6844/NCKU201900538

6-3-4 Expected thrusts

According to formula (19), (20), the evaporation rate of $(2.2\pm0.4)\times10^{-4}$(g/s) and the ionization rate of 0.03±0.01%, the theoretical thrust T*(μN)*:

$$F_{ion} = (0.03\pm0.01\%)(2.2\pm0.4\times10^{-4}) \times \sqrt{\frac{2\times5000V\times1.6\times10^{-19}}{65\times1.67\times10^{-27}}} = 9.0\pm1.0 \quad \mu N.$$

6-3-5 Expected I_{sp}

According to formula (13), we can calculate the specific impulse I_{sp} (sec)*:*

$$I_{sp} = \frac{1}{9.8} \times \sqrt{\frac{2\times5000V\times1.6\times10^{-19}}{65\times1.67\times10^{-27}}} = 12{,}300 \text{ sec}$$

6-4 Result of MIT-MEB of 1 kV/15 mA E-beam

In this section I will show the results of MIT-MEB using 1 kV accelerating voltage with 15 mA E-beam current (1 kV/15 mA). All results are averages of 5 sets of experiments.

6-4-1 Electrical characteristics of the E-beam

The current curve of the E-beam is shown in Fig. 6.15. The voltage and the current of the E-gun filament is shown in Fig. 6.16. It is to heat the filament of the E-gun. The voltage and the current of the neutralizer are shown in Fig. 6.17. It is to heat the filament of the neutralizer. The total power is

$$W = (HV\times I_e)+(V_f\times I_f)+(V_{nf}\times I_{nf})$$

$$= (1000\times(15.7\pm0.4)\times10^{-3})+((2.01\pm0.03)\times(2.26\pm0.03))+((2.4\pm0.1)\times(2.49\pm0.01))$$

$$= 26.2\pm0.7 \text{ W}$$

doi:10.6844/NCKU201900538

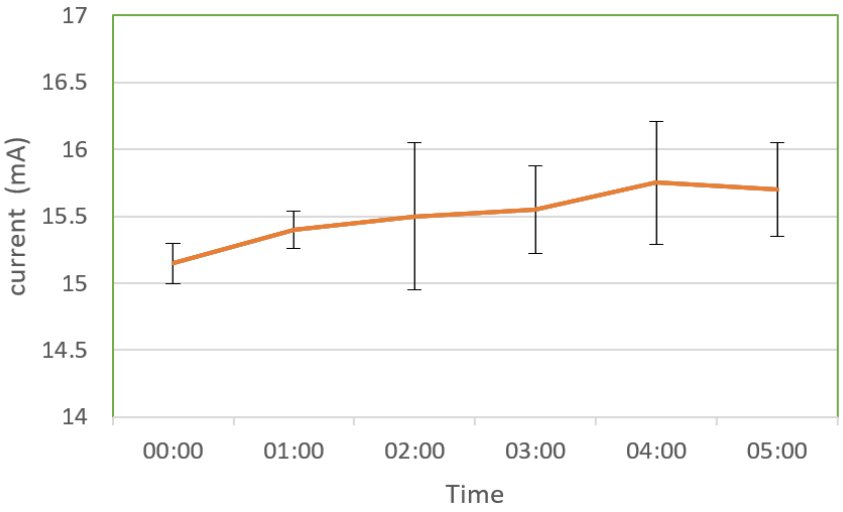

Figure 6.15: The current curve of the E-beam of MIT-MEB at 1 kV.

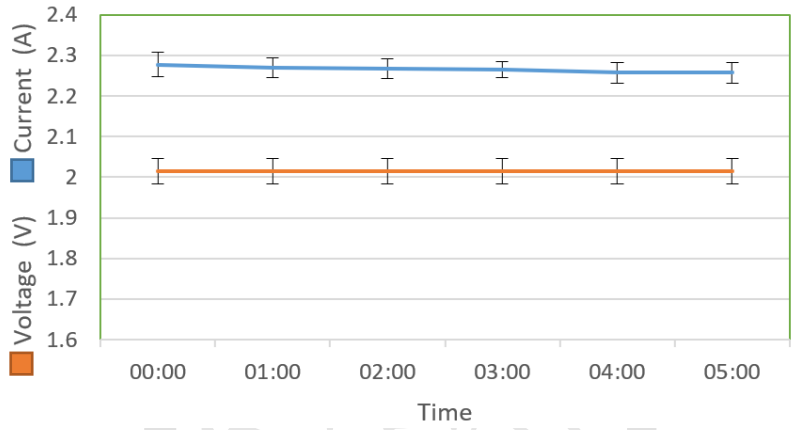

Figure 6.16: The discharge curve of voltage and current of the E-gun filament.

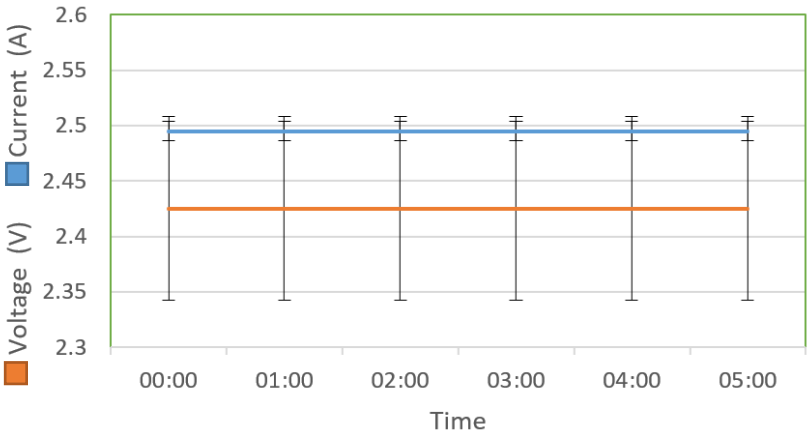

Figure 6.17: The discharge curve of voltage and current of the Neutralizer.

doi:10.6844/NCKU201900538

6-4-2 Evaporation rates

The mass different of the target is $(5.6\pm1.1)\times10^{-3}$ (g). The evaporation rate is $(1.8\pm0.3)\times10^{-5}$ (g/s) as shown in Fig. 6.18. This is about ten times smaller than the evaporation rate of 5 kV/3 mA. This result shows that the 5 kV E-beam accelerating voltage can heat and evaporate the metallic target more effectively.

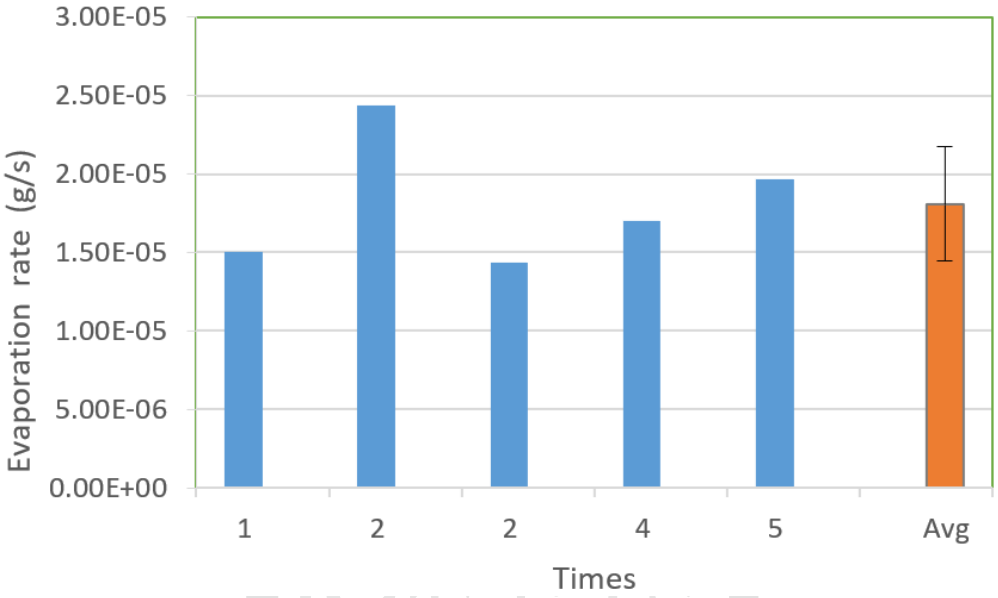

Figure 6.18: The evaporation rate of MIT-MEB at 1 kV.

6-4-3 Ionization rates

The current curve of the neutralizer of MIT-MEB is shown in Fig. 6.19. The maximum 0.27±0.03 mA occurs at the fifth minute. Since In gradually become saturated, we choose the maximum value to calculate. According to formula (18), the ionization rate is

$$\beta = \frac{(0.27\pm0.03)\times10^{-3}}{1.6\times10^{-19}} \div \frac{(1.8\pm0.3)\times10^{-5}}{65\times1.67\times10^{-24}} = 1.1\pm0.3\ \%$$

This result shows that the 1 kV electron beam accelerating voltage can be more effective to ionize the metallic vapor.

doi:10.6844/NCKU201900538

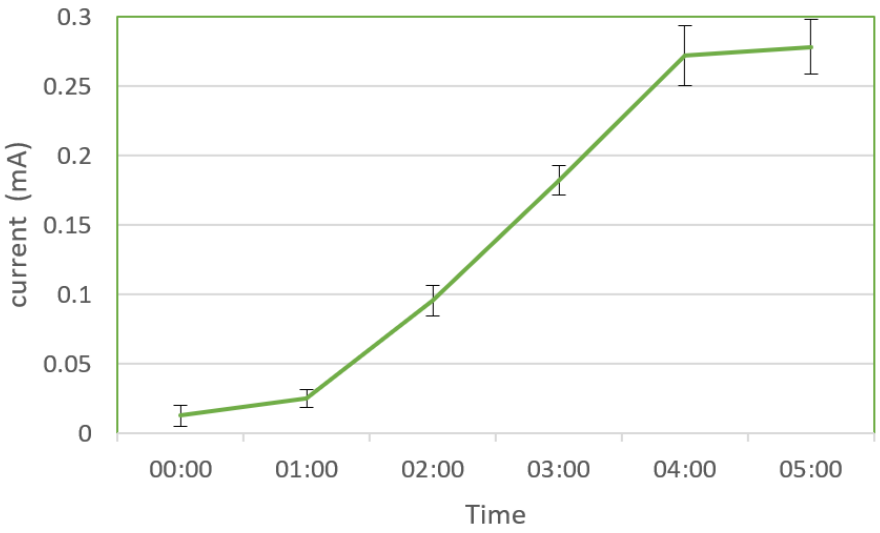

Figure 6.19: The current curve of the Neutralizer of MIT-MEB at 1 kV.

6-4-4 Expected thrusts

According to formula (19), (20), we can calculate the theoretical thrust T(μ N)*:*

$$F_{ion} = (1.1\pm0.3\ \%)(1.8\pm0.3)\times10^{-5} \times \sqrt{\frac{2\times1000V\times1.6\times10^{-19}}{65\times1.67\times10^{-27}}} = 10.3\pm0.7 \quad \mu N.$$

6-4-5 Expected I_{sp}

According to formula (13), we can calculate the specific impulse I_{sp} (sec*):*

$$I_{sp} = \frac{1}{9.8} \times \sqrt{\frac{2\times1000V\times1.6\times10^{-19}}{65\times1.67\times10^{-27}}} = 5{,}500 \text{ sec.}$$

6-5 Comparison

Comparison of propulsion parameters of MIT-MEB under experimental conditions of 1 kV and 5 kV accelerating voltage is shown in Table. 6.1. Although the evaporation rate of 5 using kV is 10 times higher than that of using 1 kV, the ionization rate is 30 times lower than that of using 1 kV. This shows that although 5 kV has better evaporation capability, the ability of ionizing gas is lower. This eventually lead to two thrusts almost. I will discuss this

doi:10.6844/NCKU201900538

phenomenon in Chapter 7 which seems to be related to the number of electrons and the cross section of different energy electrons.

Condition	*Power*	*Evaporation rate*	*Ionization rate*	*Thrust of ions*	I_{sp}
5 kV/3 mA	24.8±1.1 W	$(2.2\pm0.4)\times10^{-4}$ (g/s)	0.03±0.01 %	9.0±1.0 μN	12,300 s
1 kV/15 mA	26.2±0.7 W	$(1.8\pm0.3)\times10^{-5}$ (g/s)	1.1±0.3%	10.3±0.7 μN	5,500 s

Table 6.1: Comparison of thruster parameters of 1 kV and 5 kV of MIT-MEB under same E-beam power.

doi:10.6844/NCKU201900538

Chapter 7

Discussions

In this chapter, I will discuss the experimental results, the contribution of propulsion from vapor and the future work of improving the ionization rate. The experimental results show that the electron impact ionization efficiency with the energy of 1 keV is much higher than that of 5 keV at the same electron beam power (15 W). Although the number of electrons of E-beam at 1 kV accelerating voltage is only five times than that of 5 kV, the ionization rate of using 1 kV accelerating voltage is 30 times more than that of using 5 kV. This shows that other mechanisms cause a huge gap difference in ionization rate between 1 kV and 5 kV. This may be related to the cross section of electron impact ionization for zinc, the number of secondary and backscattered electrons.

7-1 Cross section of electron impact ionization for zinc

I mentioned in section 2-2-2-4 that the first ionization energy of zinc is 9.4 eV. This means that the energy of the electrons must be at least 9.4 eV to ionize the zinc atom. When energetic electrons (5 keV is used) collide with the zinc target, about 30 % of them collide with the solid target elastically and are backscattered with the energy of $E_{BSE} \approx 0.51E_0 = 2.55$ keV [25]. Rest electrons collide with the target inelastically and create true secondary electrons, those originally in the solid and are ejected by energies delivered by incoming-energetic electrons, with energies typically less than 15 eV [26, 27]. The true secondary electron yield which defined as the ratio between the secondary electrons to the incoming electrons is more than unity for most materials for incoming electrons with energy in the order of 1 keV or less. The yield goes

doi:10.6844/NCKU201900538

down to ~ 0.1 when the energy of incoming electrons is in the order of 5 keV or higher [26, 28]. In any cases, secondary electrons, including backscattered and true secondary electrons, are confined by the electric potential and the magnetic field in a small region forming an electron cloud on top of the target surface. Shown in Fig. 7.1 is the cross section of electron impact ionization for zinc [29]. The cross section peaks at ~ 50 eV according to Tawara and Kato's measurements [30]. Comparing energies of the accelerated and backscattered electrons to the first ionization energy of 9.4 eV for zinc [31] and the energy with the largest ionization cross section, the energy of electrons in the cloud is more than sufficient to ionize atoms. Therefore, it can be seen that the lower the acceleration voltage the better. Not only can the cross section be maximized but also the number of electrons can be increased with the same power. According to the above theory, the ideal E-beam accelerating voltage may fall around 100V.

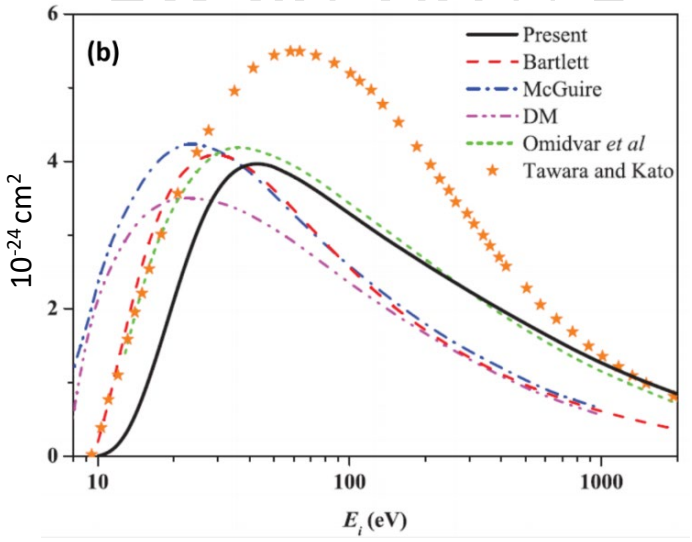

Figure 7.1: Cross section of electron impact ionization for zinc [29].

7-2 The contribution of thrust from vapor

The experimental results show that the ionization rate is very low. This shows that more than 99 % of the gas particles are not accelerated by the electric

doi:10.6844/NCKU201900538

field but are moving at the thermal speed. Therefore, considering the contribution of thermal velocity. $F_{total} = F_{th} + F_{ion}$, we can rewrite Eq. (1 & 19) as

$$F_{total} = \dot{m}_{th} \times V_{th} + \dot{m}_{ion} \times V_{ion} \ ,$$

$$F_{total} = [(1-\beta) \times \dot{m}_{Metal} \times \sqrt{\frac{2k_B T}{m}}] + [\beta \times \dot{m}_{Metal} \times \sqrt{\frac{2E_k}{m}}]$$

where V_{th} is thermal velocity, k_B is the Boltzmann constant, T is the temperature in Kelvin, and m is the mass of a particle. We assume that the temperature of zinc vapor is 300 ˚C because the vapor pressure of Zn is about 0.01 Torr at this temperature. The thermal velocity of 300 ˚C vapor is 381m/s, the corresponding I_{sp} is 38.8 sec. We calculate the thrust of thermal vapor based on experimental data of 5 kV and 1 kV:

F_{th} of 5 kV = $[(99.07\pm0.01\ \%)\times(2.2\pm0.4)\times10^{-4}\times381] = 90\pm40$ μN ,

F_{th} of 1 kV = $[(98.9\pm0.3\ \%)\times(1.8\pm0.3)\times10^{-5}\times381] = 7\pm4.0$ μN ,

and the total thrust is

F_{total} of 5 kV = $(90\pm40)+(9.0\pm1.0) = 99\pm40$ μN ,

F_{total} of 1 kV = $(7\pm4.0)+(10.3\pm0.7) = 17.3\pm4.0$ μN .

It can be seen that at the acceleration voltage of 5 kV, the thrust contributed from the vapor is dominant. At an acceleration voltage of 1 kV, the thrust contributed by the steam is similar to the thrust contributed by the ion.

7-3 Comparisons with other ion thrusters

In Table 7.1, comparisons between MIT-MEB with some well-known ion thrusters are given [12]. Note that we only calculate the thrust contributed by the ion current. Our thruster is smaller in diameter compared to other ion thrusters but the thrust is comparable to any other ion thrusters with a much higher specific impulse if it is linearly scaled up. The thrusts and the I_{sp} can be increased by

doi:10.6844/NCKU201900538

simply adding an extra accelerator. It provides the possibilities to explore deeper space such as Moon or Mars missions using CubeSats.

Name	*Propellant (Element)*	*Diameter (cm)*	*Power (W)*	I_{sp} *(sec)*	$M_{propellant}$ *(kg/s)*	β *(%)*	*Thrust (mN)*
MIT-MEB[a] 5 kV	Zn	~ 5	24.8	12,300	2.2×10^{-7}	0.03	9×10^{-3}
MIT-MEB[a] 1 kV	Zn	~5	26.2	5500	1.8×10^{-8}	1.1	1.1×10^{-2}
13-cm XIPS[b]	Xenon	13	421	2507	7.0×10^{-7}	78	17.2
25-cm XIPS[c]	Xenon	25	4300	3550	4.8×10^{-6}	87	166
NSTAR[d]	Xenon	28.6	577 - 2567	1979 – 3127	N/A	N/A	20.7 - 92.7
T5 Kaufman[e]	Xenon	10	476	3200	5.7×10^{-7}	78	18
RIT-10 RF[f]	Xenon	10	459	3400	4.5×10^{-7}	71	15
μ10 ECR[g]	Xenon	10	340	3090	2.7×10^{-7}	70	8.1
ETS-8 Kaufmanh	Xenon	12	541 – 611	2402 - 2665	8.9×10^{-7}	74	20.9 - 23.2

Table 7.1: Comparisons between our design to current ion thrusters [32].

[a]Metallic ion thruster using magnetron e-beam bombardments.
[b]Huges 13-cm Xenon Ion Propulsion System (XIPS)
[c]Huges 25-cm Xenon Ion Propulsion System (XIPS)
[d]NASA Evolutionary Xenon Thruster
[e]by Qinetiq in England
[f]Radio-frequency Ion Thruster Assembly
[g]by Japan Aerospace Exploration Agency (JAXA)
[h]Mitsubishi Electric Corporation on the Engineering Test Satellite VIII

7-4 Diffusion of metallic vapor in a vacuum chamber

At the end of the experiment, we found an interesting phenomenon. As shown in Fig. 7.2, clear projection marks of zinc on the evaporator and turbo molecular pump were observed. Since this is the projection of the accelerating grid, we are sure that it comes from downstream of the thruster. We suspect that this may be caused by metal vapors impinging on the vacuum chamber wall and

doi:10.6844/NCKU201900538

then reflecting back to the thruster. It is not clear how it will affect the performance on the thruster yet. If this is the ions attracted back to the thruster by static electricity, this will be a big problem. Because this means that the neutralizer cannot completely neutralize the charge. If this is from the neutral particles hitting the wall and being bounced back, we need to improve the experiment in the future to avoid it.

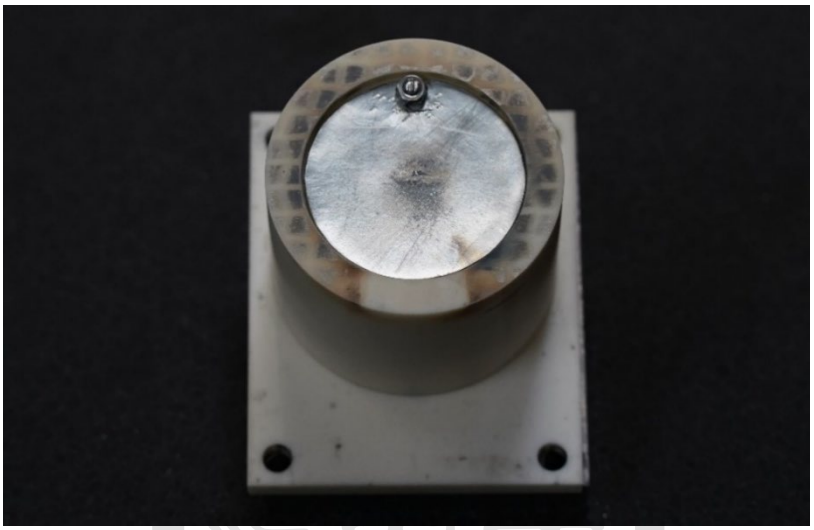

Figure 7.2: Zinc vapor projection on the evaporator.

In addition, we found a similar phenomenon on the blade of the turbomolecular pump as shown in Fig. 7.3. Since the turbomolecular pump is directly below the MIT-MEB, the vapor particles can only be reflected by the wall back into the pump.

doi:10.6844/NCKU201900538

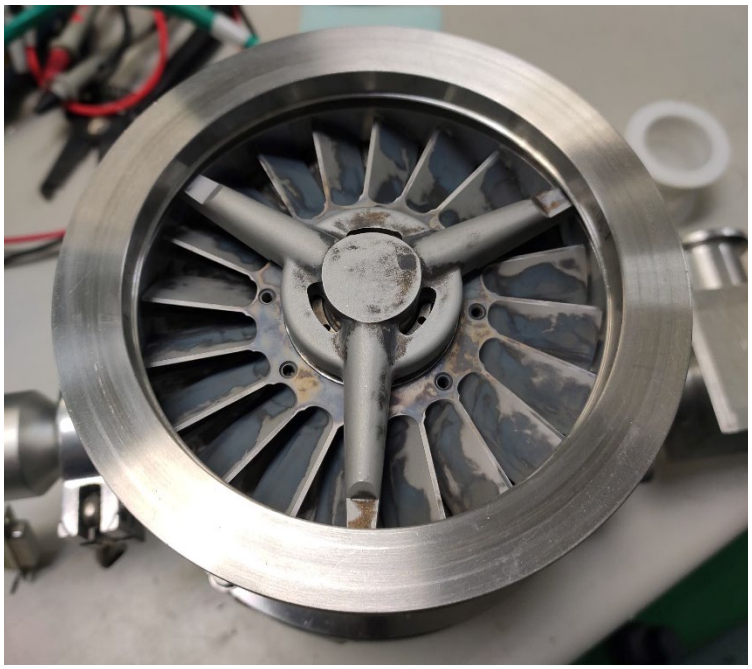

Figure 7.3: Zinc coated on the blade of the turbo molecular pump.

7-5 Future work

According to the results of our experiments, the prototype of MIT-MEB has a very low ionization rate. In order to achieve practical purposes, we must increase the ionization rate. We believe that the reason for the low ionization rate is due to the fact that electrons cannot be confined between the target and the grid for a long time. We went through designs of gridded ion thrusters and the Hall thrusters and found that both of them confine electrons for a long time. This is to increase probability of the collision between electrons and vapors. According to the structure of MIT-MEB, I design the corresponding magnetic field trap to confine the electrons. As shown in Fig. 7.4, I add a ring magnet to confine electrons.

doi:10.6844/NCKU201900538

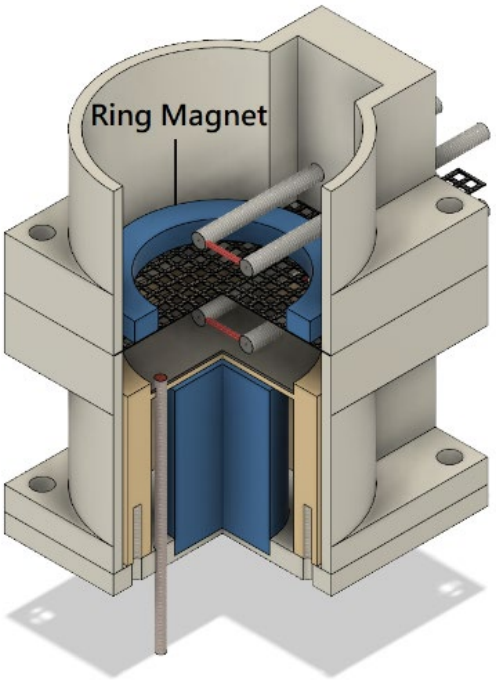

Figure 7.4: Add a ring magnet to confined the electrons.

Shown in Fig. 7.5 is the simulated magnetic field where a ring magnet is added above the grid that separates the ion source region and the accelerator region. When electrons propagate toward the target, they may be reflected due to the magnetic mirror effect. For those electrons penetrate through the magnetic mirror point, they will collide and heat the target. Further, for electrons reflected from the magnetic mirror point and backscattered from the target, they first move upward but are reflected back down by the electric potential between the filament and the target. Furthermore, electrons are confined radially by the magnetic field. As a result, electrons are confined in the triangle region in Fig. 7.5. The ionization fraction supposes to be increased.

doi:10.6844/NCKU201900538

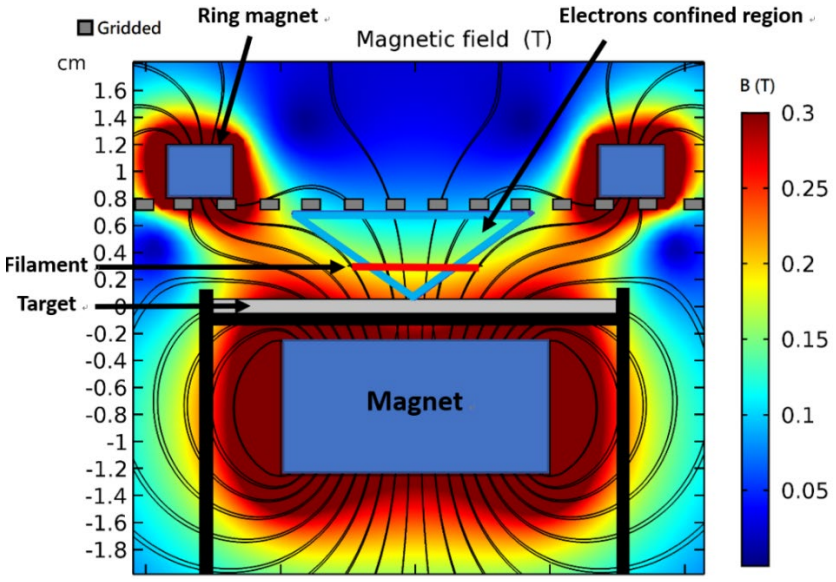

Figure 7.5: Concept of confining electrons in the gray triangle region using a ring magnet.

Power consumption is critical if the thruster is used in a CubeSat. In this design, a significant amount of power goes to heat the filament. Therefore, instead of using thermal-emitted electrons, we plan to use field-emitted electrons so that we don't need to waste energy on heating the filament. The heated filament will be replaced by a fine tip made of tungsten. The tip will also be placed closer to the target so that the electric field on the tip is large enough for electron field emissions. The power consumption is expected to be reduced dramatically.

In order to achieve 100% utilization of the propellant, we can make the propellant into wire shape. It is because the width of the electron beam bombardment area is very small, less than 1 mm. Therefore, as long as the diameter of the wire is less than 1 mm, the electron beam can 100 % erode the tip of the target. As shown in Fig. 7.6, a wire-shaped metal as the propellant of MIT-MEB is used. We can roll up the propellant and push it into the center of

doi:10.6844/NCKU201900538

the evaporator using a spring or motor. Not only the propellants are fully used, the storage density is maximized.

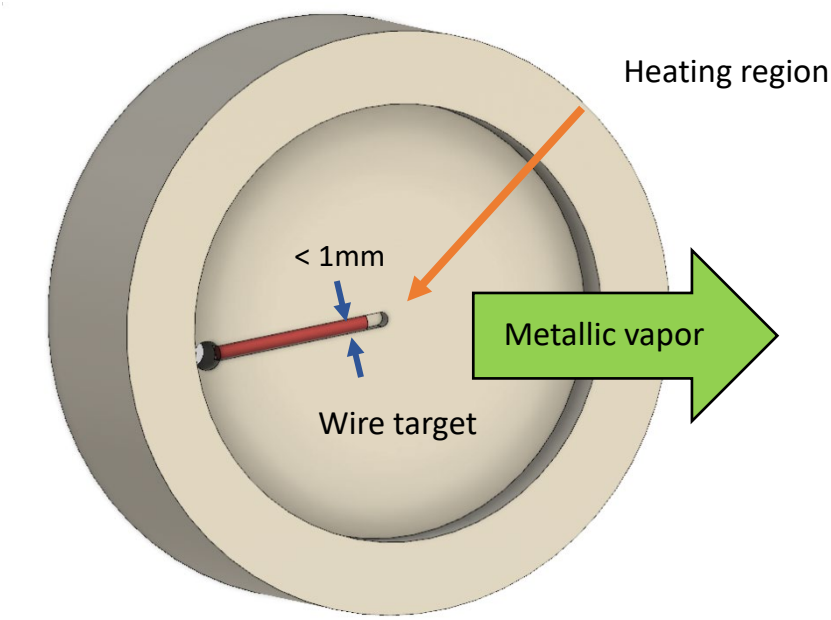

Figure 7.6: The wire-shaped propellant of MIT-MEB.

doi:10.6844/NCKU201900538

Chapter 8

Summary

It is a new idea of making an ion thruster that is much smaller in size but with comparable performance to any ion thrusters to date. Metallic Ion Thruster using Magnetron E-beam Bombardment uses a metallic target as the propellant. Different from the inert gas used in conventional plasma thrusters, the metal target is in the solid state, high density, easy to be stored and cheap. The design is divided into three parts: a metal evaporator and an ion accelerator and a neutralizer. The principle of E-beam evaporation, where a metallic target is evaporated and ionized by E-beam, is used. A focusing magnet with a magnetic field about 0.2~0.3 T between the target surface and the filament is used to guide electrons toward the center of the target so that the metal is evaporated and ionized. A prototype has been built and tested. The metallic targets were heated to more than 415 °C by electron bombardment. A mass flow rate of $(2.2\pm0.4)\times10^{-4}$ (g/s) and $(1.8\pm0.3)\times10^{-5}$ (g/s) using Zn at 5 kV/3 mA and 1 kV/ 15 mA E-beam current was measured. An ionization rate of 0.03±0.01 % and 1.1±0.3 % using Zn at 5 kV and 1 kV E-beam current was measured. Therefore, the estimated thrust of ions is 9.0±1.0 μN and 10.3±0.7 μN corresponding to 5 kV/3 mA and 1 kV/15 mA E-beam current, respectively, with a power of about 25 W. The Estimated I_{sp} of ions is 12,300 s and 5,500 s, respectively. Considering the contribution of vapors, the total thrust is 99±40 μN and 17.3±4.0 μN respectively.

In the future, we have two goals to improve the performance of the MIT-MEB. First, due to the low ionization rate of the prototype of MIT-MEB, we plan

doi:10.6844/NCKU201900538

to add a ring magnet to confine electrons. Looking forward to increasing the chance of collision between electrons and vapor. Second, we want to use an energy-free electron source to further reduce power consumption and suitable for CubeSat.

doi:10.6844/NCKU201900538

References

[1] Ming-Hsueh Shen. Development of a micro ecr ion thruster for space propulsion. Master's thesis, National Cheng Kung University, 2016. Replotted form Kuriki, K. and Arakawa. Y., Introduction to electric propulsion, U. Tokyo Press., Tokyo, 2003.

[2] K. Kuriki and Y. Arakawa. *Introduction to electric propulsion*. University of Tokyo Press, 2003.

[3] Ashkenazy, Joseph & Appelbaum, G & Ram-Cohen, T & Warshavsky, A & Tidhar, I & Rabinovich, L. (2007). VENμS Technological Payload - The Israeli Hall Effect Thruster Electric Propulsion System. 10.13140/2.1.4172.4801.

[4] Burton, Rodney L. "*Pulsed plasma thrusters.*" Encyclopedia of Aerospace Engineering (2010).

[5] Ulrich Walach. *Schematic layout of a Pulsed Plasma Thruster*, Wikipedia.

[6] Changsha Mingguan Metal Technology Co. http://www.tungstenmoly.com/html/Pure-Tungsten/79.html.

[7] Kurt J. Lesker Company. Deep Cup Evaporation Boat. Tungsten Wire/Evaporation Coil, https://www.lesker.com/newweb/evaporation_sources/thermal_boat_notched.cfm?pgid=4

[8] Jatosado. *Electron Beam Deposition, Wikipedia.*

[9] Crowell, C. R. "*The Richardson constant for thermionic emission in Schottky barrier diodes.*" Solid-State Electronics 8.4 (1965): 395-399.

[10] K.S Sree Harsha. Principle of Vapor Deposition of Thin Films. Elsevier Science, 2006

[11] SPM Science. *Thermionic Emission*. http://spmphysics.onlinetuition.com.my/2013/06/thermionic-emission.html

[12] Giubileo, F.; Di Bartolomeo, A.; Iemmo, L.; Luongo, G.; Urban, F. Field

doi:10.6844/NCKU201900538

Emission from Carbon Nanostructures. Appl. Sci. 2018, 8, 526.

[13] Inductiveload. *Beta-minus Decay.svg. Wikipedia.*

[14] Jaro.p. *Lorentz force.svg. Wikipedia.*

[15] Marcin Białek. Cyclotron motion wide view.jpg. Wikipedia.

[16] Magnetic mirror
https://cnx.org/contents/pmp6Kk2R@7/Force-on-a-Moving-Charge-in-a-Magnetic-Field-Examples-and-Applications

[17] Märk, Tilmann D., and Gordon H. Dunn, eds. Electron impact ionization. Springer Science & Business Media, 2013.

[18] First Ionization Energy. Wikipedia.

[19] Goldstein, Joseph I., et al. Scanning electron microscopy and X-ray microanalysis. Springer, 2017.

[120] K. Burak Ucer/L06-Vacuum_Evaporation/Department of Physics Wake Forest

[21] [Online] https://luxel.com/wp-content/uploads/2013/04/Luxel-Vapor-Pressure-Chart.pdf.

[22] Gao-Yu Hsiung, Vacuum Technology The sixth OCPA Accelerator School (OCPA2010),July 29 to August 7, in Beijing, China
http://csns.ihep.ac.cn/english/conference/ocpa2010/school_courses/images/PDF/T5-Vacuum%20Technology.pdf

[23] Turbomolecular pump structure
https://www.lesker.com/newweb/faqs/question.cfm?id=477

[24] Structure of hot cathode ion gauge
https://www.slideshare.net/LukeHinkle/complex2-simple-vacuum-training-quick-demo-presentation

[25] Jaya Mukherjee, V Dileep Kumar, S P Yadav, Tripti A Barnwal, and Biswaranjan

doi:10.6844/NCKU201900538

Dikshit. Plasma diagnosis as a tool for the determination of the parameters of electron beam evaporation and sources of ionization. Measurement Science and Technology, 27(7):075007, jun 2016.

[26] J.J Scholtz, D Dijkkamp, and R.W.A Schmitz. Secondary electron emission properties. Philips Journal of Research, 50(3):375 – 389, 1996. New Flat, Thin Display Technology.

[27] David M. Suszcynsky and Joseph E. Borovsky. Modified sternglass theory for the emission of secondary electrons by fast-electron impact. Phys. Rev. A, 45:6424–6428, May 1992.

[28] R. K. Yadav and R. Shanker. Contribution of backscattered electrons to the total electron yield produced in collisions of 8–28 kev electrons with tungsten. Pramana, 68(3):507–515, Mar 2007.

[29] Jaspreet Kaur, Dhanoj Gupta, Rahla Naghma, Debdeep Ghoshal, and Bobby Antony. Electron impact ionization cross sections of atoms. Canadian Journal of Physics, 93(6):617–625, 2015.

[30] H. Tawara and T. Kato. Total and partial ionization cross sections of atoms and ions by electron impact. Atomic Data and Nuclear Data Tables, 36(2):167 – 353, 1987.

[31] A. Kramida, Yu. Ralchenko, J. Reader, and and NIST ASD Team. NIST Atomic Spectra Database (ver. 5.5.1), [Online]. Available: https://physics.nist.gov/asd [2017, December 24]. National Institute of Standards and Technology, Gaithersburg, MD., 2017.

[32] Dan M. Goebel and Ira Katz. Fundamentals of Electric Propulsion: Ion and Hall Thrusters. Wiley, 1st edition, November 2008.

doi:10.6844/NCKU201900538

APPENDIX A Drawings of MIT-MEB

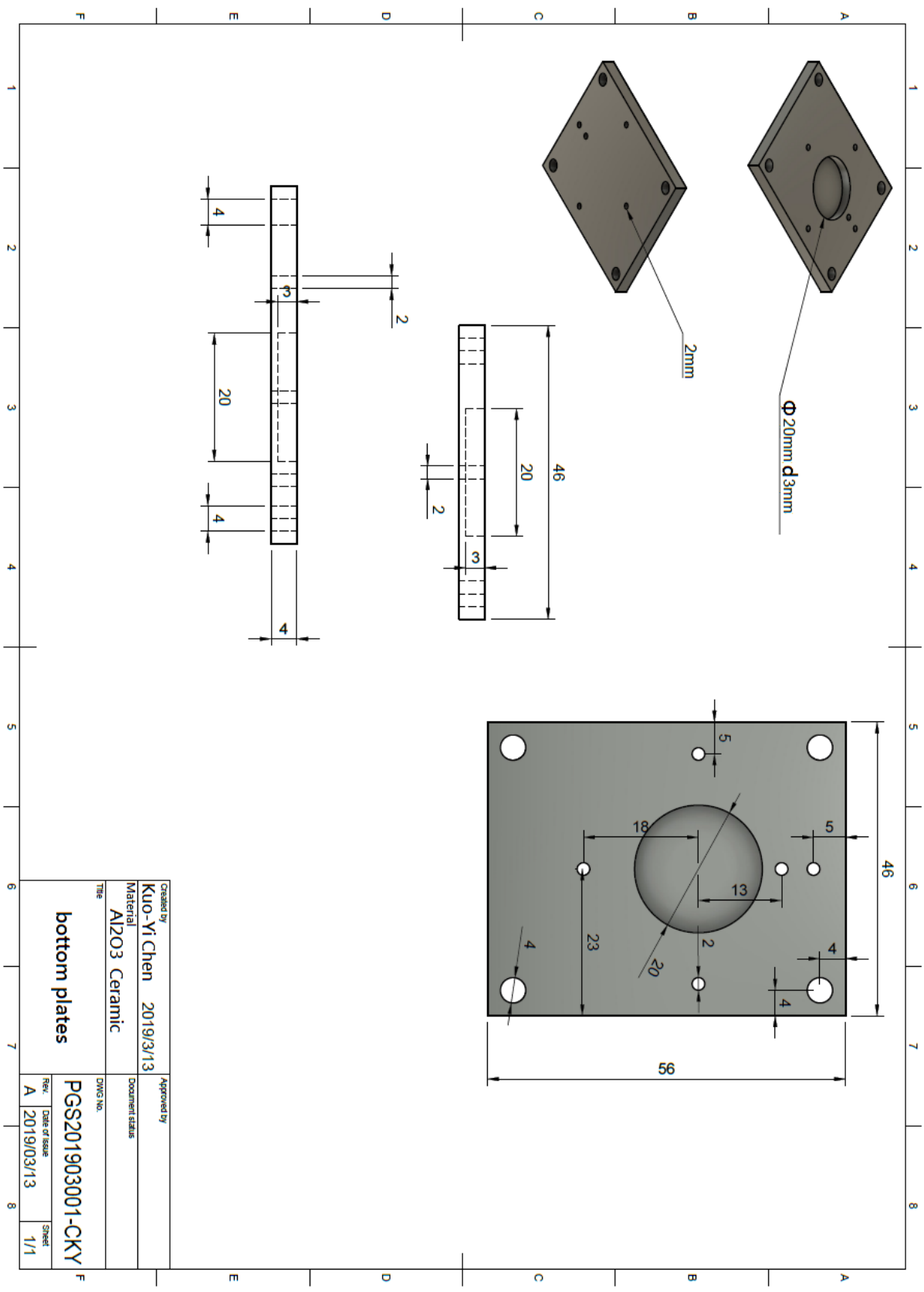

doi:10.6844/NCKU201900538

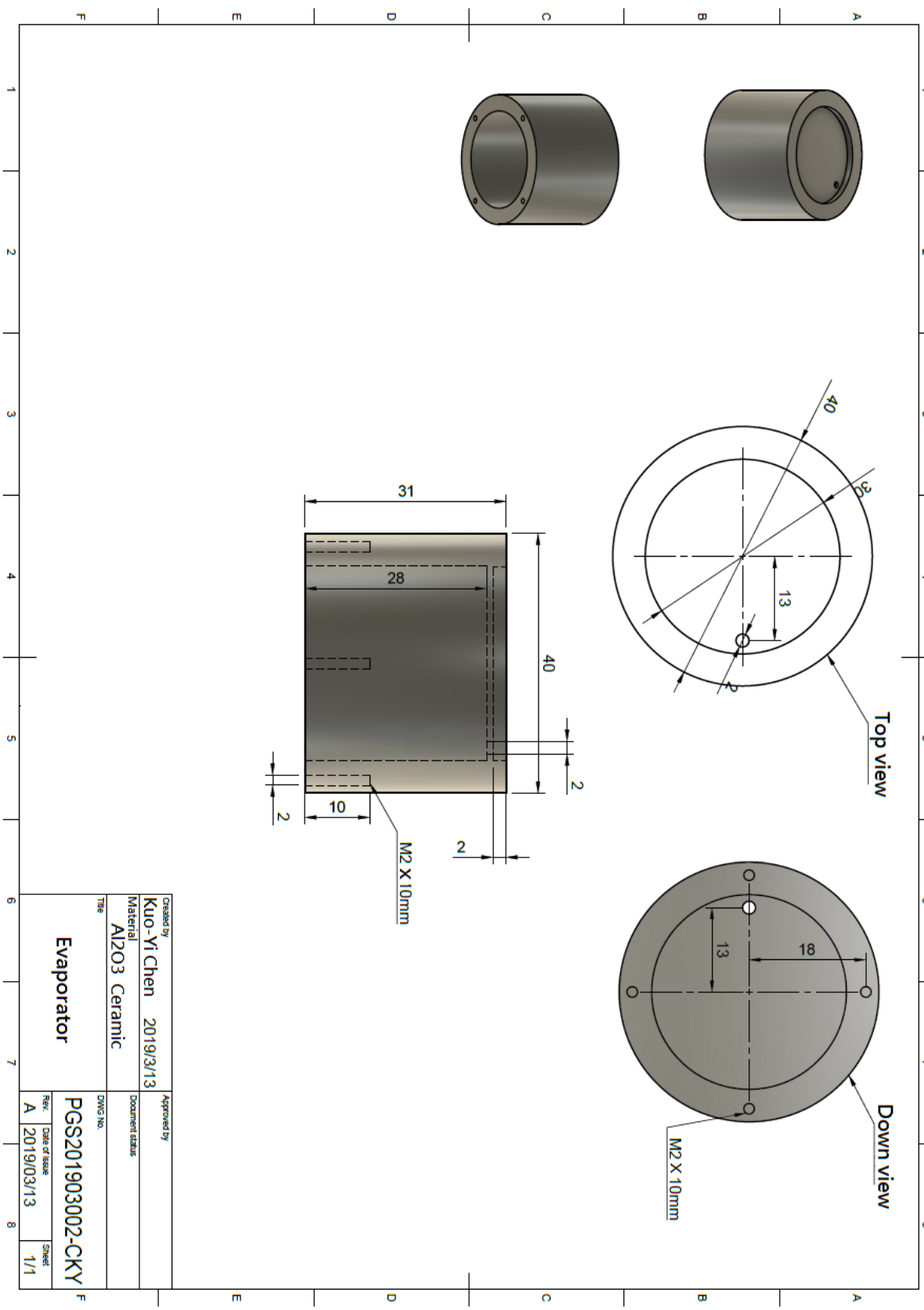

doi:10.6844/NCKU201900538

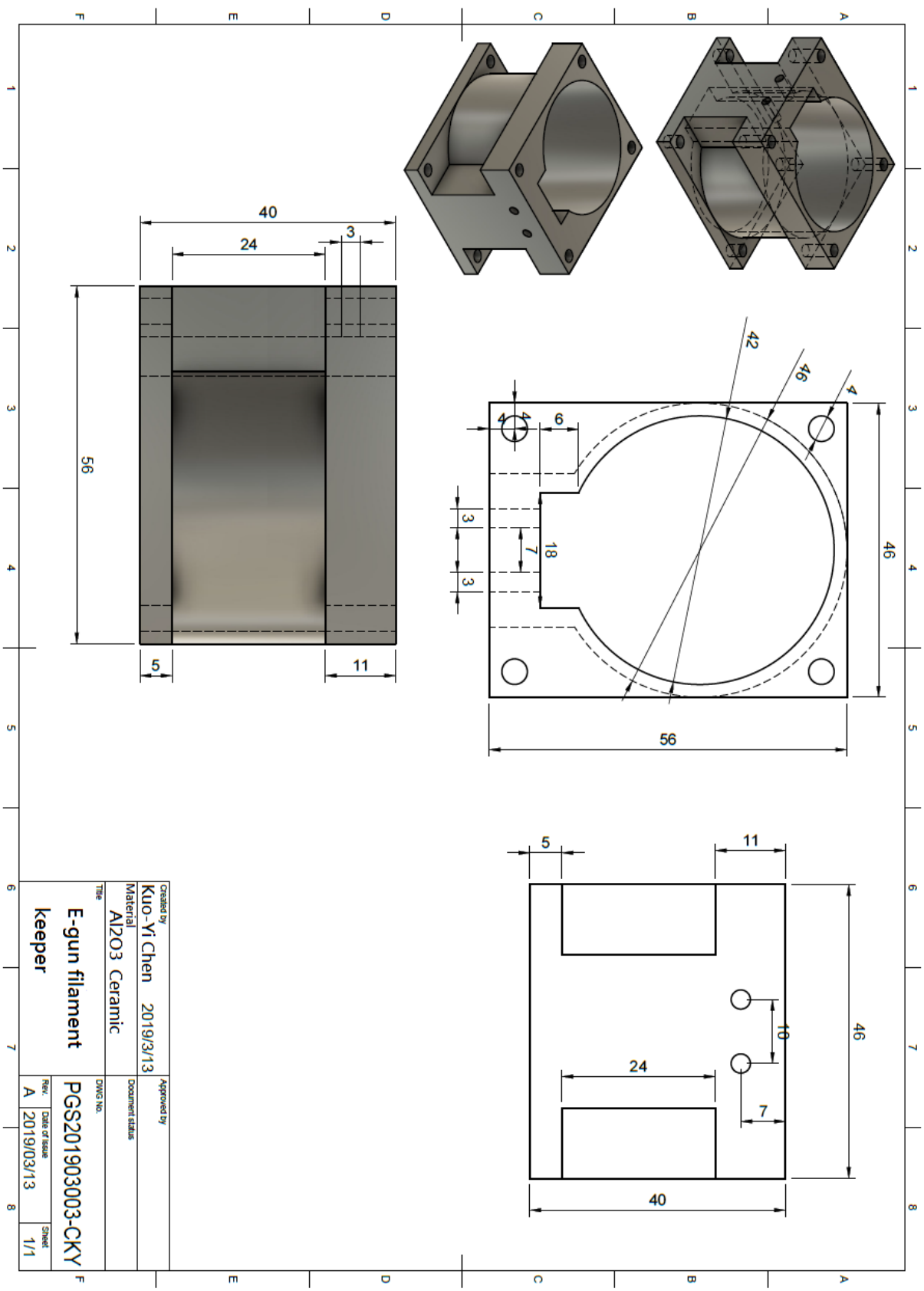

doi:10.6844/NCKU201900538

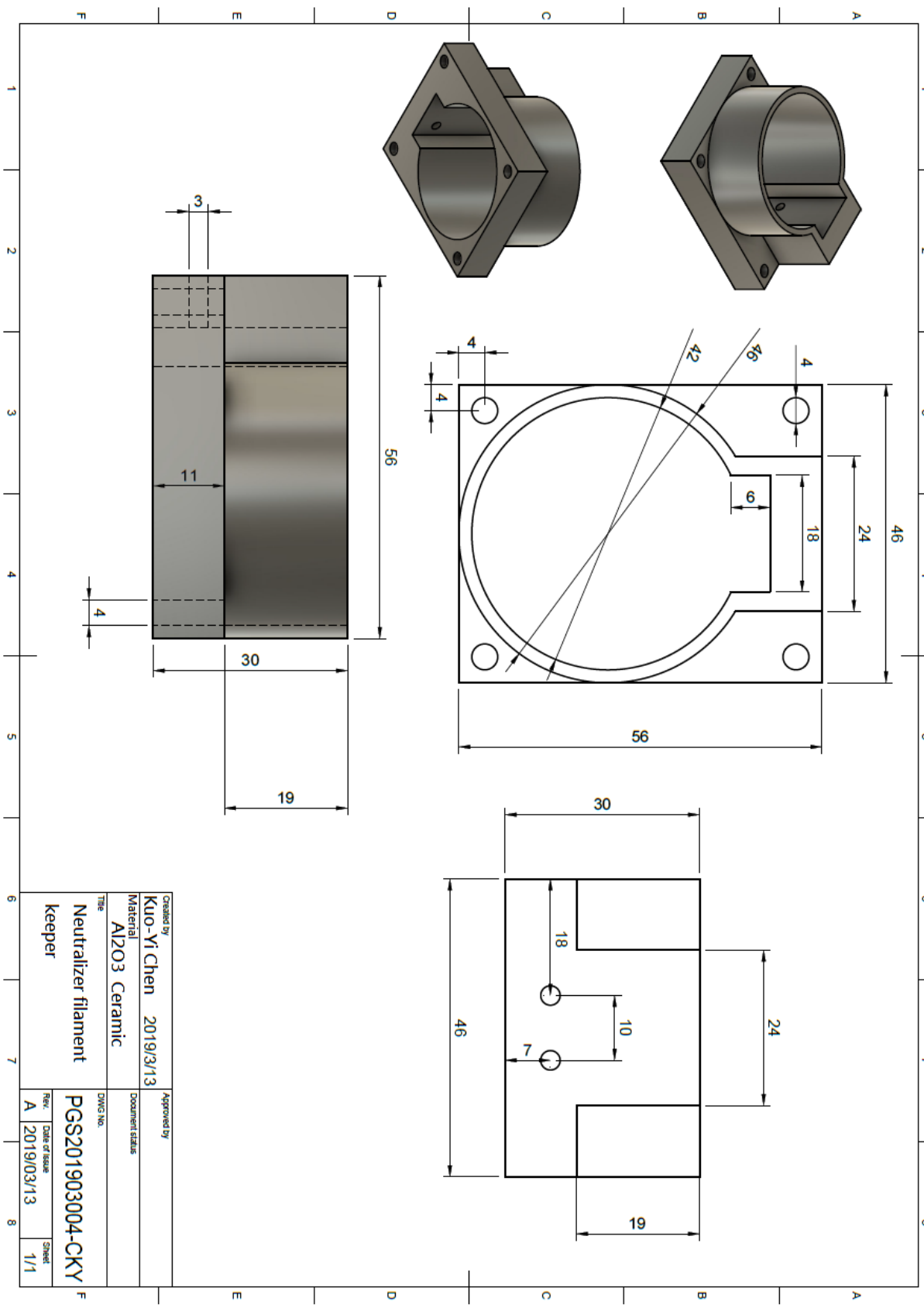

doi:10.6844/NCKU201900538

Created by	Approved by
Glori Chen 2019/7/12	
Material: Aluminum alloy	Document status:
Title: Grounding plate	DWG No.: PGS-201907001-CKY
Rev.: A	Date of issue: 2019/07/02
	Sheet: 1/1

doi:10.6844/NCKU201900538

APPENDIX B Experimental raw data

Time(min)	*2018/12/12*	*2018/12/12*	*2018/12/13*	*2018/12/17*	*2018/12/20*	*Avg*	*σ*
HV0(V)	5000	5003	5000	5002	5001	5001.2	1.16619
HV2(V)	5001	5003	5004	5003	5001	5002.4	1.2
HV4(V)	5002	5005	4997	5004	5002	5002	2.75681
HV6(V)	5001	5002	5003	5002	5003	5002.2	0.748331
HV8(V)	5001	5003	5004	5003	5002	5002.6	1.019804
HV10(V)	5002	5004	5001	5003	5004	5002.8	1.16619
$I_e0(mA)$	3.1	2.9	2.8	2.8	2.9	2.9	0.109545
$I_e2(mA)$	3.4	2.9	3	2.7	2.9	2.98	0.231517
$I_e4(mA)$	3.2	3	2.9	2.9	2.9	2.98	0.116619
$I_e6(mA)$	3.1	2.9	3.3	3	3	3.06	0.135647
$I_e8(mA)$	3.1	3	2.9	3.1	2.8	2.98	0.116619
$I_e10(mA)$	3.2	3.3	3	3	3	3.1	0.126491
$I_f0(A)$	1.802	1.818	1.904	1.913	1.899	1.8672	0.047191
$I_f2(A)$	1.802	1.824	1.905	1.917	1.895	1.8686	0.046453
$I_f4(A)$	1.804	1.824	1.898	1.919	1.897	1.8684	0.045548
$I_f6(A)$	1.801	1.817	1.894	1.913	1.879	1.8608	0.043938
$I_f8(A)$	1.8	1.818	1.883	1.899	1.893	1.8586	0.041215
$I_f10(A)$	1.802	1.815	1.879	1.896	1.91	1.8604	0.043693
$V_f0(V)$	1.8	1.8	1.7	1.6	1.8	1.74	0.08
$V_f2(V)$	1.8	1.8	1.7	1.6	1.8	1.74	0.08
$V_f4(V)$	1.8	1.8	1.7	1.6	1.8	1.74	0.08
$V_f6(V)$	1.8	1.8	1.7	1.6	1.8	1.74	0.08
$V_f8(V)$	1.8	1.8	1.7	1.6	1.8	1.74	0.08
$V_f10(V)$	1.8	1.8	1.7	1.6	1.8	1.74	0.08
P0(Pa)	9.90E-04	1.10E-03	3.20E-03	3.50E-03	5.00E-03	2.76E-03	0.001526
P2(Pa)	1.70E-03	1.10E-03	1.80E-03	2.50E-03	4.10E-03	2.24E-03	0.001031
P4(Pa)	1.30E-03	1.30E-03	1.00E-03	2.90E-03	4.50E-03	2.20E-03	0.00133
P6(Pa)	1.20E-03	1.90E-03	1.00E-03	3.70E-03	8.00E-03	3.16E-03	0.0026
P8(Pa)	1.20E-03	2.20E-03	1.30E-03	3.30E-03	7.00E-03	3.00E-03	0.002138
P10(Pa)	1.10E-03	3.00E-03	1.10E-03	2.90E-03	5.00E-03	2.62E-03	0.00145
$m_i(g)$	3.04E+00	3.23E+00	3.40E+00	3.18E+00	3.24E+00	3.21	0.116785
$m_f(g)$	2.89E+00	3.08E+00	3.24E+00	3.01E+00	3.00E+00	3.04	0.113891
$\Delta m(g)$	1.47E-01	1.51E-01	1.64E-01	1.66E-01	2.34E-01	1.72E-01	0.031888
$\dot{m}_{Zn}(g/s)$	2.45E-04	2.51E-04	2.73E-04	2.76E-04	3.91E-04	2.87E-04	5.31E-05

Test electron beam evaporation experiment (5 k/3 mA)

doi:10.6844/NCKU201900538

Time(min)	*2019/5/8*	*2019/5/27*	*2019/5/27*	*2019/6/4*	*2019/6/9*	*Avg*	*σ*
HV0(V)	5000	5000	5000	5000	5000	5000	0
HV1(V)	5000	5000	5000	5000	5000	5000	0
HV2(V)	5000	5000	5000	5000	5000	5000	0
HV3(V)	5000	5000	5000	5000	5000	5000	0
HV4(V)	5000	5000	5000	5000	5000	5000	0
HV5(V)	5000	5000	5000	5000	5000	5000	0
$I_e0(mA)$	3	3	3	3	3	3	0
$I_e1(mA)$	3	2.9	3	3.2	3	3.025	0.108972
$I_e2(mA)$	2.9	2.8	2.9	3.1	3.1	2.975	0.129904
$I_e3(mA)$	2.9	2.9	2.9	3	3.1	2.975	0.082916
$I_e4(mA)$	3	2.9	2.9	3.2	3	3	0.122474
$I_e5(mA)$	3.1	3	2.9	3.2	3	3.025	0.108972
$I_f0(A)$	2.17	2.11	2.11	2.41	2.15	2.195	0.1252
$I_f1(A)$	2.16	2.12	2.12	2.4	2.15	2.1975	0.117553
$I_f2(A)$	2.16	2.12	2.12	2.39	2.15	2.195	0.113248
$I_f3(A)$	2.14	2.12	2.12	2.38	2.15	2.1925	0.108944
$I_f4(A)$	2.13	2.12	2.12	2.38	2.15	2.1925	0.108944
$I_f5(A)$	2.14	2.12	2.12	2.38	2.15	2.1925	0.108944
$V_f0(V)$	1.8	1.8	1.8	1.9	1.84	1.835	0.040927
$V_f1(V)$	1.8	1.8	1.8	1.9	1.84	1.835	0.040927
$V_f2(V)$	1.8	1.8	1.8	1.9	1.84	1.835	0.040927
$V_f3(V)$	1.8	1.8	1.8	1.9	1.84	1.835	0.040927
$V_f4(V)$	1.8	1.8	1.8	1.9	1.84	1.835	0.040927
$V_f5(V)$	1.8	1.8	1.8	1.9	1.84	1.835	0.040927
$I_n0(mA)$	0.05	0.046	0.051	0.042	0.049	0.047	0.003391
$I_n1(mA)$	0.064	0.055	0.061	0.042	0.055	0.05325	0.006942
$I_n2(mA)$	0.071	0.099	0.061	0.07	0.055	0.07125	0.016887
$I_n3(mA)$	0.082	0.11	0.084	0.087	0.06	0.08525	0.017711
$I_n4(mA)$	0.097	0.123	0.096	0.1	0.086	0.10125	0.013553
$I_n5(mA)$	0.104	0.135	0.097	0.11	0.101	0.11075	0.014771
$I_{nf}0(A)$	2.5	2.5	2.51	2.53	2.53	2.5175	0.01299
$I_{nf}1(A)$	2.5	2.51	2.51	2.53	2.53	2.52	0.01
$I_{nf}2(A)$	2.52	2.53	2.51	2.53	2.53	2.525	0.00866
$I_{nf}3(A)$	2.51	2.52	2.53	2.53	2.53	2.5275	0.00433
$I_{nf}4(A)$	2.51	2.52	2.53	2.53	2.53	2.5275	0.00433
$I_{nf}5(mA)$	2.51	2.52	2.53	2.52	2.53	2.525	0.005
$V_{nf}0(V)$	2.2	2.4	2.4	2.2	2.2	2.3	0.1

doi:10.6844/NCKU201900538

$V_{nf}1(V)$	2.2	2.4	2.4	2.2	2.2	2.3	0.1
$V_{nf}2(V)$	2.2	2.4	2.4	2.2	2.2	2.3	0.1
$V_{nf}3(V)$	2.2	2.4	2.4	2.2	2.2	2.3	0.1
$V_{nf}4(V)$	2.2	2.4	2.4	2.2	2.2	2.3	0.1
$V_{nf}5(V)$	2.2	2.4	2.4	2.2	2.2	2.3	0.1
$m_i(g)$	69.1857	68.8916	68.9443	68.9529	68.8801	68.917225	0.031783
$m_f(g)$	69.1314	68.821	68.8862	68.8716	68.809	68.84695	0.032641
$\Delta m(g)$	0.0543	0.0706	0.0581	0.0813	0.0711	0.07027	0.008224
$\dot{m}_{Zn}(g/s)$	1.81E-04	2.35E-04	1.94E-04	2.71E-04	2.37E-04	2.24E-04	3.25E-05

Experimental of MIT-MEB (5 kV/3 mA)

Time(min)	2019/5/7	2019/6/9	2019/6/12	2019/6/13	2019/6/14	Avg	σ
HV0(V)	1000	1000	1000	1000	1000	1000	0
HV1(V)	1000	1000	1000	1000	1000	1000	0
HV2(V)	1000	1000	1000	1000	1000	1000	0
HV3(V)	1000	1000	1000	1000	1000	1000	0
HV4(V)	1000	1000	1000	1000	1000	1000	0
HV5(V)	1000	1000	1000	1000	1000	1000	0
$I_e0(mA)$	15	15	15	15.3	15.3	15.15	0.15
$I_e1(mA)$	15.1	15.4	15.2	15.6	15.4	15.4	0.141421
$I_e2(mA)$	15.4	16.4	14.9	15.4	15.3	15.5	0.552268
$I_e3(mA)$	15.6	15.8	15.8	15	15.6	15.55	0.327872
$I_e4(mA)$	15.6	16.1	15.2	16.3	15.4	15.75	0.460977
$I_e5(mA)$	16	16.3	15.5	15.4	15.6	15.7	0.353553
$I_f0(A)$	2.31	2.32	2.25	2.25	2.29	2.2775	0.029475
$I_f1(A)$	2.31	2.31	2.25	2.25	2.27	2.27	0.024495
$I_f2(A)$	2.31	2.31	2.25	2.25	2.26	2.2675	0.024875
$I_f3(A)$	2.31	2.3	2.25	2.25	2.26	2.265	0.020616
$I_f4(A)$	2.31	2.3	2.23	2.25	2.25	2.2575	0.02586
$I_f5(A)$	2.31	2.3	2.23	2.25	2.25	2.2575	0.02586
$V_f0(V)$	2.04	2.04	2.03	2.03	1.96	2.015	0.032016
$V_f1(V)$	2.04	2.04	2.03	2.03	1.96	2.015	0.032016
$V_f2(V)$	2.04	2.04	2.03	2.03	1.96	2.015	0.032016
$V_f3(V)$	2.04	2.04	2.03	2.03	1.96	2.015	0.032016
$V_f4(V)$	2.04	2.04	2.03	2.03	1.96	2.015	0.032016
$V_f5(V)$	2.04	2.04	2.03	2.03	1.96	2.015	0.032016
$I_n0(mA)$	0.01	0.003	0.018	0.022	0.008	0.01275	0.007595

doi:10.6844/NCKU201900538

$I_n1(mA)$	0.023	0.016	0.022	0.034	0.028	0.025	0.006708
$I_n2(mA)$	0.099	0.089	0.093	0.114	0.086	0.0955	0.010966
$I_n3(mA)$	0.198	0.177	0.168	0.197	0.187	0.18225	0.010848
$I_n4(mA)$	0.281	0.238	0.279	0.298	0.273	0.272	0.021691
$I_n5(mA)$	0.286	0.245	0.284	0.296	0.288	0.27825	0.019677
$I_{nf}0(A)$	2.5	2.5	2.5	2.48	2.5	2.495	0.00866
$I_{nf}1(A)$	2.5	2.5	2.5	2.48	2.5	2.495	0.00866
$I_{nf}2(A)$	2.5	2.5	2.5	2.48	2.5	2.495	0.00866
$I_{nf}3(A)$	2.5	2.5	2.5	2.48	2.5	2.495	0.00866
$I_{nf}4(A)$	2.5	2.5	2.5	2.48	2.5	2.495	0.00866
$I_{nf}5(mA)$	2.5	2.5	2.5	2.48	2.5	2.495	0.00866
$V_{nf}0(V)$	2.4	2.4	2.5	2.5	2.3	2.425	0.082916
$V_{nf}1(V)$	2.4	2.4	2.5	2.5	2.3	2.425	0.082916
$V_{nf}2(V)$	2.4	2.4	2.5	2.5	2.3	2.425	0.082916
$V_{nf}3(V)$	2.4	2.4	2.5	2.5	2.3	2.425	0.082916
$V_{nf}4(V)$	2.4	2.4	2.5	2.5	2.3	2.425	0.082916
$V_{nf}5(V)$	2.4	2.4	2.5	2.5	2.3	2.425	0.082916
$m_i(g)$	69.1604	68.8648	68.9017	68.8187	68.9071	68.873075	0.035363
$m_f(g)$	69.1559	68.8575	68.8974	68.8136	68.9012	68.867425	0.035478
$\Delta m(g)$	4.50E-03	7.30E-03	4.30E-03	5.10E-03	5.90E-03	0.00565	0.001108
$\dot{m}_{Zn}(g/s)$	1.50E-05	2.43E-05	1.43E-05	1.70E-05	1.97E-05	1.81E-05	3.64E-06

Experimental of MIT-MEB (1 kV/15 mA)

doi:10.6844/NCKU201900538

APPENDIX C Parts in this study and manufacturers

Source	*Product*	*Location*	*Contact information*
東昕實業有限公司	Vacuum product	Tainan Taiwan	台南市永康區中正南路 220 巷 39 號 Tel: 06 253 5687
南一電子有限公司	Electronic parts	Tainan Taiwan	台南市中西區民族路二段 95 號 Tel: (06) 226 0808
三美玻璃儀器行	Quartz processing	Tainan Taiwan	台南市東區富農街二段 109 巷 5 號 Tel: (06) 268 8397
GND3dp 3D	3D Printer	Taipei Taiwan	https://class.ruten.com.tw/user/index00.php?s=gnd3dp Tel: (02) 2957-6099
肥貓小舖	Aluminum electrode	New Taipei Taiwan	https://class.ruten.com.tw/user/index00.php?s=logicqq Tel: 0922361808
连云港玥霖石英科技有限公司	Quartz processing	Nanjing China	https://shop551916174.world.taobao.com/index.htm?spm=2013.1.w5002-18338120199.2.57881281zuJmVb
昱博精工	Ceramic processing	Suzhou, Jiangsu China	https://yuboce.world.taobao.com/index.htm?spm=2013.1.w5002-8510246850.2.2bf1514cZkxJF5
恒搏电源世界	High voltage power supply	Tianjin China	https://hbgydy.world.taobao.com/?spm=2013.1.1000126.3.678a2bf2pAJwOe
逸翰電子儀表	Gaussmeter	Guangzhou China	https://shopee.tw/product/60435599/983596940 Tel:
京宁机械	Vacuum Feedthrough (KF、CF)	Beijing China	https://shop550298987.world.taobao.com/shop/view_shop.htm?spm=a1z09.2.0.0.6d4f2e8dWcNP5B&user_number_id=2207920371
凯发新材	Ceramic tube	Beijing China	https://kftztc.world.taobao.com/shop/view_shop.htm?spm=a1z09.2.0.0.6d4f2e8dWcNP5B&user_number_id=178593891
成都创新电子电器厂	High voltage power supply	Chengdu, Sichuan China	https://item.taobao.com/item.htm?spm=a1z09.2.0.0.6d4f2e8dWcNP5B&id=41590765115&_u=otooesbdd5c
温州畅奇管控科技	Vacuum Flange O'ring	Wenzhou China	https://shop113266846.world.taobao.com/index.htm?spm=a312a.7700824.w5002-8559099191.2.1c45745e3YJiV7
东海县东烨石英制品有限公司	Giant quartz tube	Jiangsu China	https://item.taobao.com/item.htm?spm=a1z09.2.0.0.6d4f2e8dWcNP5B&id=541399637108&_u=otooesbb3d5
深圳市鸿金泰镀膜科技	Vacuum gauge	Shenzhen China	https://shop100460724.world.taobao.com/index.htm?spm=2013.1.w5002-9176756312.2.39184755NF8WhH
聚优汇轴承	Ceramic bearing	Jiangsu Wuxi China	https://item.taobao.com/item.htm?spm=a1z09.2.0.0.6d4f2e8dWcNP5B&id=45111832092&_u=otooesbf509

doi:10.6844/NCKU201900538

上海杨氏阀门管件	Vacuum Flange	Shanghai China	https://shop58585738.world.taobao.com/shop/view_shop.htm?spm=a1z09.2.0.0.6d4f2e8dWcNP5B&user_number_id=259686914
达邦金属	Stainless steel laser cutting	Fuzhou China	https://item.taobao.com/item.htm?spm=a1z09.2.0.0.6d4f2e8dWcNP5B&id=549113584358&_u=otooesb4210
东莞市圣泽金属材料有限公司	Tungsten wire	Dongguan China	https://shop124822164.world.taobao.com/?spm=2013.1.0.0.42be380bQHtTdD

doi:10.6844/NCKU201900538